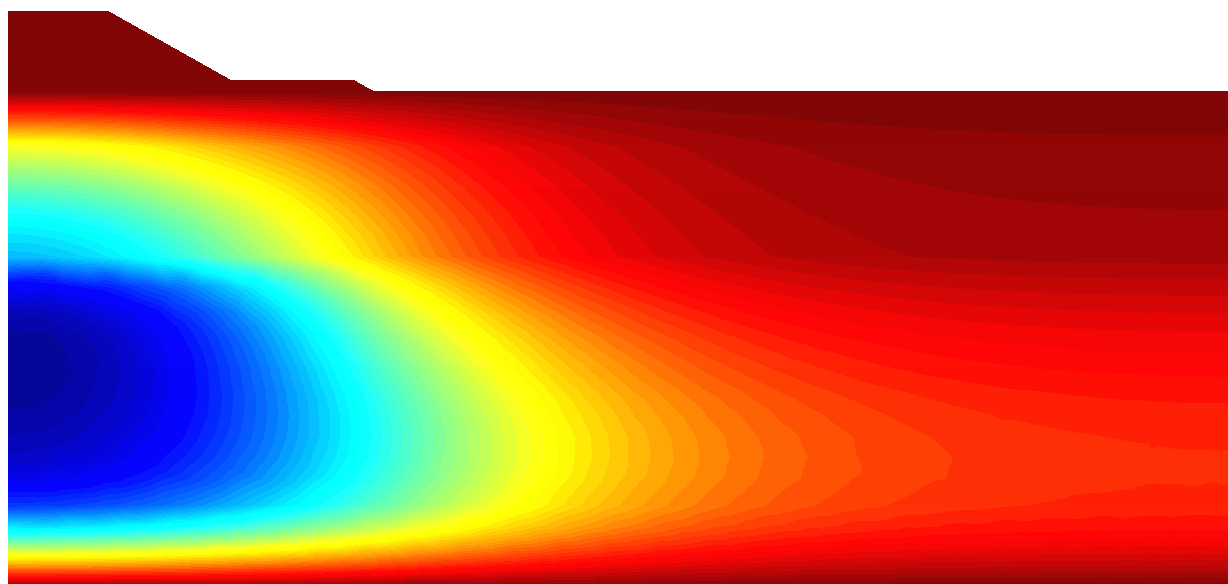




CHALMERS



Y
Z X

Numerical Analysis of Embankments on soft soil

Haarajoki Test Embankment

Master's thesis in Structural Engineering and Building Technology

AMARDEEP AMAVASAI

Department of Civil and Environmental Engineering

Division of Geo Engineering

CHALMERS UNIVERSITY OF TECHNOLOGY

Göteborg, Sweden 2015

Master's thesis 2015:37

MASTER'S THESIS IN STRUCTURAL ENGINEERING AND BUILDING TECHNOLOGY

Numerical Analysis of Embankments on soft soil

Haarajoki Test Embankment

AMARDEEP AMAVASAI

Department of Civil and Environmental Engineering
Division of Geo Engineering
CHALMERS UNIVERSITY OF TECHNOLOGY
Göteborg, Sweden 2015

Numerical Analysis of Embankments on soft soil
Haarajoki Test Embankment
AMARDEEP AMAVASAI

© AMARDEEP AMAVASAI, 2015

Master's thesis 2015:37
ISSN 1652-8557
Department of Civil and Environmental Engineering
Division of Geo Engineering
Chalmers University of Technology
SE-412 96 Göteborg
Sweden
Telephone: +46 (0)31-772 1000

Cover:
Numerical simulation of Haarajoki embankment for pore-pressure distribution after 1500 days

Chalmers Reproservice
Göteborg, Sweden 2015

Numerical Analysis of Embankments on soft soil
Haarajoki Test Embankment
Master's thesis in Structural Engineering and Building Technology
AMARDEEP AMAVASAI
Department of Civil and Environmental Engineering
Division of Geo Engineering
Chalmers University of Technology

ABSTRACT

The purpose of this thesis is to benchmark Creep-Sclay1S model, an advanced constitutive model for soft soil analysis, against a well-documented field observation. The objective include parameter determination for Creep-Sclay1S model in an automated environment using a series of newly developed algorithms in MATLAB. A test embankment constructed at Haarajoki in 1997 by the Finnish National Road Administration is considered in this thesis for the validation of Creep-Sclay1S model due to well documented long term behaviour of soft soil under embankment loading. Half of the area is improved with prefabricated vertical drains. In this thesis, the other half comprising of unimproved ground is considered for the analysis. From geological investigation, the soil deposit in Haarajoki has a high amount of variation due to its history of intermittent saline and fresh water influx. The initial 2m thick desiccated clay layer is heavily overconsolidated. The quality of laboratory tests for most of the soil samples from Haarajoki exhibit poor standard suffering from sampling effects, noisy data and lack of key information. The soil deposits from Haarajoki have been divided into 6 layers based on the index tests provided. Data from incremental loading tests of Haarajoki samples are digitized and stored in separate arrays in MATLAB. The data is then manipulated and necessary parameters are derived by using a set of newly developed algorithms in MATLAB. Experimental simulations using Creep-Sclay1S model show good accordance with laboratory results for oedometer incremental loading tests and triaxial tests. However, simulation for oedometer with Constant Rate of Strain (CRS) shows deviation from its laboratory results. A sensitivity analysis of parameters on CRS simulation shows that preoverburden pressure has the highest influence followed by isotropic parameters and initial stress condition. Since pre-consolidation pressure is highly strain rate dependant, sample disturbance before CRS testing can be a key reason for the observed deviation. Soil behaviour under embankment loading is simulated with the same model parameters used for simulation of element tests. The predictions are in good accordance with field measurements for settlement and pore-pressure distribution. The most influential parameters for embankment simulation includes the permeability, dry crust stiffness and modified creep index. The settlements are exaggerated when creep index values corresponding to in-situ stress condition are used. This value does not have a significant impact on the element test simulations due to short duration of tests and smaller domain. Dry crust has been found to be the most sensitive layer followed by initial soft soil layer (2-4m depth) which is similar to field observations. It is recommended to use a spatial differential stiffness model for dry crust analysis with proper capturing of OCR variation. Sensitivity analysis for permeability, dry crust layer and effects from geometry and line load analysis on the overall simulation are investigated.

Keywords: Embankment, Soft soil, Creep-Sclay1S, parameter determination

CONTENTS

| | |
|---|------------|
| Abstract | i |
| Contents | iii |
| Acknowledgements | iv |
| List of Figures | vi |
| List of Tables | ix |
| List of Notations | x |
| 1 Introduction | 1 |
| 1.1 Background | 1 |
| 1.2 Aim and Objective | 2 |
| 1.3 Thesis structure | 3 |
| 2 Literature review | 4 |
| 2.1 Constitutive model for simulating soft soil behaviour | 4 |
| 3 Geological History | 6 |
| 4 Test Embankment | 9 |
| 4.1 General information | 9 |
| 4.2 Field Observations | 9 |
| 4.3 Embankment | 10 |
| 4.4 Soil Profile | 11 |
| 4.5 Layering | 12 |
| 5 Parameter Determination | 13 |
| 5.1 Initial stress state parameters | 13 |
| 5.2 Isotropic parameters | 14 |
| 5.3 Anisotropic parameters | 18 |
| 5.4 Destructuration parameters | 19 |
| 5.5 Viscous parameters | 20 |
| 6 Simulation of Laboratory results | 22 |
| 6.1 Geometry | 22 |
| 6.2 Loading condition | 22 |
| 6.3 Results | 23 |
| 6.3.1 Oedometer IL test | 23 |
| 6.3.2 Oedometer CRS test | 25 |
| 6.3.3 Triaxial test | 28 |

| | |
|--|-----------|
| 7 Embankment simulation | 29 |
| 7.1 Initial condition | 29 |
| 7.2 Results from simulation | 30 |
| 7.3 Drycrust sensitivity | 36 |
| 7.4 Permeability sensitivity | 37 |
| 7.5 Load type sensitivity | 39 |
| 7.6 Geometry sensitivity | 41 |
| 7.7 Mesh sensitivity | 42 |
| 8 Conclusions & Recommendations | 44 |
| 8.1 Conclusions | 44 |
| 8.2 Recommendations | 45 |
| References | 46 |
| A Instrument installation | 48 |
| A.1 Layout | 48 |
| A.2 Installation procedure | 48 |
| A.3 Instrument position | 49 |
| B Embankment construction schedule | 50 |
| C Layering | 51 |
| D Summary of parameters | 55 |
| E Initial in-situ stress condition | 56 |
| F Other methods of determining pre-consolidation pressure | 57 |
| G Determination of modified intrinsic creep index | 59 |
| H Experimental procedure | 60 |
| H.1 Oedometer test | 60 |
| H.2 Triaxial test | 61 |
| I Parameter sensitivity analysis on CRS simulation | 62 |
| J Flow equation | 63 |
| K Settlement results from embankment simulation | 64 |
| L Pore pressure results from Embankment simulation | 66 |

Acknowledgements

Foremost, I would like to sincerely thank my supervisor, Dr. Jelke Dijkstra, for his guidance, understanding, and most importantly, his patience during my work. His mentorship was paramount who has always been available and encouraged me to grow as an independent thinker.

I would like to thank Prof. Minna Karstunen, the examiner, for providing me this opportunity. Her experience and immense knowledge in numerical analysis has saved me from many critical situations during this thesis. I am extremely grateful as not many graduate students are given the opportunity to develop their own individuality and work with such independence.

I would also like to thank Dr. Jean-Philippe Gras from Chalmers University of Technology and Dr. Nallathamby Sivasithamparam from Norwegian Geotechnical Institute, Norway, for providing guidance with Creep-Sclay1S model before starting this thesis. Additionally, I would like to thank Dr. Mats Karlsson from Chalmers University of Technology for providing guidance on some basic concepts and sharing his expertise.

Finally, I would like to thank my friends and family who, with their constant love and support, provided the necessary motivation and encouragement to overcome several obstacles in my life and moulded me into a person that I am today.

List of Figures

| | | |
|-----|--|----|
| 1.1 | Schematic diagram of Thesis structure | 3 |
| 2.1 | Illustration of constitutive yield surface used in Creep-Sclay1S model | 4 |
| 3.1 | (a.) Map illustrating the extent of Eemian Sea at 130000-115000 BP (Forsström and Eronen 1985) (b.) Map illustrating the retreat of ice sheet towards northern Baltic in different time periods after Weichselian glaciation (Nenonen and Portaankorva 2009) | 6 |
| 3.2 | (a) Map illustrating the extent of Baltic Ice Lake at 12600-10300 BP (Björk 2008) (b) Yoldian Sea at 10300-9300 BP (Björk 2008) | 7 |
| 3.3 | (a) Map illustrating the extent of Ancylus Lake at 9500–8000 BP (Björk 2008) (b) Littorina Sea at 7500-4000 BP (Björk 2008) | 8 |
| 4.1 | Illustration of Haarajoki embankment cross-section (Yildiz et al. 2009) | 10 |
| 4.2 | Typical characteristics of soil deposit from Haarajoki | 11 |
| 4.3 | Illustration of layering of typical samples from Haarajoki deposit based on similar characteristics | 12 |
| 5.1 | Illustration of pre-consolidation stress determination for typical Haarajoki samples . | 13 |
| 5.2 | (a) Distribution of pre-consolidation stress and σ'_v with depth (b) Distribution of overconsolidation ratio with depth | 14 |
| 5.3 | Illustration of determination of compression and swelling index for a typical Haarajoki sample from $e - \log(\sigma'_v)$ plot | 15 |
| 5.4 | Distribution of λ^* , λ_i^* and κ^* along soil depth | 16 |
| 5.5 | Illustration of K and OCR distribution along Oedometer IL stress path for Haarajoki sample from depth 4.13-4.22m (ID = 1648V) | 17 |
| 5.6 | Determination of parameters from $\epsilon_v - \ln(p')$ plot | 17 |
| 5.7 | Illustration of bonding relation between intact and reconstituted clay (Yin, and Karstunen 2011) | 19 |
| 5.8 | (a) Determination of modified creep index from $\epsilon_v - \ln(t)$ plot (b) from $e - \log(t)$ plot | 20 |
| 5.9 | Illustration of Reference time determination for a typical Haarajoki sample | 21 |
| 6.1 | Comparison of Oedometer IL simulation result with laboratory data for typical Haarajoki sample at depths 6.13-6.22m and 4.34-4.37m | 23 |
| 6.2 | (a) Relation between Permeability and Void ratio from Taylor's formula (b) Difference between constant and dynamic permeability analysis for typical Haarajoki sample at depth 15.2-15.23m | 24 |
| 6.3 | Mesh sensitivity analysis in oedometer IL simulation for typical Haarajoki sample . | 25 |
| 6.4 | (a) Comparison with CRS simulation with Laboratory data for a typical Haarajoki sample from a depth of 15.1m (b) 5.1m | 25 |
| 6.5 | (a) Modification of Strain rate to match Lab data for a typical Haarajoki sample at depth 15.1m (b) 5.1m | 26 |
| 6.6 | Comparison of different simulations with hydraulic properties modification for typical Haarajoki sample at depth 5.1m | 26 |
| 6.7 | (a) Modification of pre-consolidation stress to fit CRS lab data for typical Haarajoki sample at depth 15.1m (b) Modification of Initial bonding to fit CRS lab data for typical Haarajoki sample at depth 2.1m | 27 |
| 6.9 | Comparison of triaxial simulation result with laboratory data for typical Haarajoki sample at depths 8.03-8.15m and 12.87-12.97m | 28 |
| 7.1 | Embankment geometry | 29 |

| | | |
|------|---|----|
| 7.2 | In-situ stress equilibrium prior to embankment loading in Tochnog | 30 |
| 7.3 | (a) Comparison of Creep-Sclay1S simulation with field data for settlement along embankment centre line at Haarajoki (b) Difference between original and modified values of μ_i^* on settlement prediction along embankment centre line at Haarajoki . . | 31 |
| 7.4 | (a) Comparison of Creep-Sclay1S simulation with field data for settlement along 4m right of embankment centre line (b) along 9m right of embankment centre line at Haarajoki | 31 |
| 7.5 | Comparison of simulation with field data for pore pressure measurements at different depths in Haarajoki | 32 |
| 7.6 | Simulation result of groundflow pressure distribution after 1500 days generated in Gmsh for Haarajoki soil | 33 |
| 7.7 | Creep-Sclay1S prediction for settlement along embankment centre line at Haarajoki after 1000 years | 33 |
| 7.8 | (a) Comparison of Creep-Sclay1S simulation with field data for lateral displacement along 4m right of embankment centre line after 1 year (b) after 3 years | 34 |
| 7.9 | (a) Comparison of Creep-Sclay1S simulation with field data for lateral displacement along 9m right of embankment centre line after 1 year (b) after 3 years | 34 |
| 7.10 | (a) Settlements along embankment centre line from simulation for different time period (b) Pore pressure distribution along embankment centre line from simulation for different time period | 35 |
| 7.11 | (a) Ground flow pressure after 1500 days from simulation with high stiff dry crust layer (b) Comparison of settlement from simulation of high stiff dry crust layer with field data | 36 |
| 7.12 | (a) Comparison of pore pressure distribution for high stiff dry crust layer analysis with original simulation after 35 days embankment construction (b) after 1500 days | 37 |
| 7.13 | Comparison between analyses with different values of permeability with field data for settlement along embankment centre line | 38 |
| 7.14 | (a) Comparison of simulation with field data for pore pressure dissipation at depth of 4m (b) 15m | 38 |
| 7.15 | (a) Comparison between line load and embankment material analysis with field data for settlement along embankment centre line (b) 9m right of embankment centre line | 39 |
| 7.16 | (a) Comparison of line load with embankment material analysis for lateral deformations at 4m right of embankment centre line (b) 9m right of embankment centre line . . . | 39 |
| 7.17 | (a) Comparison between line load and embankment material analysis for pore pressure distribution after 35 days embankment construction (b) after 365 days | 40 |
| 7.18 | (a) Comparison between line load and embankment material analysis for pore pressure distribution after 1500 days (b) Simulation from line load analysis for ground flow pressure after 1500 days in Haarajoki | 40 |
| 7.19 | (a) Comparison of Creep-Sclay1S simulation of different geometries with field data for settlement along embankment centre line (b) Lateral deformation after 1 year for different geometries at 4m right of embankment centre line | 41 |
| 7.20 | (a) Comparison of pore pressure distribution of different geometries after 35 days embankment construction (b) after 1500 days | 42 |
| 7.21 | (a) Comparison of simulation with 900 and 22000 elements with field data for settlement along embankment CL (b) for lateral displacement at 4m right of embankment CL . | 43 |

| | | |
|------|--|----|
| 7.22 | (a) Comparison of simulation with 900 and 22000 elements for pore pressure behaviour after 35 days embankment construction (b) after 365 days | 43 |
| A.1 | Layout of Haarajoki test embankment with instrument positions (Yildiz et al. 2009) | 48 |
| B.1 | Illustration of schedule for embankment construction at Haarajoki | 50 |
| F.1 | Illustration of Casagrande’s method for determination of pre-consolidation stress (Holtz and Kovacs 1981) | 57 |
| F.2 | Illustration of Schmertmann’s proposal of eventual intersection of virgin compression line between laboratory and in-situ samples at $e = 0.42e_0$ (Knappett and Craig 2014) | 58 |
| F.3 | Principle for evaluation of pre-consolidation stress according to Sällfors (1975) | 58 |
| G.1 | Determination of intrinsic creep value from Grimstad and Degago 2010 | 59 |
| H.1 | Schematic diagram of an Oedometer apparatus (Knappett and Craig 2014) | 60 |
| H.2 | Schematic diagram of a commonly used triaxial apparatus (Knappett and Craig 2014) | 61 |
| K.1 | Settlement with maximum value of 0.149m under embankment centre line after 35 days of embankment construction at Haarajoki | 64 |
| K.2 | Settlement with maximum value of 0.261m under embankment centre line after 365 days at Haarajoki | 64 |
| K.3 | Settlement with maximum value of 0.422m under embankment centre line after 1500 days at Haarajoki | 65 |
| K.4 | Settlement with maximum value of 1.060m under embankment centre line after 1000 years at Haarajoki | 65 |
| L.1 | Groundflow with maximum excess pore pressure upto 58 kPa around 16m depth after 35 days of its construction for Haarajoki soil deposit | 66 |
| L.2 | Groundflow with maximum excess pore pressure upto 42 kPa around 12 - 16m depth after 365 days of embankment loading for Haarajoki soil deposit | 66 |
| L.3 | Groundflow with maximum excess pore pressure upto 32 kPa around 8 - 15m depth after 1500 days of embankment loading for Haarajoki soil deposit | 67 |
| L.4 | Groundflow with no excess pore pressures after 1000 years of embankment loading for Haarajoki soil deposit | 67 |

List of Tables

| | | |
|-----|---|----|
| A.1 | Location of instruments under Haarajoki embankment for unimproved ground | 49 |
| D.1 | Summary of Creep-Sclay1S parameters derived from laboratory tests for Haarajoki samples | 55 |
| E.1 | Initial in-situ stress condition prior to embankment loading in Haarajoki soil profile | 56 |
| I.1 | Sensitivity of Creep-Sclay1S model's parameters on oedometer CRS simulation for Haarajoki samples | 62 |

List of Notations

Abbreviations

| | |
|------------|-----------------------------|
| <i>BP</i> | Before Present |
| <i>CRS</i> | constant rate of strain |
| <i>IL</i> | Incremental Loading |
| <i>OCR</i> | overconsolidation ratio |
| <i>PCP</i> | pre-consolidation pressure |
| <i>POP</i> | preoverburden pressure |
| CL | centre line |
| DMT | Dilatometer test |
| OC | overconsolidated |
| PMT | Borehole pressuremeter test |

Greek Symbols

| | |
|-------------------------|-----------------------------------|
| α | scalar rotation of yield function |
| α_0 | initial value of α |
| α_d | deviatoric rotational vector |
| χ | degree of bonding |
| χ_0 | initial bonding |
| $\dot{\epsilon}_{ij}^c$ | creep strain rate |
| $\dot{\Lambda}$ | visco-plastic multiplier |
| ϵ_d^p | plastic deviatoric strain |
| ϵ_v | volumetric strain |
| ϵ_v^p | plastic volumetric strain |
| ϵ_v^p | plastic volumetric strain |
| η | stress ratio |

| | |
|-----------------|--|
| η_0 | initial stress ratio |
| η_{K_0} | Mobilization with K_0 loading |
| γ | unit weight (kN/m^3) |
| γ_f | unit weight of fluid (kN/m^3) |
| κ | slope of the swelling path |
| κ^* | modified swelling index |
| λ^* | modified compression index |
| λ_i | slope of the intrinsic compression path |
| λ_i^* | modified intrinsic compression index |
| μ^* | modified creep index |
| μ_i^* | modified intrinsic creep index |
| ∇ | Del operator in three dimensional cartesian coordinate system |
| ω | parameter controlling absolute rate of rotation of yield surface |
| ω_d | parameter controlling relative effectiveness of plastic strain |
| ϕ'_{cv} | friction angle at critical state |
| ψ' | dilatancy angle |
| ρ_f | density of fluid (t/m^3) |
| ρ_s | density of solid (t/m^3) |
| σ'_{p0} | preconsolidation pressure of intact sample (kPa) |
| σ'_{pi0} | preconsolidation pressure of reconstituted sample (kPa) |
| σ'_h | effective horizontal stress (kPa) |
| σ'_v | effective vertical stress (kPa) |
| τ | reference time (days) |
| θ | value of lode angle |
| ξ | parameter controlling absolute rate of destructuration |
| ξ_d | parameter controlling relative effectiveness of destructuration rate |

Roman Symbols

| | |
|------------|---|
| A | cross-sectional area (m^2) |
| c | cohesion (kPa) |
| C_α | secondary compression index |
| C_c | compression index |
| c_k | constant of proportionality used in Taylor's relation |
| C_s | swelling index |
| c_v | vertical coefficient of consolidation ($m^2/year$) |
| e | void ratio |
| e_0 | Initial void ratio |
| g | gravity (m/s^2) |
| G_s | specific gravity |
| H | Total head (m) |
| h_v | velocity head (m) |
| k | Hydraulic conductivity (m/s) |
| K_0 | Coefficient of lateral earth pressure at rest |
| K_0^{NC} | Coefficient of lateral earth pressure at rest in normally consolidated region |
| M | slope of critical state line |
| m | ratio of critical state slope in extension to compression |
| M_c | slope of critical state line in Triaxial compression |
| M_e | slope of critical state line in extension |
| p' | mean effective stress (kPa) |
| p'_{eq} | size of current stress surface in p'-q plane (kPa) |
| p'_{eq} | size of current stress surface in p'-q plane (kPa) |
| p'_{mi} | size of intrinsic yield curve in p'-q plane (kPa) |
| p'_p | size of normal consolidation surface in p'-q plane (kPa) |

| | |
|-------------|---|
| Q | volumetric flow of fluid (m^3/s) |
| q | mean deviatoric stress (kPa) |
| q_v | discharge velocity(m/s) |
| R_{ref} | time resistance value at reference time |
| $r_{s,min}$ | time resistance number for undisturbed sample |
| r_{si} | time resistance number for reconstituted sample |
| r_s | time resistance number |
| S_t | sensitivity factor |
| t | time (days) |
| u | pore pressure (kPa) |
| v | specific volume |
| z | elevation head (m) |
| R | time resistance |

1 Introduction

1.1 Background

The Industrial revolution in the mid-nineteenth century has led to a sharp rise in social and economic development creating new opportunities and progressive scientific advancement in a short period of time. As a consequence, demand for infrastructure in small scale construction such as roads, railways, dwellings etc. and large scale construction such as harbours, dams and airports has increased tremendously, creating densely populated coastal regions covered with silt and clayey deposits. This situation has forced construction to move into marshy terrains and sites with highly compressible soft soils due to eventual scarcity of good quality sites.

Soft soil is a highly anisotropic material due to its depositional history. During deposition, the orientation of clay particles determine the characteristic of the soil along with conditions such as pore water properties and changes in loading history. Clay is composed of irregularly arranged particles bonded together to form an anisotropic fabric. Upon loading, the particle contacts are gradually destroyed due to plastic strain increment and this process of bond degradation is known as destructuration (Rouainia and Muir Wood 2000). Additionally, soft soils exhibit viscous behaviour leading to long term deformations.

Due to insufficient data, attempts to fully understand this complex behaviour in engineering applications has been difficult and pose a serious challenge for Geotechnical engineers around the globe. Several innovative ideas has been proposed by researchers for modelling soft soil but due to its extreme variation in nature and complex behaviour coupled with insufficient data has proven difficult for a complete validation. Hence several methods were resorted to gain insight in soil's behaviour to observe patterns and formulate models. Among them, construction of trial embankments on soft soil deposits has been used more commonly around the world due to its simple execution. With advancement in instrumentation, measuring devices such as piezometers, inclinometers etc. have been used to accumulate more detailed information and gain a better understanding about the real nature of soft soil's behaviour. Even with the available data, conventional calculation methods did not prove to be accurate, forcing engineers and researchers to resort to numerical analysis. The advent of Finite element method paved the way for advanced computations and take into account the non-linear nature of soft soils. The incorporation of simplified continuum models to analyse complex reality is more commonly used in soft soil analysis. Recently developed advanced constitutive models such as Creep-Sclay1S provide more accurate predictions than conventional calculations as they take into account anisotropy, bond degradation and viscous behaviour of soft soil.

A trial embankment with data comprising of long term field observation is required for a comprehensive validation of Creep-Sclay1S model. In order to choose a benchmark case, the quality of available test data and site investigation for different trial embankments are surveyed. The Test embankment constructed at Haarajoki, Finland in 1997 by the Finnish National Road Administration is chosen as the benchmark case for validating Creep-Sclay1S model in this thesis due to availability of long term data. Several finite element studies have been published in recent years for the Haarajoki embankment (Cundy and Neher 2003; Stapelfeldt et al. 2009;

Yildiz et al. 2009). The analysis from Näätänen et al. 1998 uses an isotropic elasto-plastic model with small strain analysis and does not consider many of the key features in soft soil property. Cundy and Neher 2003 uses the multi-laminate constitutive model accounting for anisotropy by directional distribution of state variables responsible for bonding but does not consider viscous properties in soft soil. Stapelfeldt et al. 2009 uses an elasto visco-plastic model, EVP-SCLAY1S, based on overstress theory (Perzyna 1963 and Perzyna 1966) which accounts for anisotropy, destructuration and soil viscosity. Although most of the previous studies account for anisotropy and destructuration, not many deal with viscous behaviour of soft soil for Haarajoki embankment. Also, the parameters used in the analysis has not been discussed in detail in any of the published results, hence querying the reliability of the analysis itself. In this thesis, emphasis is given to consistent parameter determination for Creep-Sclay1S model from existing laboratory results. The sensitivity of parameters on experimental simulation and embankment analysis is investigated. Also, other factors such as boundary effects, permeability and numerical issues affecting the results are investigated in detail.

1.2 Aim and Objective

The aim of this thesis is to benchmark Creep-Sclay1S model, an advanced constitutive model for soft soil analysis, against a well documented field observation. The objectives of this thesis include

- Interpretation of data from laboratory experiments and site investigation.
- Determination of parameters for Creep-Sclay1S model in an automated environment using a series of newly developed algorithms in MATLAB.
- Simulation of oedometer and triaxial experiments in Tochnog using Creep-Sclay1S model and comparison with available laboratory results.
- Boundary value level comparison of model vs. site.

1.3 Thesis structure

Initial part of the work includes literature review to gain knowledge about the fundamentals of soft soil behaviour, constitutive modelling and surveying previous publications. Evaluation of laboratory data includes digitisation of results from oedometer and triaxial experiments, inclinometer and piezometer measurements, soil profile etc. The digitised data is imported into MATLAB software for manipulation and interpretation. Parameters necessary for Creep-Sclay1S model are determined from imported data in MATLAB using customized and default algorithms. The algorithm is encoded to process large sets of data in a fully automated environment and time efficient manner with focus on accuracy. Using these parameters, oedometer and triaxial tests are simulated with Creep-Sclay1S model in Tochnog, a finite element analysis tool and validated with existing laboratory results. After finalisation of parameters, the embankment with soil profile is simulated with the model in Tochnog. The final settlement from the simulation is compared with field measurements and the prediction is validated.

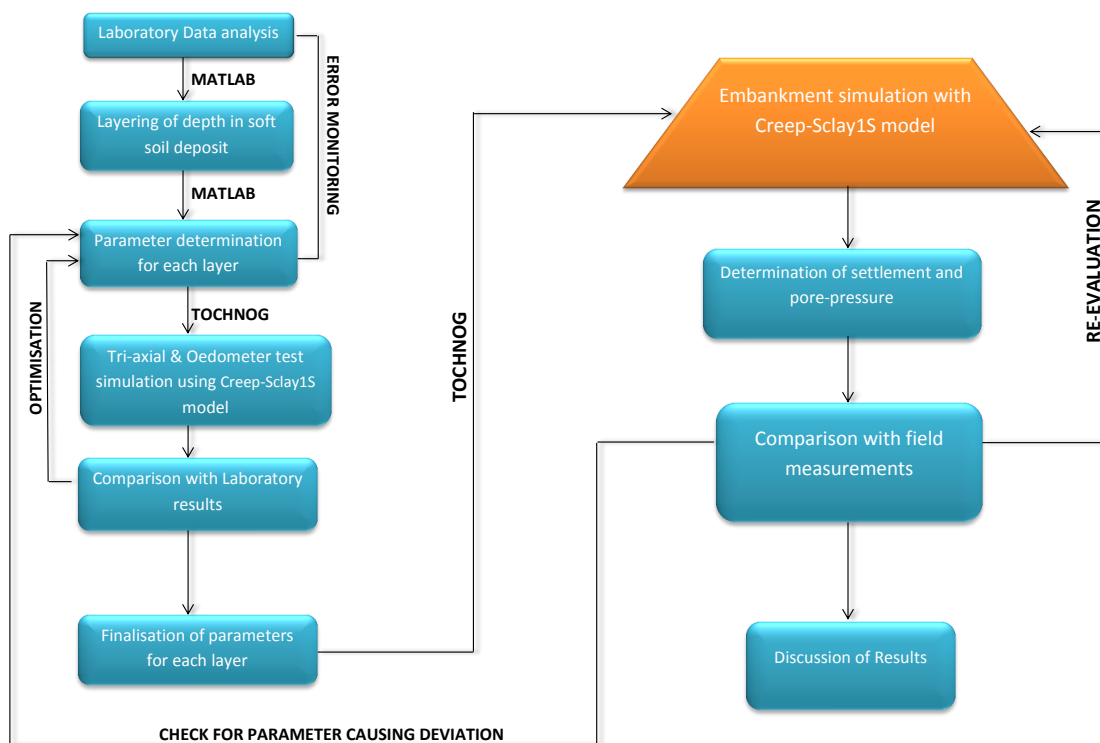


Figure 1.1: Schematic diagram of Thesis structure

2 Literature review

2.1 Constitutive model for simulating soft soil behaviour

Soft soils are highly anisotropic material due to depositional history. During deposition, the orientation of clay particles can influence the anisotropic characteristics resulting in time dependant behaviour. Hence advanced constitutive models with incorporation of anisotropy, bonding and rate dependency are required to better represent soft soil behaviour. The recently developed Creep-Sclay1S model (Sivasithamparam 2012) is based on Anisotropic creep model (Leoni et al. 2008) and SCLAY1S model (Karstunen et al. 2005). The model uses a constitutive yield surface as shown in Figure 2.1.

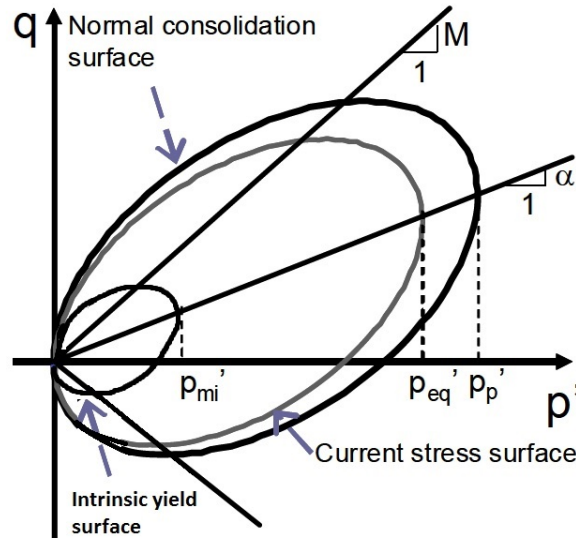


Figure 2.1: Illustration of constitutive yield surface used in Creep-Sclay1S model

The yield criterion comprises of an intrinsic surface represented by p'_{mi} , a current stress state surface an outer rotated ellipse denoting the normal consolidation surface in the p' - q plane and its evolution with respect to volumetric strains are described according to hardening law from equation 2.1.

$$\Delta p'_p = \frac{p'_p}{\lambda_i^* - \kappa^*} \Delta \epsilon_v^p \quad (2.1)$$

where p'_p is the size of the normal consolidation surface. λ_i^* and κ^* denotes the modified compression index and modified swelling index respectively. The size of the current stress surface is represented by p'_{eq} which can be derived from equation 2.2.

$$p'_{eq} = \frac{p'^2 + (q - \alpha p')^2}{(M^2 - \alpha^2) p'} \quad (2.2)$$

The model uses the concept of visco-plastic multiplier presented by Grimstad et al. 2008 for capturing creep behaviour in soft soil. The viscoplastic multiplier is given by equation 2.3.

$$\dot{\Lambda} = \frac{\mu_i^*}{\tau} \cdot \left(\frac{p^{eq}}{(1 + \chi) \cdot p'_{mi}} \right)^{\frac{\lambda_i^* - \kappa^*}{\mu_i^*}} \cdot \frac{M_c^2 - \alpha_0^2}{M_c^2 - \eta_0^2} \quad (2.3)$$

where M_c denotes the critical state slope in Triaxial compression, μ_i^* is the intrinsic creep index which can be derived from standard laboratory test, α_0 refers to the initial inclination of the yield surface and η_0 refers to the initial stress ratio. With incorporation of the visco-plastic multiplier, the analysis can go above the Critical state line (into dry side) similar to the MCC model. However, this in most cases can result in higher values of undrained shear strength for OC soils. Due to assumption of an associated flow rule, the creep strain rate and plastic strain increment are represented by the viscoplastic multiplier from equation 2.4.

$$\dot{\epsilon}_{ij}^c = \dot{\Lambda} \frac{\partial p'_{eq}}{\partial \sigma'_{ij}} \quad \Delta \epsilon_{ij}^c = \Delta t \dot{\Lambda} \frac{\partial p'_{eq}}{\partial \sigma'_{ij}} \quad (2.4)$$

The model uses three hardening laws which are similar to the S-CLAY1S model except that the plastic strains were replaced with creep strains. The first hardening law describes the evolution of the size of intrinsic yield surface p'_{mi} from equation 2.5.

$$dp'_{mi} = \frac{vp'_{mi}}{\lambda_i - \kappa} d\epsilon_v^p \quad (2.5)$$

If the destructuration parameter χ is neglected, the first hardening law reduces to Modified Cam Clay analysis (equation 2.1). The second hardening law describes the change in orientation of the yield surface which can also be called as the rotational hardening law proposed by Wheeler et al. 2003 is given in equation 2.6.

$$d\alpha_d = \omega \left(\left[\frac{3\eta}{4} - \alpha_d \right] \langle d\epsilon_v^p \rangle + \omega_d \left[\frac{\eta}{3} - \alpha_d \right] d\epsilon_d^p \right) \quad (2.6)$$

where η is the stress ratio, ω and ω_d are model constants. ω controls the absolute rate of rotation of the yield surface whereas ω_d controls the relative effectiveness of plastic strains. The third hardening law describes the degradation of inter-particle bonding with plastic straining. Here a bonding parameter χ is introduced which gets reduced to a target value of zero with increase in plastic strains. The evolution of the bonding parameter χ is given in equation 2.7.

$$d\chi = \xi ([0 - \chi] |d\epsilon_v^p| + \xi_d [0 - \chi] d\epsilon_d^p) = -\xi\chi (|d\epsilon_v^p| + \xi_d d\epsilon_d^p) \quad (2.7)$$

From equation 2.7, the bonding parameter χ depends on two additional soil properties ξ and ξ_d . ξ controls the absolute rate of destructuration whereas ξ_d controls the relative effectiveness of plastic strains during bond degradation. The critical state (M) in Creep-Sclay1S model is incorporated as a function of Lode angle. This gives a smooth yield surface comparable to the Drucker-Pragar failure criterion. The formulation of lode angle dependency in Creep-Sclay1S model is given by equation 2.8.

$$M(\theta) = M_c \left(\frac{2m^4}{1 + m^4 + (1 - m^4) \sin 3\theta_\alpha} \right)^{\frac{1}{4}} \quad (2.8)$$

where m is the ratio of critical state slope in extension to the critical state in compression.

3 Geological History

In order to understand the variation in soil property, it becomes necessary to survey the geological history of the region to avoid misinterpretation. The geography for southern Finland slightly differs from other Scandinavian regions, bordering several water bodies such as Baltic Sea, Gulf of Finland and Gulf of Bothnia. Hence, periods of glaciation and melting has predominantly influenced the region's geological characteristics. The late Pleistocene epoch lasting from 130,000 to 12,000 BP (Before Present) experienced several glacial events with constant variation in temperature and climate patterns (Clayton et al. 1991). During the initial stages of this period, Scandinavia region was completely surrounded by the Eemian Sea with southern Finland completely inundated by this saline inflow (Forsström and Eronen 1985). The location of the Eemian Sea is approximately close to the present day Baltic Sea. This is known as the Eemian stage (Marine Isotope Stage 5e) that existed roughly around 130,000 to 115,000 BP (NEEM 2013) during the interglacial period when temperatures were 4–10°C warmer than present. From Figure 3.1 (a), it is evident that southern Finland including Haarakajoki was completely inundated by saline water during this period.

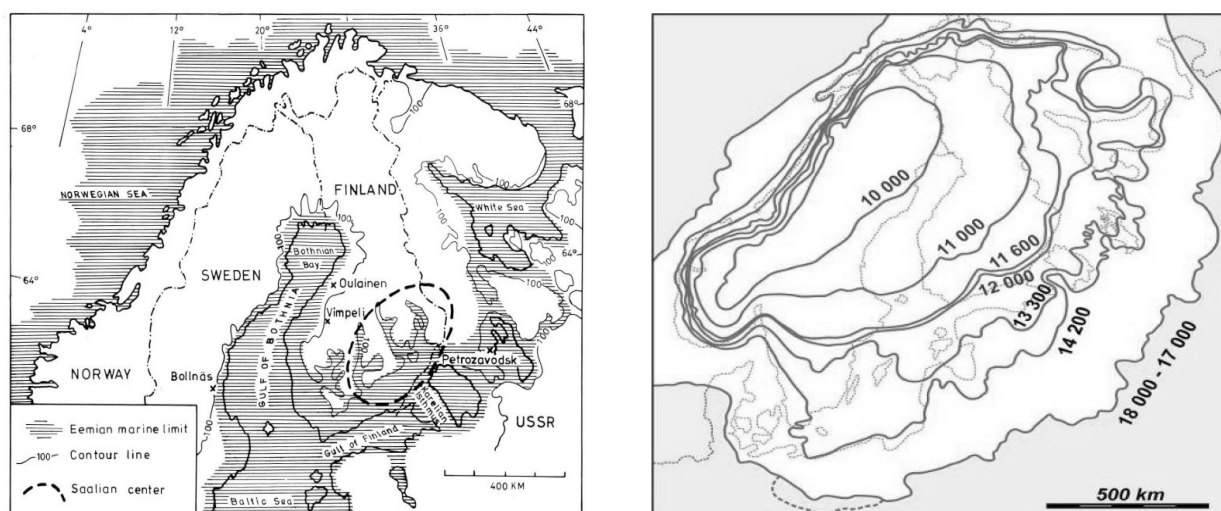


Figure 3.1: (a.) Map illustrating the extent of Eemian Sea at 130000-115000 BP (Forsström and Eronen 1985) (b.) Map illustrating the retreat of ice sheet towards northern Baltic in different time periods after Weichselian glaciation (Nenonen and Portaankorva 2009)

The Weichselian glaciation started with the prelude of gradual cooling and intermittent interstadial periods where ice sheets overwhelmed the whole Scandinavian region. The ice sheets reached its maximum around 20,000 BP reaching 3 kilometers thick after which glaciers started to melt and reached southern Finland around 13,100 BP. The quaternary deposits found in this region were deposited by the late Weichselian glaciation (Nenonen and Portaankorva 2009). The retreat of the Weichselian glaciers marked the formation of Baltic Ice Lake in front of the receding ice sheet. As the ice sheet retreated north, glacio-lacustrine sediments such as clay and silt were deposited in the Baltic. The growing fresh water Baltic Ice Lake from melt-waters was isolated from the saline Atlantic ocean by the Danish straits land bridge along with ice barriers extending across Mount Billingen in south-central Sweden blocking the saline water entry from the western North sea and northern Arctic sea towards Finland (Wefer

et al. 2002). Due to isostatic rebound of land, the elevation of Öresund strait was uplifted and dammed the ice lake to increasingly higher levels from 7m below current sea level to +28m. The sediments contained low organic carbon and varved feature of clay became thinner and blended into homogenous clay in distal areas (Wefer et al. 2002).

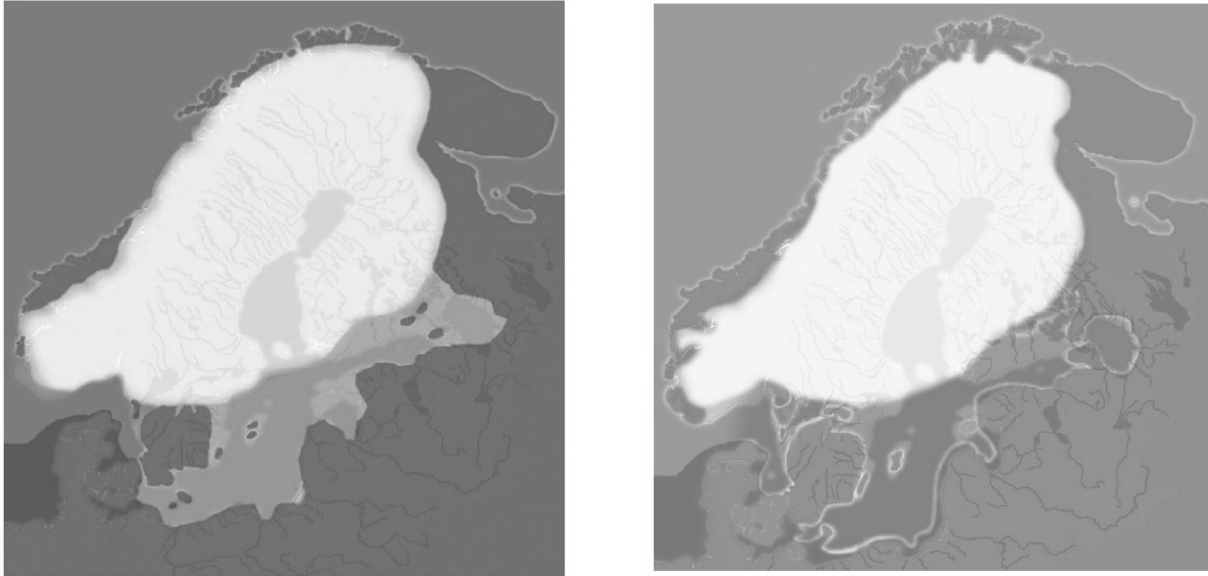


Figure 3.2: (a) Map illustrating the extent of Baltic Ice Lake at 12600-10300 BP (Björk 2008) (b) Yoldian Sea at 10300-9300 BP (Björk 2008)

With further melting and retreat of ice sheet from south-central Sweden, the water level in the dammed Baltic Ice Lake started to reduce, giving away 25m of water around 10,300 BP and established a connection to marine water. This event is marked by a color change in clays and change in sediment density. During this period, the elevation of sills in Danish straits were 20m above current sea level and saline water inflow predominantly occurred from south-central Sweden (Figure 3.2 (b)). This period marked the transition from fresh water Baltic Ice Lake to saline Yoldian Sea stage (Wefer et al. 2002).

The Yoldian Sea stage (10,300 – 9300 BP) is the period between the final drainage of Baltic Ice Lake until a new barrier impeded the saline water inflow into Baltic Sea. The varved feature of clay sediments in the Gotland Basin remained for atleast for another 300 years followed by an increase in iron-sulphide minerals giving rise to high magnetic susceptibility. There is a sharp increase in organic carbon content during this interval.

The continuous uplift of south-central Sweden restricted the flow of marine waters and with an elevated basin level marked the end of the Yoldian Sea stage and gave rise to the fresh water Ancylus Lake with maximum water elevation of 7m below the current sea level. The Ancylus Lake stage existed between 9300 BP and 8700 BP and created fjords with inundation in large areas. The organic content during this stage was low due to retreating saline conditions. The further north, the more glacially influenced the sediment deposits existed. Since land uplift subsided during this period, the relative sea level increased significantly and flooded the marine coasts of western Baltic around 9000 BP. This marked the beginning of a gradual end for the Ancylus Lake stage after the flooding of the Öresund strait by the marine ocean from west.

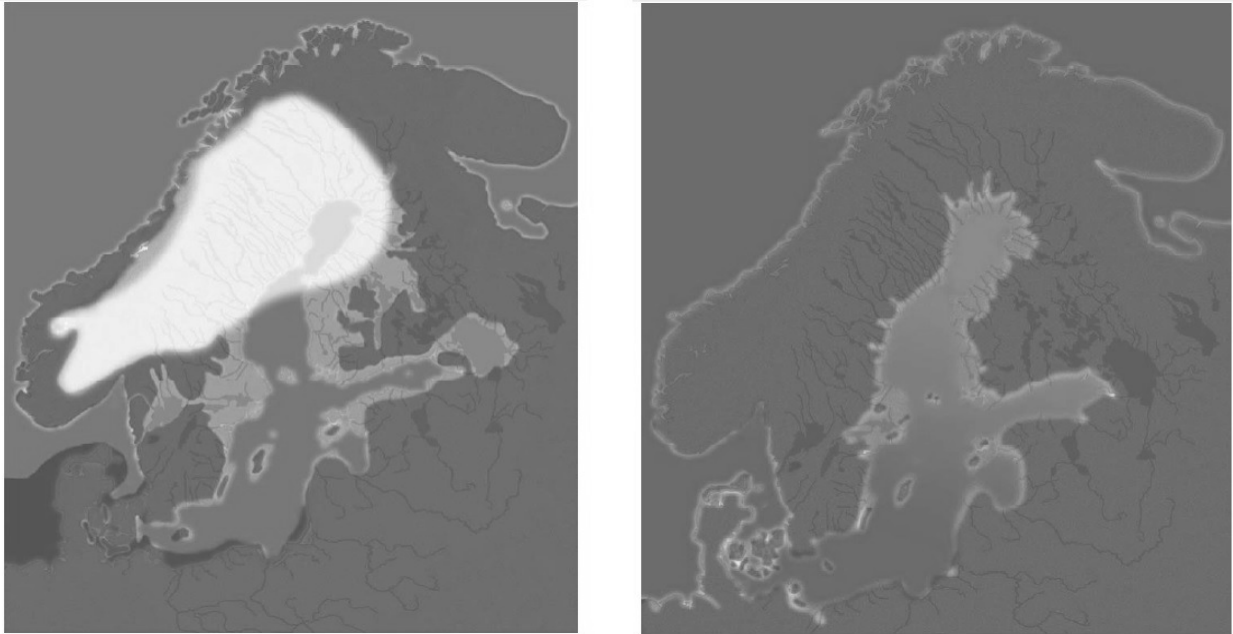


Figure 3.3: (a) Map illustrating the extent of Ancyclus Lake at 9500–8000 BP (Björk 2008) (b) Littorina Sea at 7500–4000 BP (Björk 2008)

The transition from fresh water Ancyclus Lake stage to brackish Littorina Stage (initial stages of this period is referred as the Mastogloia Sea Stage) was gradual. The gradual increase in water level had inundated many of the coastal regions including Haarajoki in the Baltic around 7000 BP (Wefer et al. 2002). During this transition, the bottom waters became dense and increasingly salty due to gradual intrusion of marine water. The nutrients from the saline bottom rose to the surface and supported biological productivity. At the end of the transgression, the transition from the Atlantic to the Sub-boreal Chrono zone created a drastic climate change with a period of cooling lasting for 500 years. Due to cooler conditions, there is abrupt drop in salinity with decrease in organic carbon and biological production, decreasing tendency for anoxia production and increasing abundance of species indicative of cold conditions which lasted from 5000 to 3700 BP.

The transition from Littorina to post-Littorina environment around 3700 BP (Wefer et al. 2002) is a period with fluctuating rainfall conditions. The sediments are much lighter in color indicating lack of salinity due to continuous leaching from rainfall. Climate fluctuations from 2000 BP have been less than 2°C. Land continued to rise and regions around Gulf of Bothnia and Gulf of Finland rose out of sea. Sediments in the Gotland basin are homogeneous due to well oxygenated environment from cooler conditions during 400 – 300 BP. The spread of agriculture around the Baltic Sea region caused changes in vegetation, pollen patterns, increase in land erosion and sedimentation rates of Lakes. This could have affected the over-consolidation ratio for soft soil deposits at top layer which is attributed predominantly by human activity.

4 Test Embankment

4.1 General information

The test embankment at Haarakajoki, situated in the vicinity of Järvenpää, Finland is constructed between July and August, 1997 by the Finnish National Road Administration (Vepsäläinen et al. 1997) to organize a competition with tasks involving evaluation of settlements, horizontal displacements and pore pressure. The 2.9m high embankment is constructed as a noise barrier and is founded on soft soil deposits. The deposits in this area are characterized by a high degree of anisotropy and natural inter-particle bonding (Yildiz et al. 2009) which influences its stress-strain behaviour. Half of the embankment is constructed on virgin soil with no ground improvement whereas the other half on ground improved area with prefabricated vertical drains installed in a regular pattern with 1m intervals in a square grid. The prefabricated drains are 100mm wide and 3-4mm thick (Vepsäläinen et al. 1997). Experiments such as oedometer tests (both Incremental Loading (IL) and Constant Rate of Strain (CRS)) and triaxial tests has been conducted by Road Administration Consulting Laboratory along with Laboratory of Soil mechanics and Foundation Engineering at Helsinki University of Technology, Finland. Since clay is highly anisotropic, there is large variation with respect to depth which is also evident from laboratory results from oedometer IL tests. Hence depths exhibiting similar stress-strain behaviour and initial conditions are grouped in a single layer and this process of layering samples with respect to depth would be discussed later in this Chapter. The lab results combined with field monitoring data from FinnRA is used for the validation of Creep-Sclay1S and the extent of accuracy depends on the quality of data provided. Several results has already been published regarding Haarakajoki test embankment analyses with different constitutive models as mentioned in Chapter 2, however no comparison shall be made with previous analysis since the main objective of this thesis limits to accurate derivation of parameters and validation of model therewith.

4.2 Field Observations

It has been observed that even on ground improved areas, primary consolidation continues significantly after three years of embankment construction (Vepsäläinen et al. 1997). The strain effects is found to be minor below a depth of 10 meters. The effects of three year consolidation period is clearly observed on layers closer to the embankment. The increase of undrained shear strength and pre-consolidation pressure are small for subsoil that was slightly overconsolidated before embankment construction. Hence it is clear from field observations that the most critical region should exist around 2 – 4m for soft soil layer combined with dry crust behaviour. The 2m thick dry crust layer can distort the prediction accuracy since even advanced models are unable to capture the stress strain behaviour for dry crust soils due to difficulty in its parameter derivation.

4.3 Embankment

An illustration of the Haarajoki embankment cross-section is shown in Figure 4.1. The embankment is 2.9 m high and 100 m long. The crest of the embankment is 8 m wide with slopes constructed at a gradient of 1:2. The phreatic level is at the ground surface. The embankment material varies from sandy gravel to gravel with a moisture content of 2.5 % and maximum dry density of 2.20 g/cm^3 . Size distribution includes 18 % of 32 to 64 mm fraction and 20 % for more than 64 mm. The density of the embankment material is 21 kN/m^3 . Class-3 geotextile has been spread on the levelled ground over the entire embankment. The embankment is underlain by heavily overconsolidated crusted clay layer. The dry crust layer is 2 m thick and is followed by 20.2 m thick soft clay deposit as shown in Figure 4.1. Deposits that are more permeable than clay such as silt and till can be found beneath the soft clay layer.

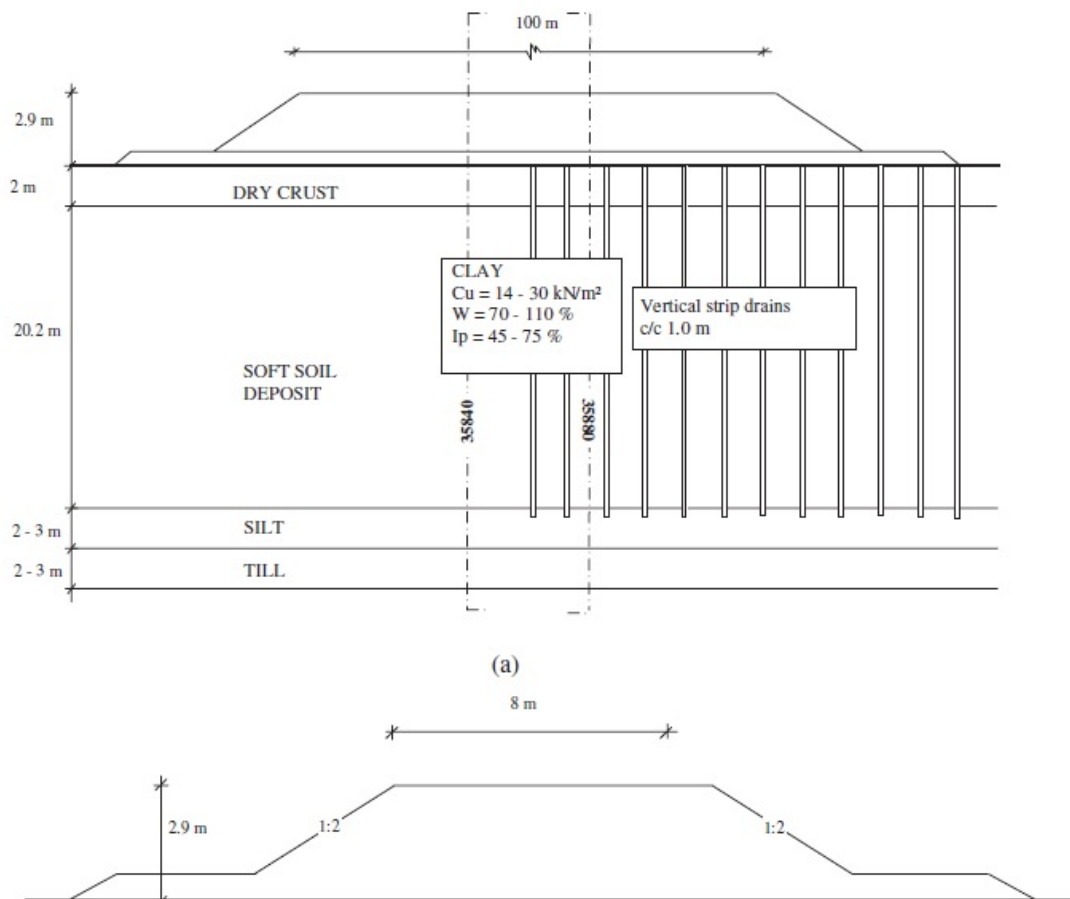


Figure 4.1: Illustration of Haarajoki embankment cross-section (Yildiz et al. 2009)

The embankment is constructed on an average of 0.5m high on every two days. The schedule for embankment construction is illustrated in Appendix B. The material is transported in such a way that the compaction effect is uniform over the entire area. Compaction is done to 90% relative density using a 6 tonne roller with regular intervals of moistening. Stones over 300mm are removed from the embankment.

4.4 Soil Profile

The water content for soft clay varies between 70 – 120 % with maximum water content in the shallow layer of soft soil and decreases with depth. The water content for soft soil is equal to or, in most cases, greater than their liquid limit. Soft soil around 3m depth exhibit the highest plasticity index and tends to decrease with depth. The dry crust layer, however, exhibits a much lower range of water content ranging between 35 – 55 %. The loss of water can be due to dessication from high temperature variation. This leads to crack propagation and high permeability properties in the first initial layers. From dessication, there is swelling in soil leading to reduction in void ratio and subsequent increase in its unit weight as shown in Figure 4.2. The unit weight for dry crust layer varies between 16.86 – 17.68 kN/m^3 whereas for soft soil, the unit weight varies between 13.72 - 16.21 kN/m^3 increasing with depth. The organic content varies between 1.2 % - 2.2 %. The sensitivity of the soil varies between 20 – 65 depending on the depth.

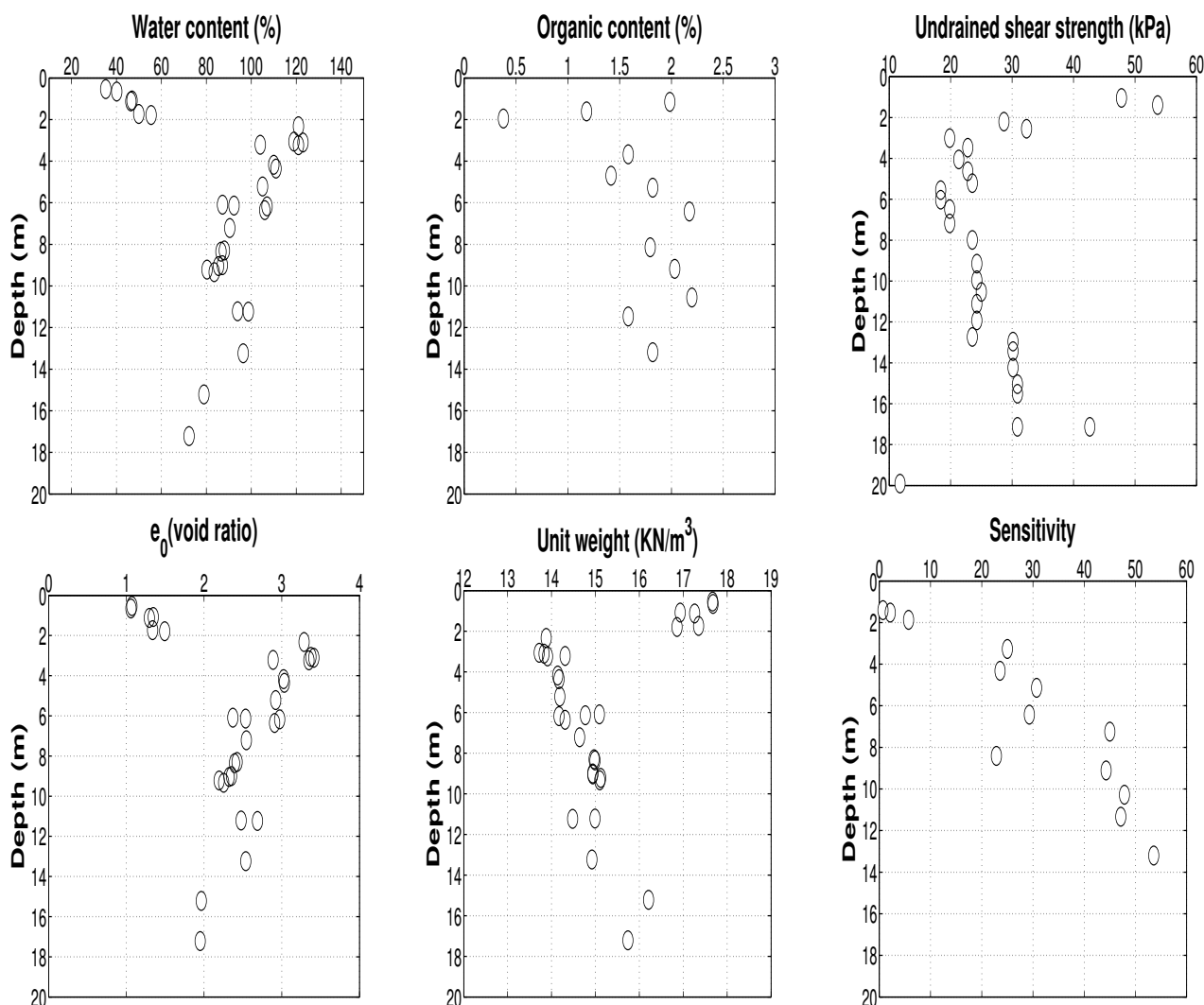


Figure 4.2: Typical characteristics of soil deposit from Haarajoki

4.5 Layering

From soil profile, there is evidence of high variation between samples from different depth and necessary measures should be taken to avoid error in the validation procedure. Hence it is necessary to divide the soil profile into layers of similar characteristics in order to perform a reliable validation. In order to test the efficiency of the model, it is necessary to investigate the soil with comparatively low number of layers. However, the number of layers should not be too less since high variation may affect the accuracy of the final result. This procedure is important for validating Creep-Sclay1S model and a comprehensive analysis should be undertaken.

In CRS tests for Haarajoki samples, two different strain rates (0.0015 mm/min and 0.0025 mm/min) are used which can be helpful to validate different parameters. However test results for samples with 0.0025mm/min beyond 10m are either missing or not done. Also, a constant strain rate cannot be representative of site condition since embankment is constructed in stages (refer Appendix B). In triaxial test data, the critical slope for compression (M_c) can be a key aspect to consider in layering of samples.

Data for oedometer tests with incremental loading for 30 samples from different depths are available with details of initial condition and stress-strain behaviour. This data is imported into MATLAB script and saved in separate arrays. These data are then processed to plot $\log(\sigma'_v) - e$ curve for all samples. Samples with similar in-situ void ratio (e_0) and stress-strain behaviour are compiled as a single layer. Other aspects such as unit weight and undrained shear strength are also considered and corrected accordingly. The initial layer comprising of dry crusted clay is treated as a separate layer with thickness 0 - 2m. Typical compiled layers 3 and 6 of soft soil deposit are shown in Figure 4.3. A complete summary of layers is reported in Appendix C.

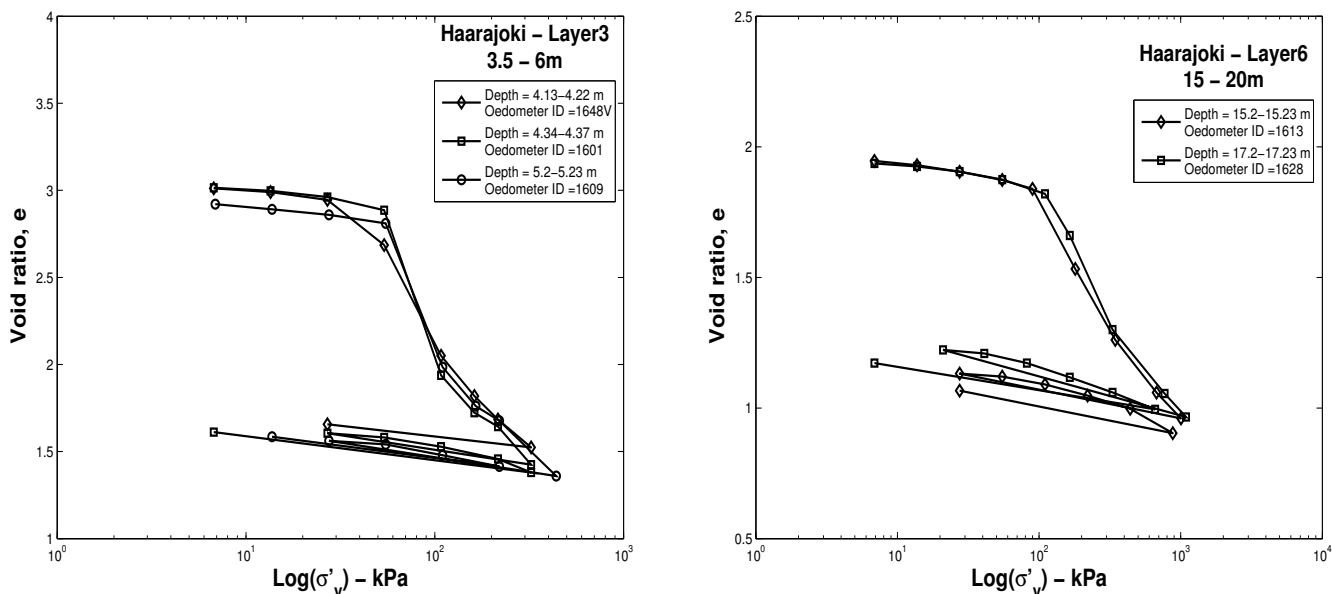


Figure 4.3: Illustration of layering of typical samples from Haarajoki deposit based on similar characteristics

5 Parameter Determination

5.1 Initial stress state parameters

Pre-consolidation pressure represents the maximum effective stress which a soil has undergone from its origin of deposit. It defines the yielding point of a soil when the stress path transits from elastic to elastic plastic region. Hence, an accurate determination of pre-consolidation stress is of major importance as its high influence on experimental simulation would be mentioned later. Several methods have been proposed to determine an accurate value for pre-consolidation pressure (refer Appendix F). Oedometer tests with Constant Rate of Strain (CRS) for Haarajoki samples does not hold sufficient information for most of the depths as mentioned in section 4.5. Hence one dimensional Oedometer Incremental Loading (IL) tests are taken due to their better consistency of data for all depth.

Data from oedometer IL tests are digitized and stored in separate arrays in MATLAB. The change in void ratio are plotted against σ'_v in log scale for all samples. A linear tangent is plotted on the swelling region (Figure 5.1). The points on the normally consolidated region are interpolated with cubic spline to obtain a smooth curve and extrapolated to intersect on the linear tangent from overconsolidated region. This intersection point is presumed as the pre-consolidation stress (PCP). The advantage of using this method is the convenience for the user to automate this process for large data sets in a simple and time efficient manner. The values derived from this method have a margin of error that is well within the range described by Casagrande (Appendix F). The sensitivity of this error margin and its influence on simulation results shall be investigated.

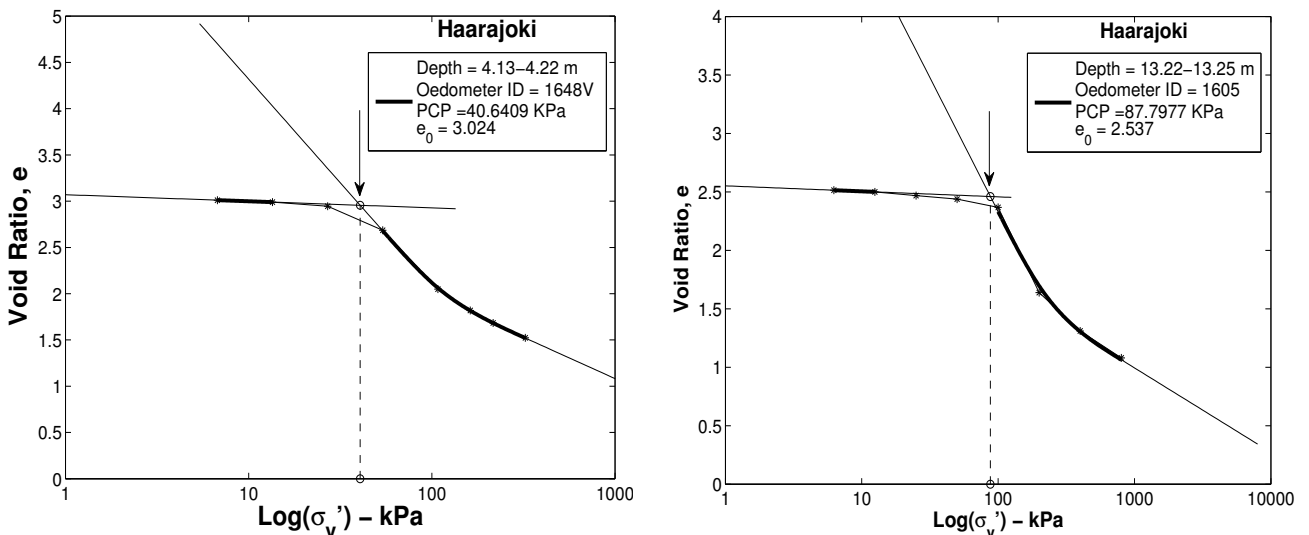


Figure 5.1: Illustration of pre-consolidation stress determination for typical Haarajoki samples

The PCP is determined for all samples and compared with the effective stress in each layer (Figure 5.2 (a)). It is clearly evident that there is sample disturbance in all layers with large variation in the fourth layer (6 - 10m). Hence this shows that the quality of laboratory

experiments undertaken for Haarajoki samples are poor and requires several approximations for curve fitting. The distribution of pre-consolidation stress with depth merges with the effective stress path around 15m which is similar to presented previous papers (Yildiz et al. 2009).

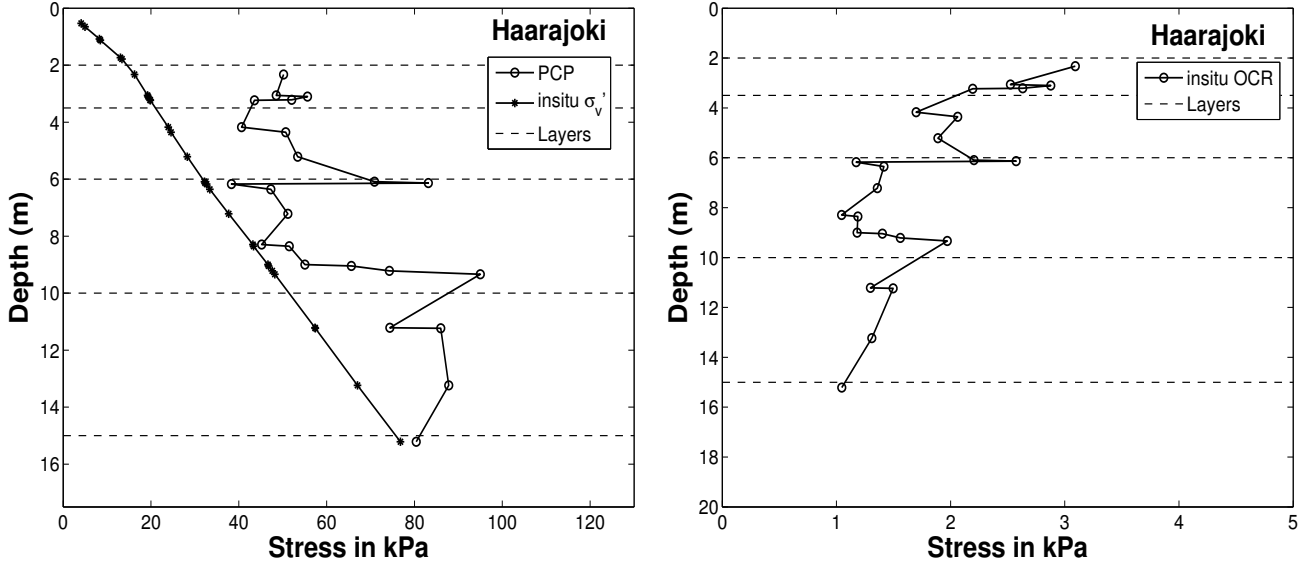


Figure 5.2: (a) Distribution of pre-consolidation stress and σ'_v with depth (b) Distribution of overconsolidation ratio with depth

The overconsolidation ratio (OCR) is defined as the ratio of pre-consolidation stress to current effective vertical stress of the soil (Muir Wood 2010). It can be formed due to several factors such as erosion of top layer in a certain period of soil's history. When the current stress state of a soil is below pre-consolidation pressure, lower settlement values are predicted due to high elastic moduli in overconsolidated region. OCR and POP (preoverburden pressure) provides information about the intensity of swelling in soil which is significant for excavation problems. Heavily overconsolidated clays exhibit plastic softening whereas normally consolidated and slightly overconsolidated clays exhibit plastic hardening (Muir Wood 1991). However this is hard to interpret from the Haarajoki samples due to poor quality of triaxial test results.

The initial void ratio (e_0) defines the ratio of volume of voids to volume of solid particles in the sample. The information about the distribution of initial void ratio with depth is shown in Figure 4.2. Other parameters such as solid density (ρ_s in t/m^3), specific gravity (G_s) and Unit weight (γ in kN/m^3) are taken from laboratory data.

5.2 Isotropic parameters

Data from one dimensional incremental loading tests with unload-reload cycles have been used to determine the isotropic parameters. In $e - \log(\sigma'_v)$ plot, the slope for normal consolidation line is measured as the compression index (C_c) and the slope of the unload-reload hysteresis loop is measured as the swelling index (C_s) as shown in equation 5.1.

Derivation of parameters from $e - \log(\sigma'_v)$ plot is straight forward, similar to procedure

mentioned in section 5.1. Isotropic parameters can also be derived directly from $e_v - \ln(p')$ plot where the slope of normal consolidation line is defined as the modified compression index (λ^*) and the slope of the unloading path gives the modified swelling index (κ^*). For calculation of mean effective stress, information about coefficient of lateral earth pressure at rest (K_0) is necessary and OCR for each stress point must be calculated for all samples. Hence the accuracy of pre-consolidation stress is significant as mentioned earlier in section 5.1. In this thesis, both cases of λ^* and κ^* emerging from $e - \log(\sigma'_v)$ plot and $e_v - \ln(p')$ are calculated for comparison. In Creep S-Clay1S model, intrinsic value for compression index and creep index are used. The slope of λ_i^* represents the stress path of a reconstituted sample in which all particle bonds are destroyed. The relation between the parameters derived from $e - \log(\sigma'_v)$ and $e_v - \ln(p')$ are given by equations 5.2 and 5.3 (Sivasithamparam 2012).

$$C_c = \frac{\Delta e}{\Delta \log(\sigma'_v)} \quad C_s = \frac{\Delta e}{\Delta \log(\sigma'_v)} \quad (5.1)$$

$$\lambda^* = \frac{\lambda}{1 + e_0} \quad \kappa^* = \frac{\kappa}{1 + e_0} \quad (5.2)$$

$$\lambda^* = \frac{C_c}{2.3(1 + e_0)} \quad \kappa^* \approx \frac{2C_s}{2.3(1 + e_0)} \quad (5.3)$$

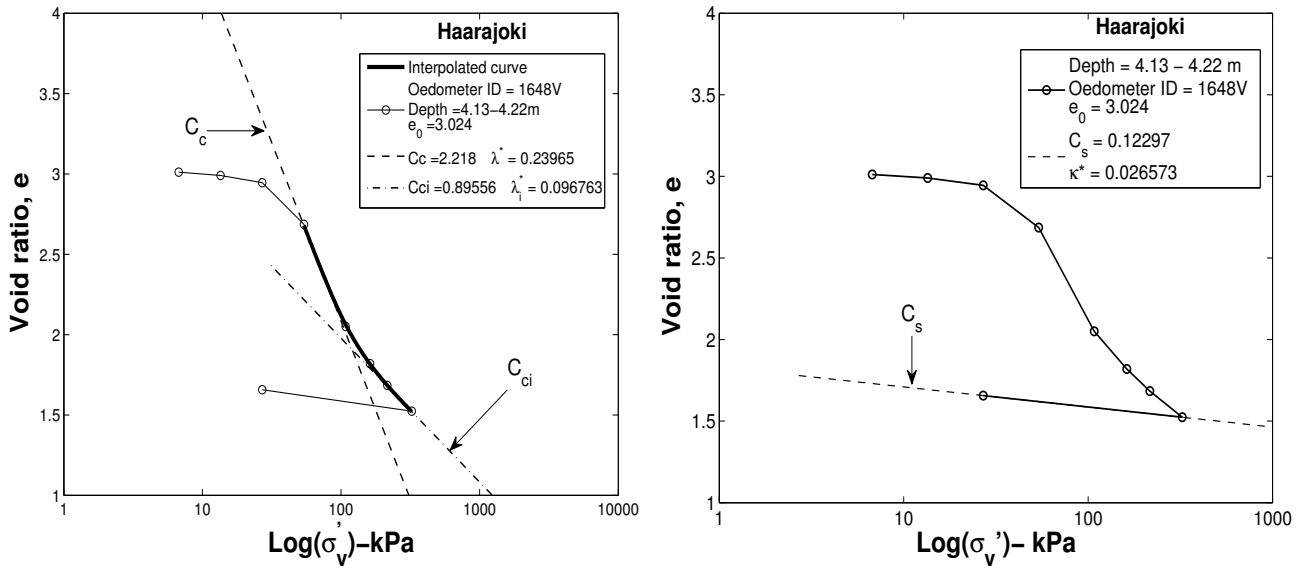


Figure 5.3: Illustration of determination of compression and swelling index for a typical Haarajoki sample from $e - \log(\sigma'_v)$ plot

For the determination of modified swelling index, the slope of the first unload stress path is considered as shown in Figure 5.3 (b). During observation of several $e - \log(\sigma'_v)$ plots of different samples from Haarajoki, it is found that the unloading path is not always constant and has a high variation. This can be an issue during analysis since this variable highly influences the elastic region in the model and yet there are no clear definition as to how to determine this parameter. It can well be due to bad quality of data, however many authors have claimed the same and refuse to give a definite statement for κ (Muir Wood 1991). Figure 5.4 shows the distribution of calculated values of λ^* , λ_i^* and κ^* in the $e - \log(\sigma'_v)$ plot. It clearly shows

that there is large variation in λ^* than in λ_i^* . Hence it is evident that using intrinsic values would give more accurate predictions than normal values. However, the parameter κ^* shares the same amount of variation as λ^* which shows that the unloading path for one dimensional oedometer tests are highly varying for each sample.

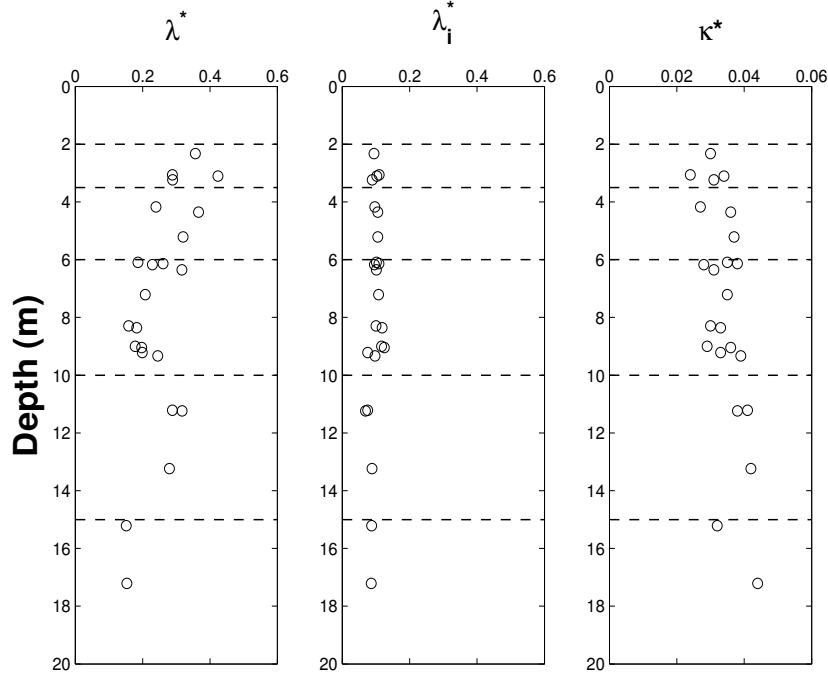


Figure 5.4: Distribution of λ^* , λ_i^* and κ^* along soil depth

In order to plot $\epsilon_v - \ln(p')$ curve, information about horizontal effective stress acting on the sample at all stress points is required to construct the mean effective stress of the sample. K_0 is defined as the ratio between horizontal and vertical effective stress of a soil. It can be accurately measured from a borehole pressuremeter test (PMT) or a Dilatometer test (DMT) (Knappett and Craig 2014), however due to high cost factors these tests are not commonly used and alternate empirical relations are resorted. Jaky 1948 proposed a relation which is commonly used for deriving the K_0 value and is given in equation 5.4 (a). However, this formula does not mention the history but only the structure of the soil. Since the value of K_0 is not constant in the overconsolidated region, equation 5.4 (a) cannot be taken for calculation of the mean effective stress. The relation formulated by Kulhawy and Mayne 1990 for the determination of K_0 takes into account the history of the soil given by equation 5.4 (b).

$$K_0^{NC} = (1 - \sin \phi') \quad K_0 = (1 - \sin \phi') \cdot OCR^{\sin \phi'} \quad (5.4)$$

Using the formula from equation 5.4 (b), it is observed that heavy OC clays exhibited higher K_0 values with sometimes values more than 1.00. However, the accuracy of the mean effective stress is bound to be affected due to the use of this empirical formula and taking into account the sample disturbance effects. Hence, values from $e - \log(\sigma'_v)$ plots, although with sampling effects, should provide a comparatively reliable result. The values from both plots, $e - \log(\sigma'_v)$ and $\epsilon_v - \ln(p')$, were analysed and found that the variation in λ^* and λ_i^* values range between 0.11 – 0.13% and 0.11 – 0.87% respectively which is very negligible. The reason can be due to

a constant value of OCR and K_0 in the normally consolidated region (as shown in Figure 5.5) leading to a constant ratio between σ'_h and σ'_v . However, a high difference in the value of κ^* between the two plots have been observed ranging 22 – 26% lower in the $\epsilon_v - \ln(p')$ plot. The proportion of change in p' and σ'_v are not constant during one-dimensional unloading of the sample due to a constant change of OCR in the swelling region.

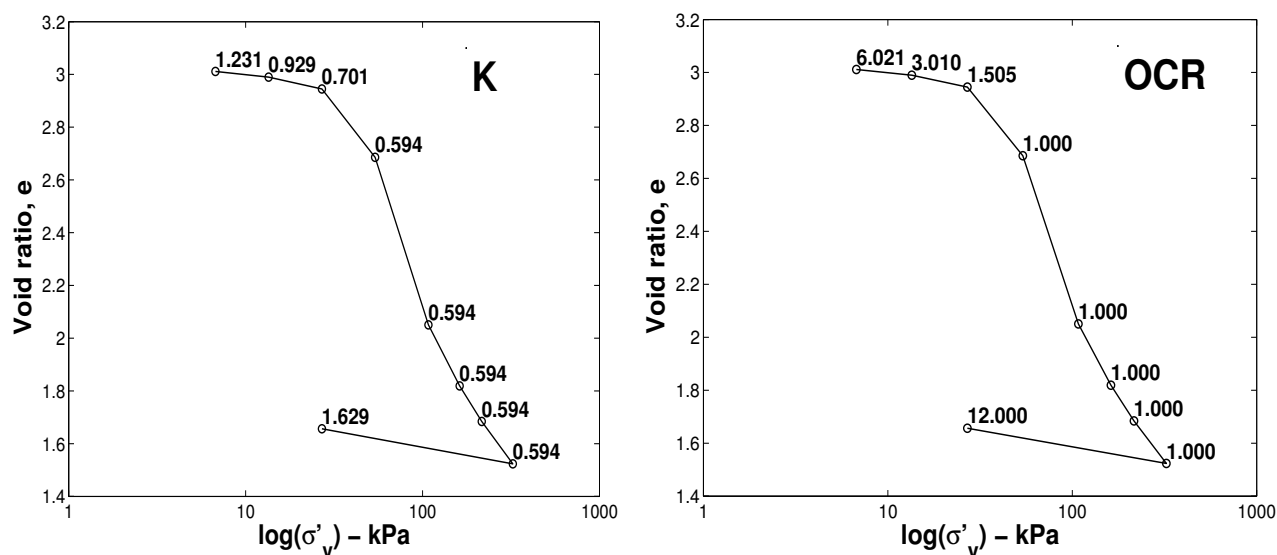


Figure 5.5: Illustration of K and OCR distribution along Oedometer IL stress path for Haarajoki sample from depth 4.13-4.22m (ID = 1648V)

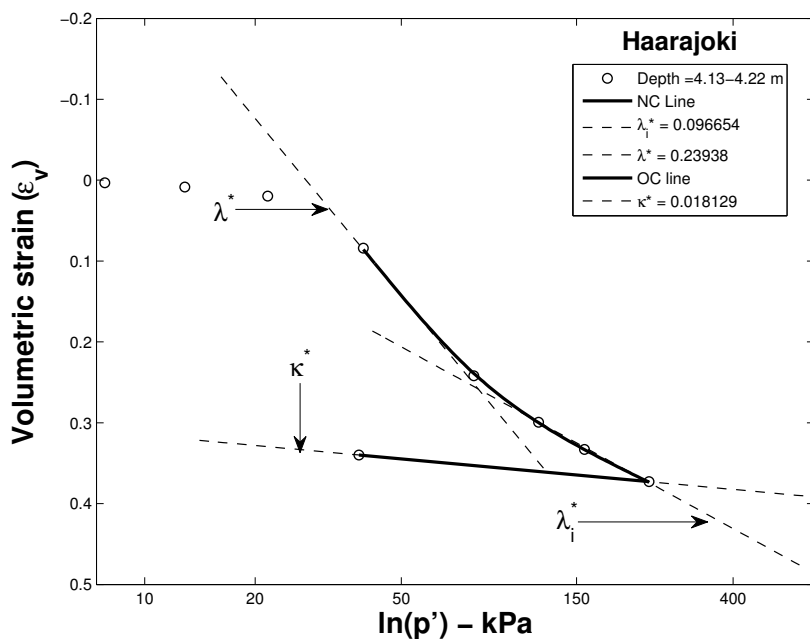


Figure 5.6: Determination of parameters from $\epsilon_v - \ln(p')$ plot

Poisson's ratio is an elastic parameter and usually ranges between 0.1 - 0.3 for soft soils. Due

to poor quality of triaxial test results for Haarajoki samples, values from previous papers (Yildiz et al. 2009) are taken for initial calculations and then optimised in experimental simulations.

The critical state line (M) is the most important parameter due to its influence on six other parameters. A sample is said to have reached its critical state when stress ratio η becomes constant with indefinite plastic shearing under constant volume. When the critical state is reached, a unique line of failure is formed in the $q - p' - v$ plane where q is the deviatoric stress, p' is the mean effective stress and v is the specific volume. In triaxial test, when cell pressure acts as a minor principal stress, then the test corresponds to triaxial compression and gives the critical state line in compression, M_c . On the contrary, when cell pressure acts as a major principal stress, then the test corresponds to triaxial extension and gives the critical state line in extension, M_e . Soft soils are highly anisotropic and the behaviour of a soil sample would depend mostly on the orientation of its particles with respect to applied stress, the amount of bonding and particle interaction. Citing this reason, the value of critical state in compression is highly unlikely to be equal to its extension counterpart and there are experimental evidences to support this statement (Gens 1982). Since no triaxial extension tests were performed for Haarajoki samples, M_e is calculated from equation 5.5 where ϕ'_{cv} is derived from triaxial compression test. The relation between M_c , M_e and ϕ'_{cv} is given by equations 5.5 (Muir Wood 1991).

$$M_c = \frac{6 \sin \phi'_{cv}}{3 + \sin \phi'_{cv}} \quad M_e = \frac{6 \sin \phi'_{cv}}{3 - \sin \phi'_{cv}} \quad (5.5)$$

5.3 Anisotropic parameters

In order to achieve better accuracy in predicting soil behaviour, Creep-Sclay1S takes into account the anisotropic characteristics that exists in soft soil due to its depositional history. The anisotropy proposed in the model describes the initial inclination of yield surface (α_0) and kinematic hardening refers to the change in inclination during plastic straining. Assuming an associated flow rule and a 0.66 ratio difference between volumetric and deviatoric plastic strains, Wheeler et al. 2003 proposed a method for determining the initial inclination of the yield surface (α_0) for normally consolidated soils which is given by the equation 5.6 (a).

$$\alpha_0 = \frac{\eta_{K_0}^2 + 3\eta_{K_0} - M_c^2}{3} \quad \eta_{K_0} = \frac{3(1 - K_0^{NC})}{(1 + 2K_0^{NC})} \quad (5.6)$$

where η_{K_0} is the normally consolidated stress ratio and M_c is the slope of critical state line in compression. By definition, stress ratio is defined as the ratio between deviatoric stress (q) and the mean effective stress (p'). Hence in order to determine the value of η_0 , it is required to estimate the horizontal effective stress which is assumed from the empirical relation given by Jaky 1948 for K_0^{NC} (equation 5.4).

The parameter ω_d , also known as shear rotation parameter, defines the relative effectiveness of plastic volumetric and shear strains in rotational hardening (Wheeler et al. 2003). The parameter ω can be determined from curve fitting from isotropic compression test or Triaxial extension test where significant change in anisotropy is observed (Yin et al. 2011). It controls the absolute rate at which the surface of normal consolidation rotates with viscous straining. Leoni et al. 2008 assumes that anisotropy is erased when α_0/α reaches 10, which allegedly occurs at 2 or 3 times the pre-consolidation stress. The value of ω can, therefore, be estimated

from equation 5.7. This relation is, however, based on several assumptions and does not yield a reliable value. For this thesis, a simple relation (Yin et al. 2011) has been used for ω ranging between $10/\lambda_i$ to $20/\lambda_i$.

$$\omega = \frac{1}{\lambda^*} \ln \left(\frac{10M_c^2 - 2\alpha_0\omega_d}{M_c^2 - 2\alpha_0\omega_d} \right) \quad \omega_d = \frac{3}{8} \cdot \frac{(4M_c^2 - 4\eta_{K0}^2 - 3\eta_{K0})}{(\eta_{K0}^2 - M_c^2 + 2\eta_{K0})} \quad (5.7)$$

5.4 Destructuration parameters

The Creep-Scly1S model incorporates the effects of bonding and destructuration which is represented by three parameters. The amount of bonding between particles is represented by a scalar quantity, χ . Based on sensitivity of the soil, the initial bonding, χ_0 , can be determined from the empirical relation, $\chi_0 = S_T - 1$. This is due to introduction of a sensitivity factor to relate intact samples containing some particle bonding to reconstituted samples where all bondings are destroyed. Hence the relation of stress between intact and reconstituted sample is given by $\sigma'_{p0} = S_T \cdot \sigma'_{pi0}$, where σ'_{p0} is the apparent pre-consolidation stress of the intact sample as shown in the Figure 5.7 and σ'_{pi0} is the pre-consolidation stress corresponding to reconstituted sample which are related by a sensitivity factor describing the amount of bonding that exists in the intact sample (Figure 5.7). The amount of bonding decreases to a value of zero with increasing plastic strains and the stress path for the intact clay would eventually merge with its reconstituted counterpart.

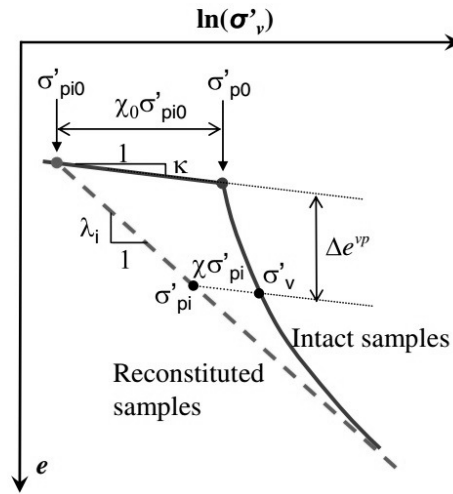


Figure 5.7: Illustration of bonding relation between intact and reconstituted clay (Yin, and Karstunen 2011)

The parameters ξ_v and ξ_d controls the rate of bond degradation due to volumetric and deviatoric strains respectively. To estimate ξ_v , the sample is isotropically compressed to erase the initial anisotropy in the sample such that there would only be volumetric strains. Leoni et al. 2008 suggests that experimental evidence show by isotropically loading the sample at values two or three times larger than the pre-consolidation pressure, it is possible to erase

the initial anisotropy of the sample. Hence, very low values of η must be simulated in the Triaxial test such that the shear strains would be small and effects from shear parameters would be negligible. In order to determine ξ_d , ξ_v is used along with high η (q/p') simulation in tri-axial test to obtain bond degradation from shear effects. This procedure is based on several presumptions and is not definite, since pre-consolidation stress varies for different strain rates. However not many alternate procedures are available for the determination of these parameters. In the laboratory data for Haarajoki samples, there are no experiments dedicated for destructuration parameters and only information regarding sensitivity of the soil at different depths are available. Citing this reason, default values are taken (Yin, and Karstunen 2011) such as 9.0 for ξ_v (from typical range of 8.0 - 12.0) and 0.20 for ξ_d (from typical range of 0.20 - 0.30).

5.5 Viscous parameters

The modified creep index μ^* can be derived from two methods. It can be directly measured in $\epsilon_v - \ln(t)$ plot and through parameter C_α (as mentioned in equation 5.9) from $e - \log(t)$ plot. However both plots would give the same value for μ^* since void ratio difference and volumetric strain are related. The scale of time does not have an effect on the value of creep index due to representation in logarithmic scale. The Creep-Sclay1S model uses intrinsic values for modified creep index (μ_i^*).

$$\mu^* = \frac{\Delta \epsilon_v}{\Delta \ln t} \quad (5.8)$$

$$C_\alpha = \frac{\Delta e}{\Delta \log t} \quad \mu^* = \frac{C_\alpha}{2.3(1 + e_0)} \quad (5.9)$$

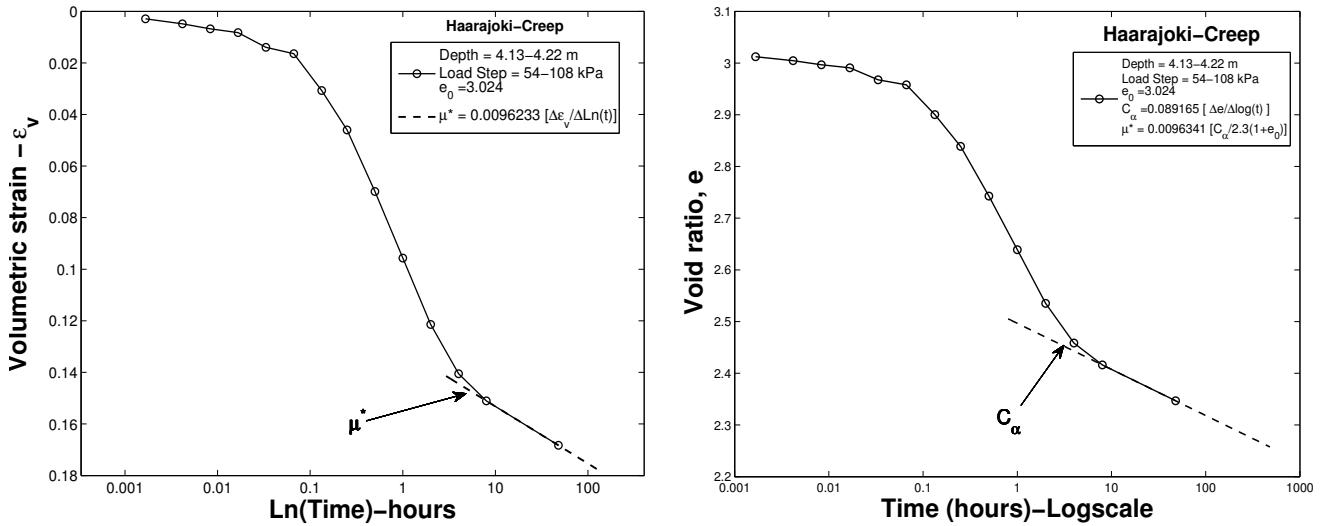


Figure 5.8: (a) Determination of modified creep index from $\epsilon_v - \ln(t)$ plot (b) from $e - \log(t)$ plot

In Laboratory tests for Haarajoki samples, there are only a maximum of two creep tests for each sample which is insufficient for estimation of the intrinsic creep index. The determination of intrinsic creep value according to Grimstad and Degago 2010 using time resistance number is

mentioned in Appendix G. Hence, load steps that represent the in-situ conditions are chosen as the value for μ_i^* and optimised during simulation. Reference time (τ) is linked to the definition of pre-consolidation stress (Brinkgreve et al. 2008). The value is usually taken as one day since Oedometer test is performed with 24 hours time step. However, lab results for Haarajoki samples show time steps longer than 7 days. Hence time step before and after attainment of pre-consolidation stress is compared and an average value is chosen for the analysis.

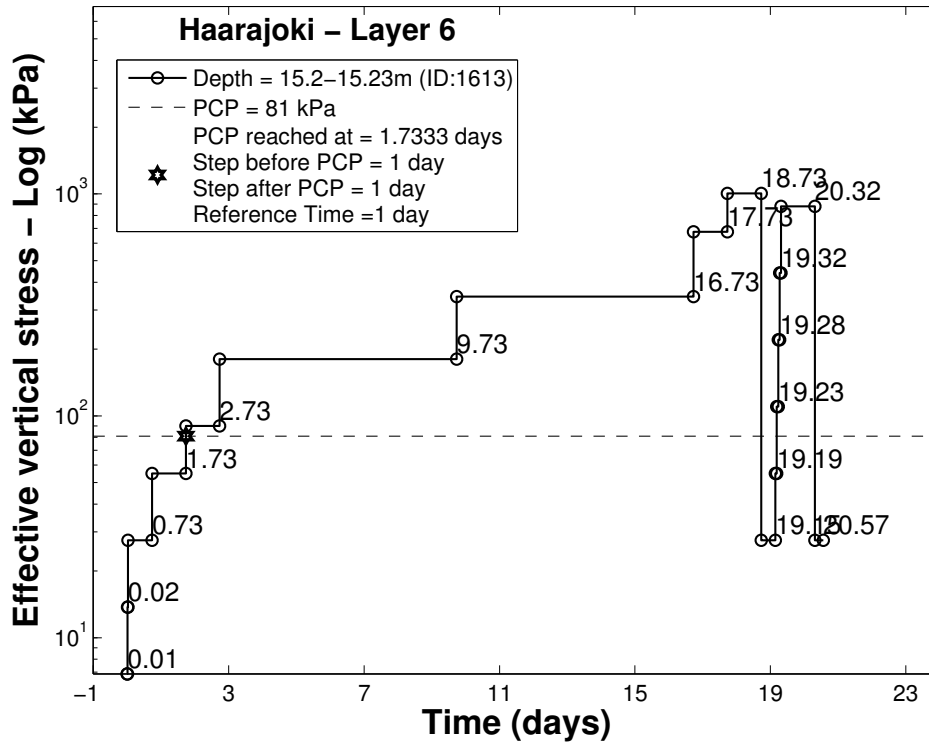


Figure 5.9: Illustration of Reference time determination for a typical Haarajoki sample

6 Simulation of Laboratory results

The objective for simulating laboratory tests is to validate the Creep-Sclay1S model's accuracy in predicting soft soil behaviour. A number of simulations has been conducted for oedometer IL, constant strain-rate (CRS) and triaxial experiments in Tochnog, a finite element software for geotechnical analysis (refer *Tochnog Professional User's manual* 2015) and compared with laboratory results.

6.1 Geometry

The geometry of the sample is meshed in Gmsh, an open source software for finite element mesh generator (refer *Gmsh reference manual* 2015). The mesh is generated with respect to second order shape function due to coupled flow analysis (refer Appendix J). Single element is modelled for all drained test simulations. The generated mesh file is incorporated in Tochnog as an input geometry file. Due to axial symmetry on the left edge and confining ring on the right edge (cell pressure in case of triaxial test), lateral movement is restricted on these boundaries. Frictional effect from confining ring is not considered in simulation due to limited scope of this thesis. Hydraulic pressure is set to zero on the upper boundary to allow vertical drainage. Vertical displacement is restrained on the lower edge. Creep-Sclay1S is a user defined model in Tochnog and parameters are given as input for samples from depth corresponding to respective layer. A summary of parameters for each layer is given in Appendix D. One sample is chosen from each layer, however due to high variation in layer-4 (6 - 10m) three samples are chosen from this layer for better validation. The load input of the sample starts around 5 - 10 kPa and preoverburden pressure (POP) is adjusted accordingly since initial stress condition of sample extracted from site cannot represent in-situ stress condition due to swelling from sampling effects and this should be taken into account before loading.

6.2 Loading condition

Initially an isotropic cell pressure of 5 kPa is assigned for all samples and then increased anisotropically corresponding to values from each test. The rate of loading is assigned as a boundary input on the upper edge of the sample until failure. For oedometer IL simulation, load input is given in increments with same magnitude and time interval as performed in laboratory testing. For each load step, a transition time of 8 seconds has been considered. For oedometer CRS tests, no load is applied as boundary condition, however, a constant displacement velocity (m/day) is set on the upper boundary of the sample. From laboratory results, all samples are tested at constant displacement rate of 0.0015 mm/min (0.6 %/hour) and is modified accordingly in Tochnog for simulation. This displacement rate results in a total span of around 2 days for all CRS tests. The quality of triaxial lab results for Haarakjoki samples are poor and hence simulation is chosen for only a select number of samples with a standard stress path. This is due to fact that most tests were conducted in partially drained condition which is not possible to simulate since the time of transition between undrained to drained condition is not clear and information about the permeability of sample is unavailable. Also, for most tests that claim to have been conducted in drained condition shows an undrained stress path with increasing pore pressure values, hence querying its reliability.

6.3 Results

6.3.1 Oedometer IL test

The results from the Oedometer IL test simulation has a very good agreement with the Laboratory data as shown in Figure 6.1. This is reasonable since highly influential parameters such as λ_i^* , κ^* and pre-consolidation stress are derived from samples of IL experiments. For some samples when started from initial values (6.75 kPa), there were excess creep deformation in the elastic region showing a high μ_i^* value and would be optimised during embankment analysis. However, when simulation is done from second load step (13.5 kPa), yields a proper elastic stress path cohering well with lab data. From the results of the IL simulations, it is safe to state that the model's prediction is close to the lab data and requires no optimisation for parameters at this stage.

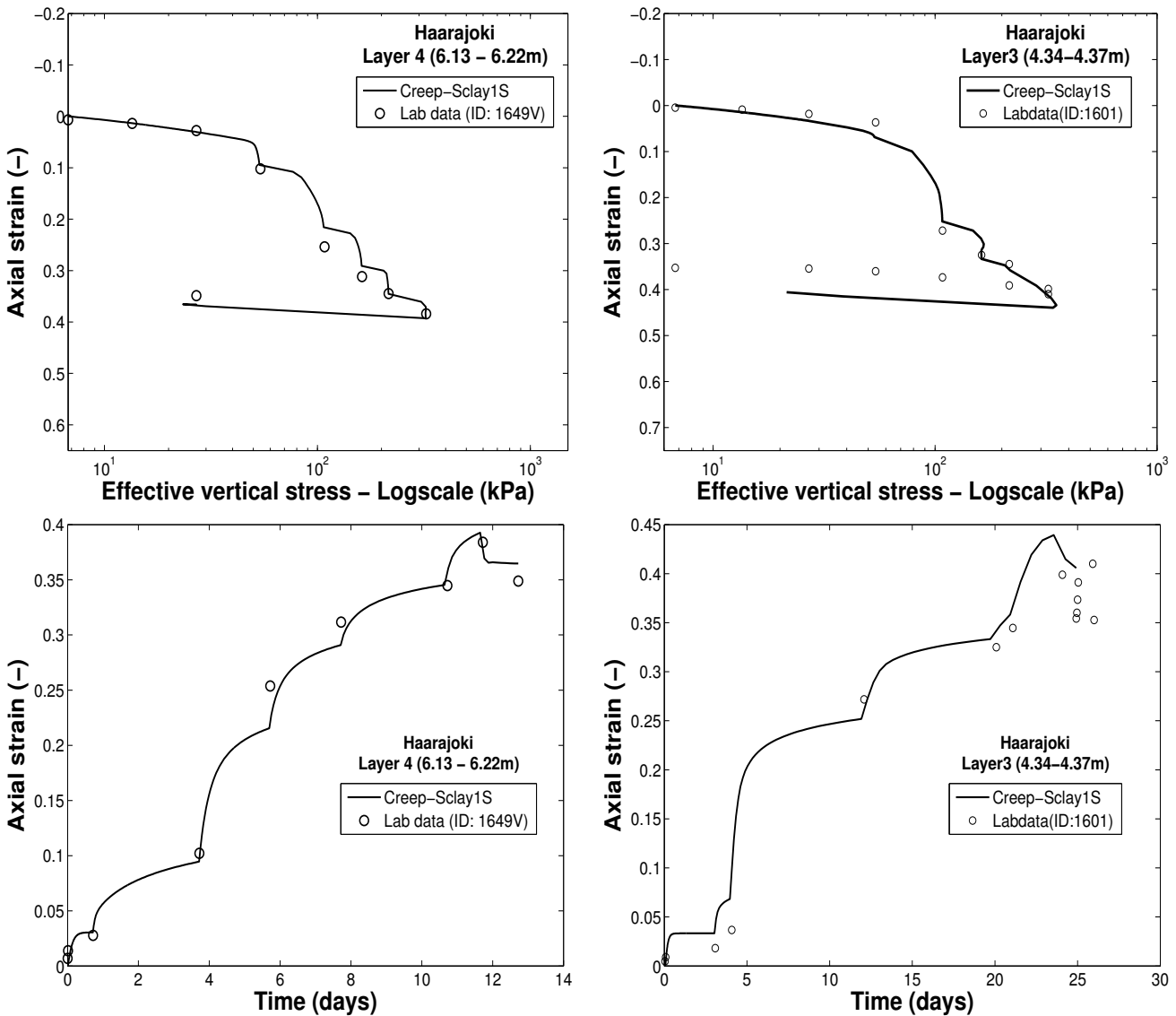


Figure 6.1: Comparison of Oedometer IL simulation result with laboratory data for typical Haarajoki sample at depths 6.13-6.22m and 4.34-4.37m

Permeability change with respect to void ratio has been modelled using dependency function in Tochnog. The relation between permeability and void ratio is calculated from Taylor's formula (Taylor 1948) which is given by, $\log(K/K_0) = \Delta e/c_k$, where $c_k = 0.5e_0$ as shown in Figure 6.2(a). Simulations with both conditions, constant and dynamic permeability, resulted in no significant difference (Figure 6.2(b)). This can be due to slow increment of load that allows faster drainage in the sample. Hence, sample should be loaded quickly so that rate of dissipation due to permeability can be validated. Changes affecting the drained stress path are largely influenced by parameter input of which preoverburden pressure is the most significant followed by isotropic parameters and initial stress input.

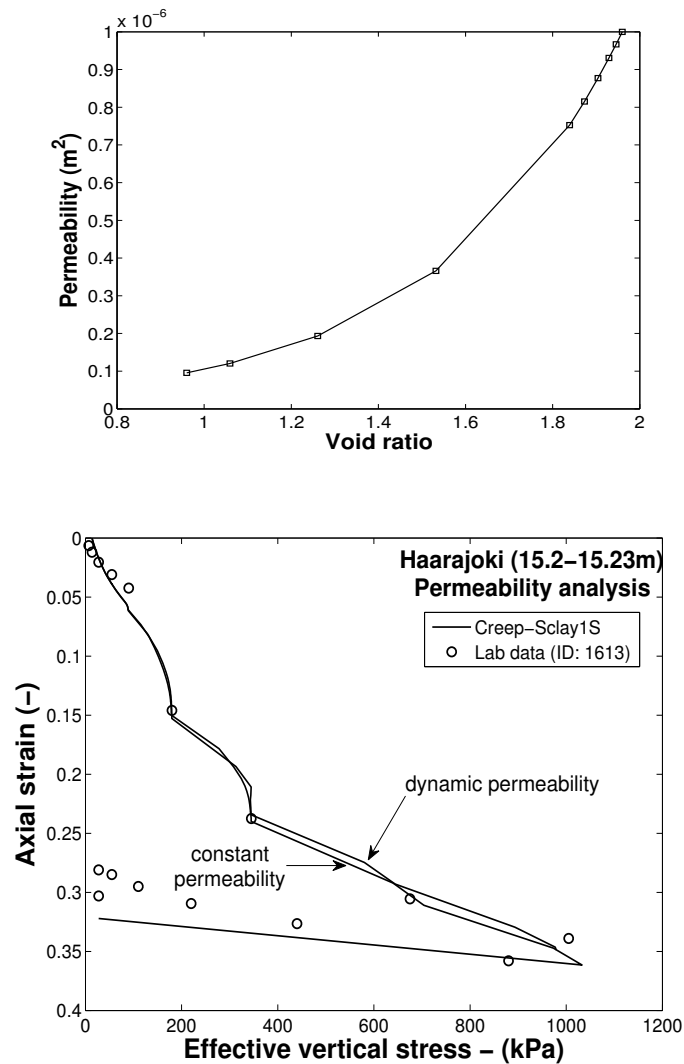


Figure 6.2: (a) Relation between Permeability and Void ratio from Taylor's formula (b) Difference between constant and dynamic permeability analysis for typical Haarajoki sample at depth 15.2-15.23m

Mesh sensitivity analysis ranging from 1 element to 750 elements have been analysed and resulted in no significant change as shown in Figure 6.3. However significant change can be expected if high amount of pore-pressure build-up is created in the sample. Hence validation of permeability and mesh sensitivity in oedometer IL, CRS and triaxial tests can only be done when there is faster loading rate.

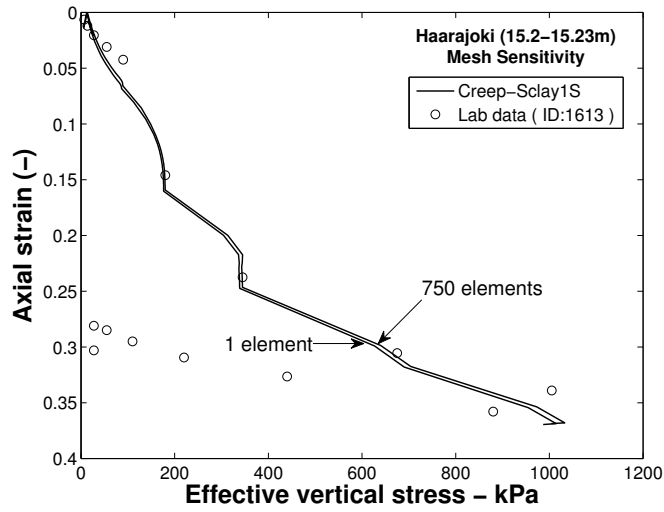


Figure 6.3: Mesh sensitivity analysis in oedometer IL simulation for typical Haarakjoki sample

6.3.2 Oedometer CRS test

The results for constant strain rate simulations, did not match with laboratory CRS data. The margin of difference is large as shown in Figure 6.4. Therefore, samples from different depths were chosen and still gave similar error. It can be due to several reasons such as bad quality of lab data, irregular monitoring of strain rate or sampling disturbance effects.

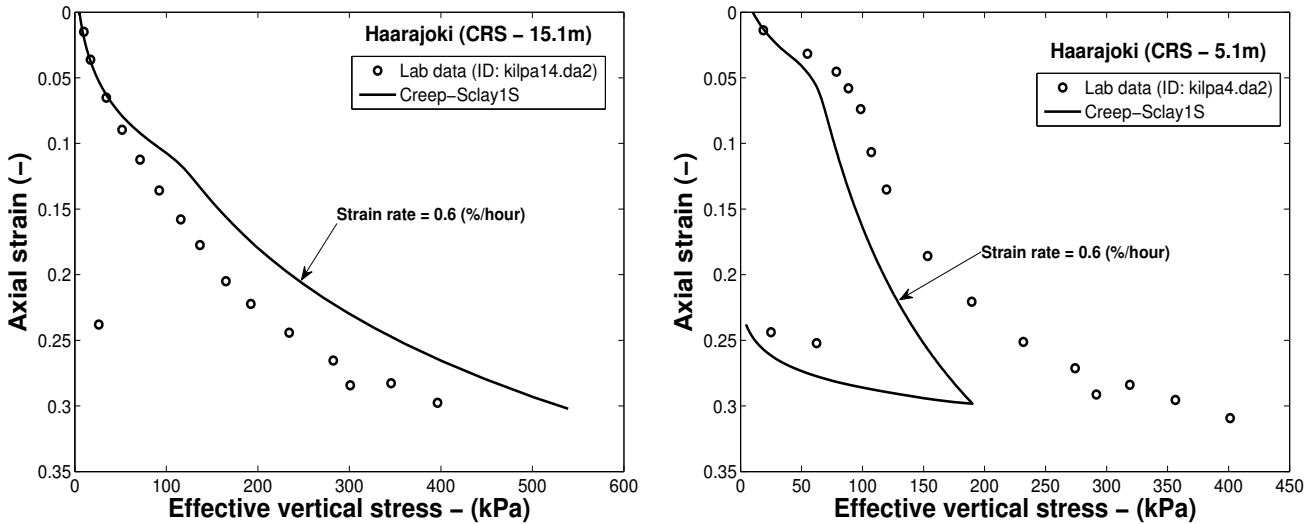


Figure 6.4: (a) Comparison with CRS simulation with Laboratory data for a typical Haarakjoki sample from a depth of 15.1m (b) 5.1m

With concern for maintaining a constant strain rate (which originally is a constant displacement rate) throughout the test in reality can be difficult, and modification is done to fit lab data. For sample taken at a depth of 15.1m, a strain modification, with the same parameters, spanning 200 days (0.006 %/hour) is required to actually match the lab data while originally it is done at a strain rate spanning 2 days (0.6 %/hour). So the margin of difference in this case seems to be around 100 times (Figure 6.5) which is unrealistic.

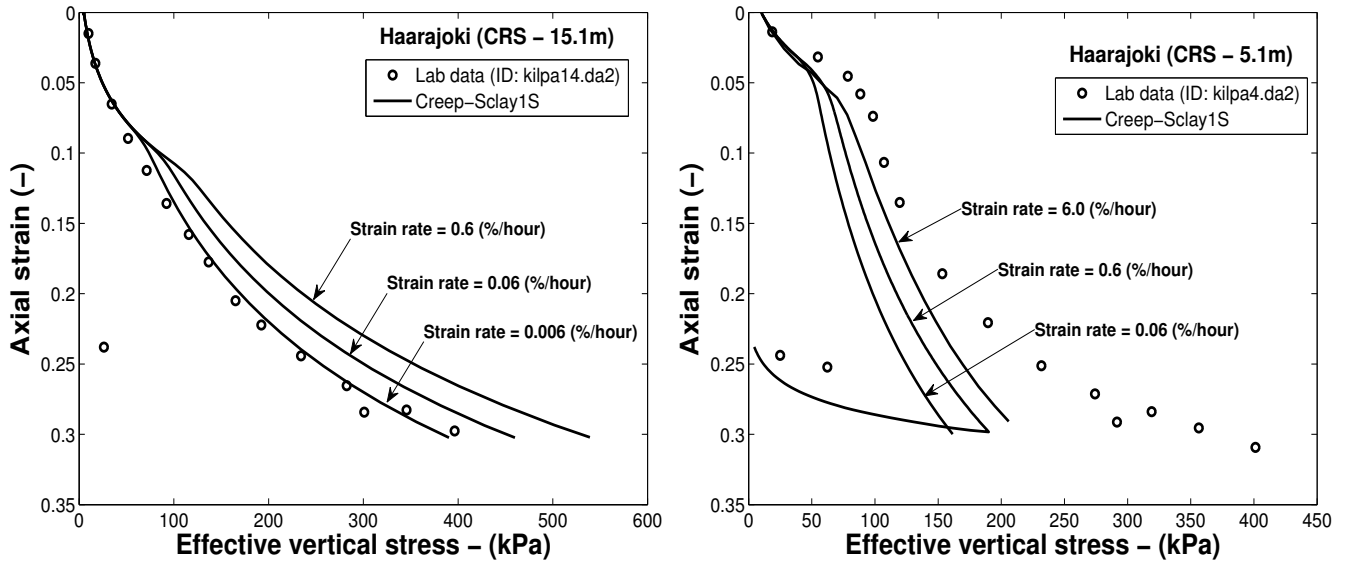


Figure 6.5: (a) Modification of Strain rate to match Lab data for a typical Haarajoki sample at depth 15.1m (b) 5.1m

Although initially hydraulic properties were taken as constant value similar to oedometer IL simulations, dynamic permeability properties combined with water stiffness input were also simulated but yielded similar or almost no difference in the final result (Figure 6.6). This is due to the rate of strain (0.0015mm/min for sample height of 15mm corresponding to 0.6 %/hour) which is slower than standard CRS tests conducted in Sweden (0.0024 mm/min with sample height of 20mm corresponding to 0.7 %/hour (Olsson 2010)) allowing complete drainage with no excess pore pressures. Hence, CRS tests for Haarajoki samples can be regarded as a fully drained test.

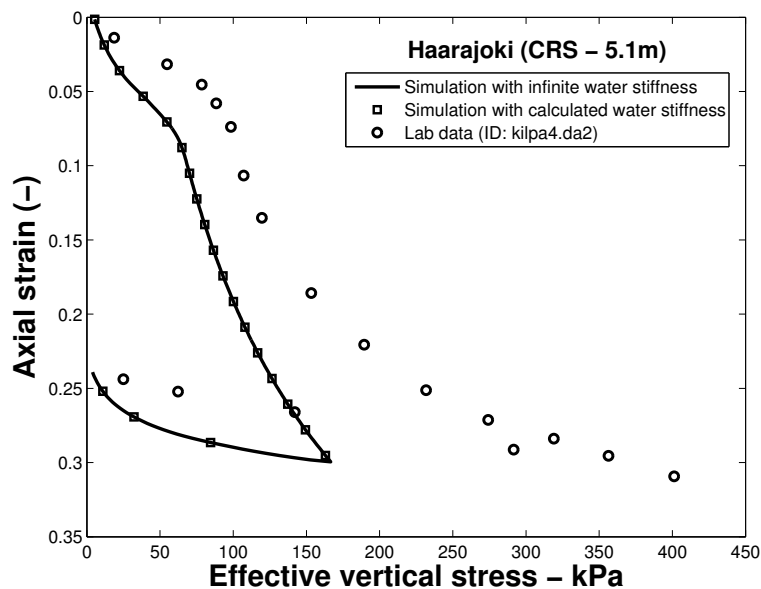


Figure 6.6: Comparison of different simulations with hydraulic properties modification for typical Haarajoki sample at depth 5.1m

Due to a large margin of difference between lab data and simulation, significant modifications in parameters such as pre-consolidation stress, intrinsic compression index and swelling index are required for optimisation. Since pre-consolidation stress is strain rate dependant, it is reasonable that sample disturbance can affect this value and subsequently the overall stress path. Also other factors such as monitoring error, instrument fault etc. are difficult to measure and can affect the stress path dearly. Figure 6.7 shows the large modification required for pre-consolidation stress and sensitivity values to fit CRS lab data.

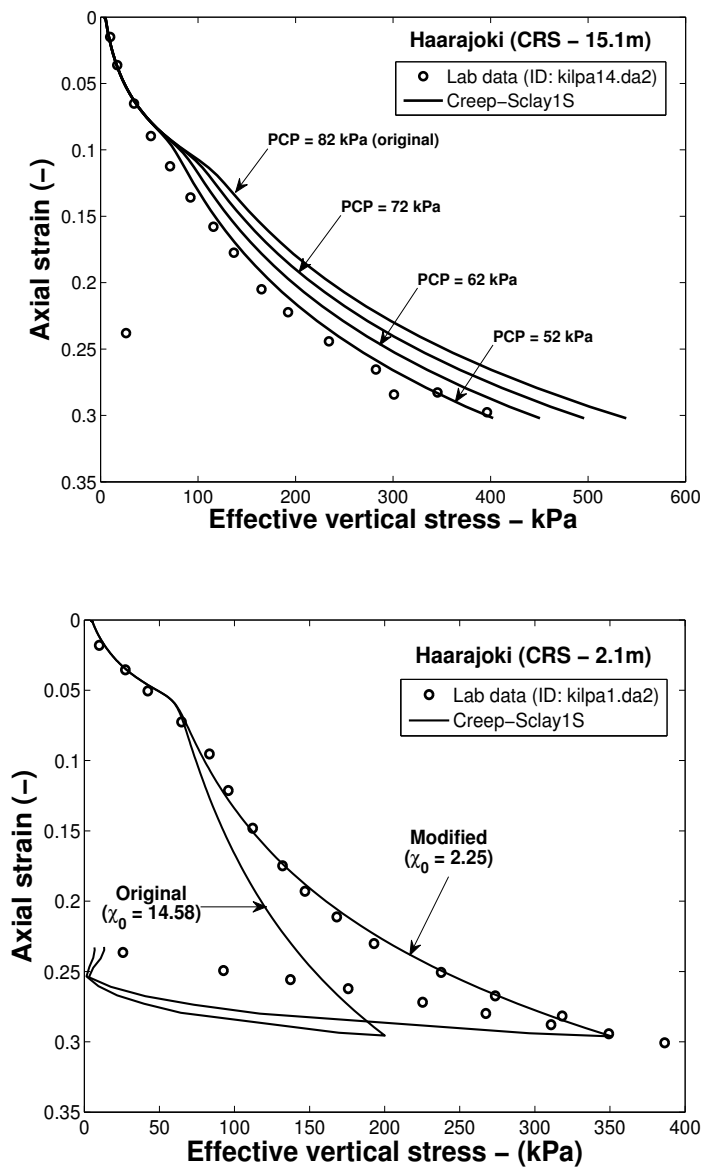


Figure 6.7: (a) Modification of pre-consolidation stress to fit CRS lab data for typical Haarajoki sample at depth 15.1m (b) Modification of Initial bonding to fit CRS lab data for typical Haarajoki sample at depth 2.1m

A separate sensitivity analysis for parameters is done and the range of effect each parameter influences on CRS stress path are recorded. It is observed that the pre-consolidation stress has the highest influence followed by isotropic parameters (summarized in Appendix D).

6.3.3 Triaxial test

Simulation is conducted for samples from depth 8.03-8.15m and 12.87-12.97m as the quality of triaxial lab results for these depths show better quality. Other samples were ignored due to poor quality as mentioned in section 6.2.

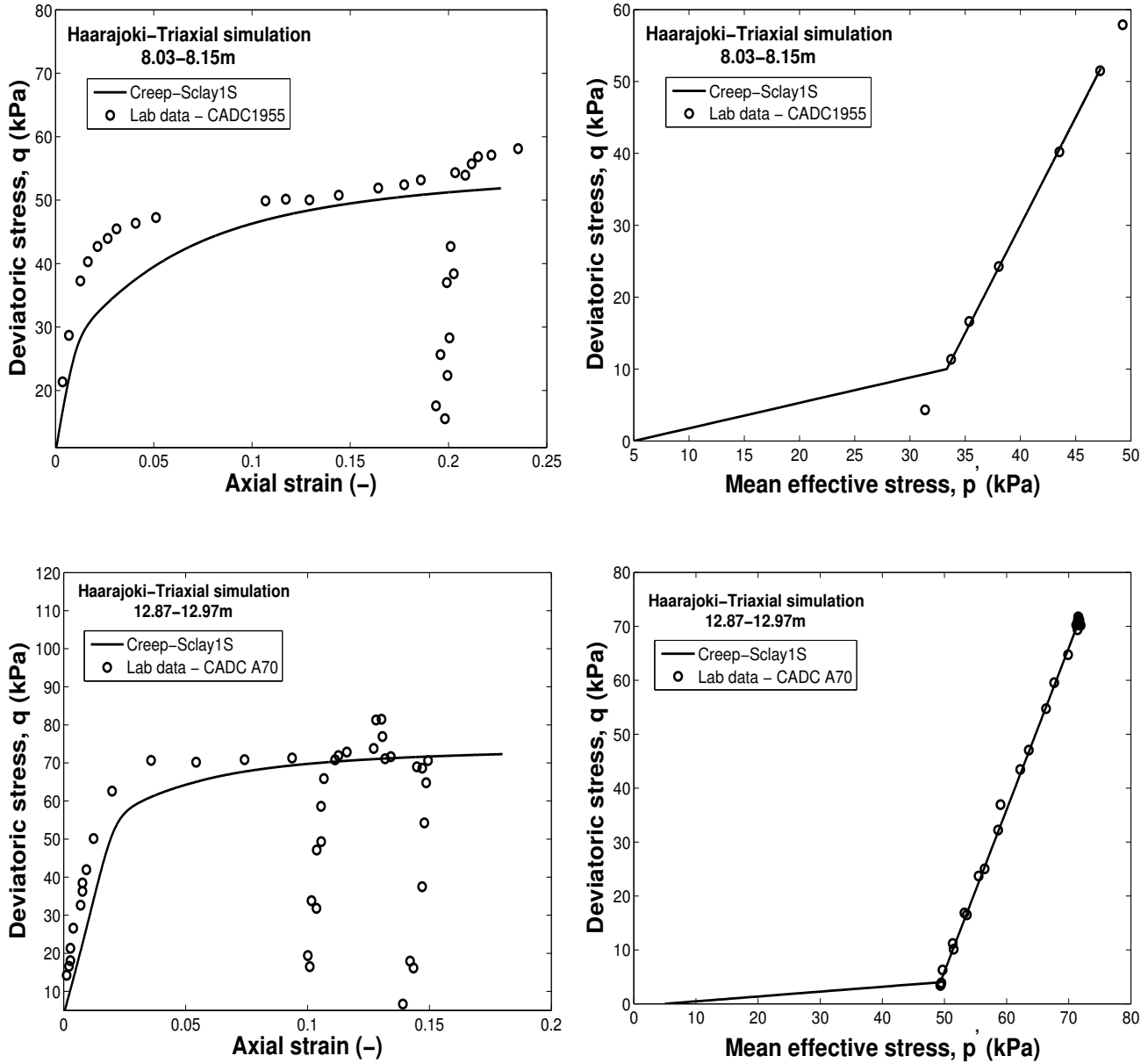


Figure 6.9: Comparison of triaxial simulation result with laboratory data for typical Haarajoki sample at depths 8.03-8.15m and 12.87-12.97m

The results from triaxial test simulation (Figure 6.9) show a good match with experimental result. Both simulations show a slight deviation in the elastic region. This can be due to consideration of purely drained condition in simulation whereas during laboratory testing a constant pore pressure around 6 - 10 kPa would exist giving additional elastic stiffness to the sample. It can be observed that after pore pressure dissipation, the effective stress path from the experimental data gradually merge with the simulation curve as shown above.

7 Embankment simulation

7.1 Initial condition

The geometry of the Haarajoki embankment is meshed in Gmsh, as shown in Figure 7.1. The right half of the geometry is modelled due to symmetrical boundary conditions and to save computation time. A length of 50m from embankment centre line has been considered to prevent boundary effects on material velocity and groundwater flow. Meshing is done using elements with second order shape functions due to incorporation of flow analysis (refer Appendix J). The mesh is locally refined in the embankment and the dry crust layer. The minimum and maximum element size is 0.25m and 1.00m respectively. The total number of elements is 5358 with 11033 nodes.

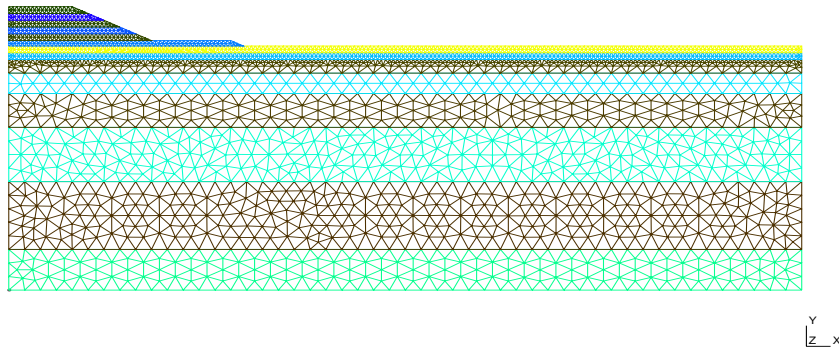


Figure 7.1: Embankment geometry

The embankment is constructed in stages (Appendix B) which is simulated in Tochnog. The Mohr-coulomb model is used for modelling embankment behaviour. The material properties for the embankment include $2.2 t/m^3$ dry density, 60000 kPa elastic modulus and poisson's ratio of 0.30. Also a cohesion of 2 kPa and 5 kPa dilatancy has been included (Vepsäläinen et al. 1997). Since the material of embankment ranges between sandy gravel to gravel, the permeability is presumed to be high. All layers of soft soils ranging from 2 to 18m are modelled by using Creep-Sclay1S model with the same parameters discussed in Chapter 6 (summarized in Appendix D). Till now the parameters are not optimised and original values derived from lab data are used. Since falling head permeability tests have not been conducted for Haarajoki samples, the value of vertical coefficient of consolidation (c_v) is taken from the CRS data to calculate hydraulic conductivity and an average value of permeability is assumed from empirical data comparison. The first 2m in the Haarajoki soil comprises of heavily overconsolidated dessicated clay. In general, Mohr-coulomb model is used for dry crust analysis, however, a definite methodology to study its behaviour is yet to be formulated. The maximum load from the embankment is measured to be 60 kPa along the centre line. From oedometer IL data for Haarajoki dry crust samples, it is observed that a load of 60 kPa corresponds to linear elastic region. Although, sampling of this clay involve large variation, It is known that the rate of dessication is large on the surface and decreases gradually to a certain depth, here assumed till 1m, suggesting a high elastic behaviour on the top surface. Hence the dessicated clay layer has

been divided into three linear elastic layers with large elastic stiffness on the top layer.

Due to symmetrical boundary, lateral movement is restrained on the left boundary (centre line of embankment) and also on the right side. Both lateral and vertical movement are restrained on the bottom boundary. The unit weight of water is taken as 9.81 kN/m^3 . Hence a pressure head of 176.58 kPa is set at the bottom boundary. The phreatic level is set on the ground level. A total of 7 post processing points have been chosen. Pore-pressures at depth of 4, 7, 10 and 15m below embankment are recorded along with settlements on centre line, 4m and 9m right of embankment. Prior to embankment loading, the in-situ stress equilibrium needs to be checked. Figure 7.2 shows the in-situ stress condition in Tochnog before embankment loading which corresponds to calculated values of initial condition. The stress distribution with depth is summarized in Appendix E.

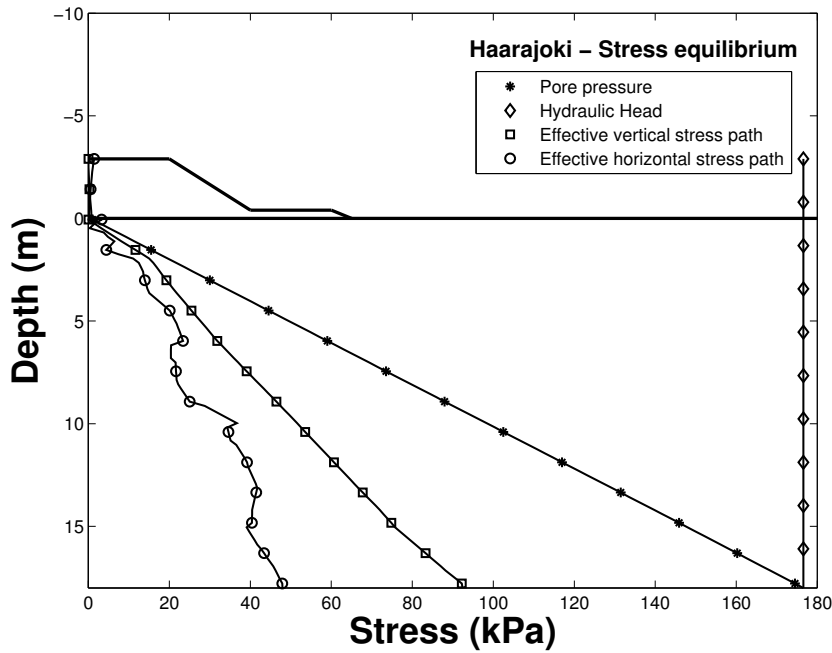


Figure 7.2: In-situ stress equilibrium prior to embankment loading in Tochnog

7.2 Results from simulation

Figure 7.3 (a) shows the comparison between Creep-Sclay1S simulation and field data for settlement along embankment centre line (CL) with respect to time. The simulation shows a good fit with field measurement, however, the modified creep index has been changed. Initially the simulation is run for 365 days to check the parameter's sensitivity on deformation and pore pressure values. The parameters μ_i^* , permeability and dry crust stiffness, dominate the overall simulation. Due to large value of modified creep index, the initial deformation during embankment construction is exaggerated as shown in Figure 7.3 (b). Since creep tests are done for only two load steps from each sample, the value of creep index taken from load steps corresponding to in-situ stress conditions have now proven to be much higher than intrinsic values. The intrinsic creep index cannot be derived from the available laboratory results and requires an assumption from empirical data. It is observed that by reducing the modified creep index to around 10 fold, a satisfactory result is achieved.

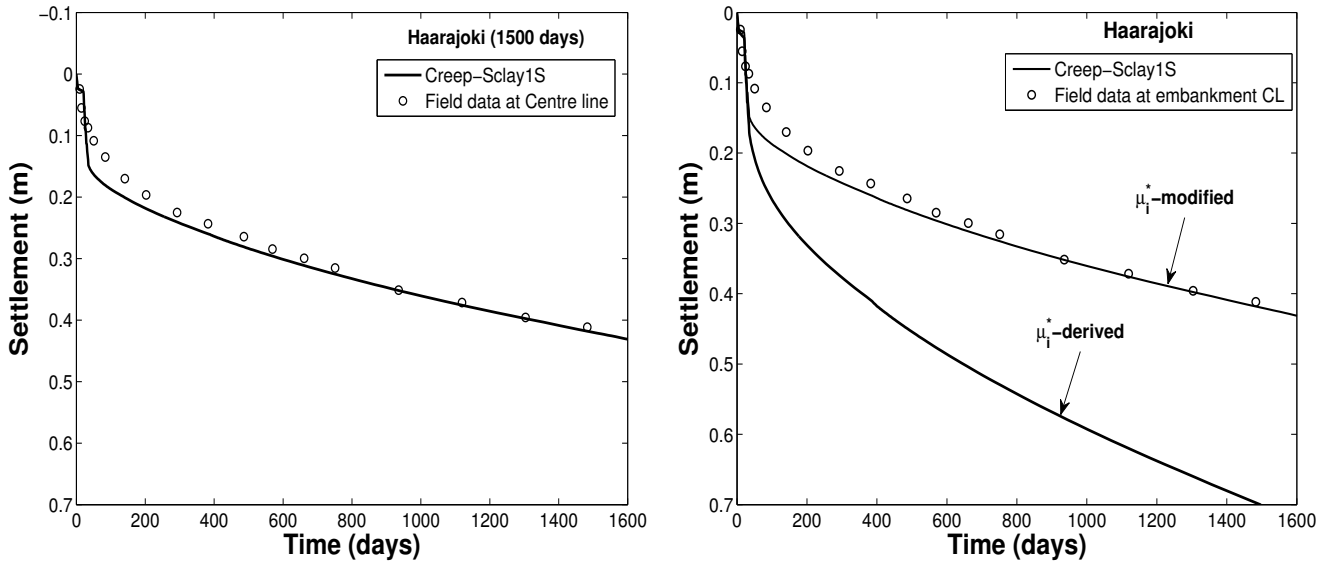


Figure 7.3: (a) Comparison of Creep-Sclay1S simulation with field data for settlement along embankment centre line at Haarakjoki (b) Difference between original and modified values of μ_i^* on settlement prediction along embankment centre line at Haarakjoki

Figure 7.4 shows the settlement prediction from Creep-Sclay1S model at 4m and 9m right of embankment CL. The slight deviation observed is attributed to the stiffness of top dry crust layer. The rate of load distribution, with respect to area, from embankment to dry crust layer and deformation therewith relies heavily on the stiffness of this layer. Due to difficulty in testing dry crust samples, information from laboratory results can be insufficient and requires examination of several other data. A detailed examination of dry crust property is beyond the scope of this thesis and values close to empirical data are assumed for now.

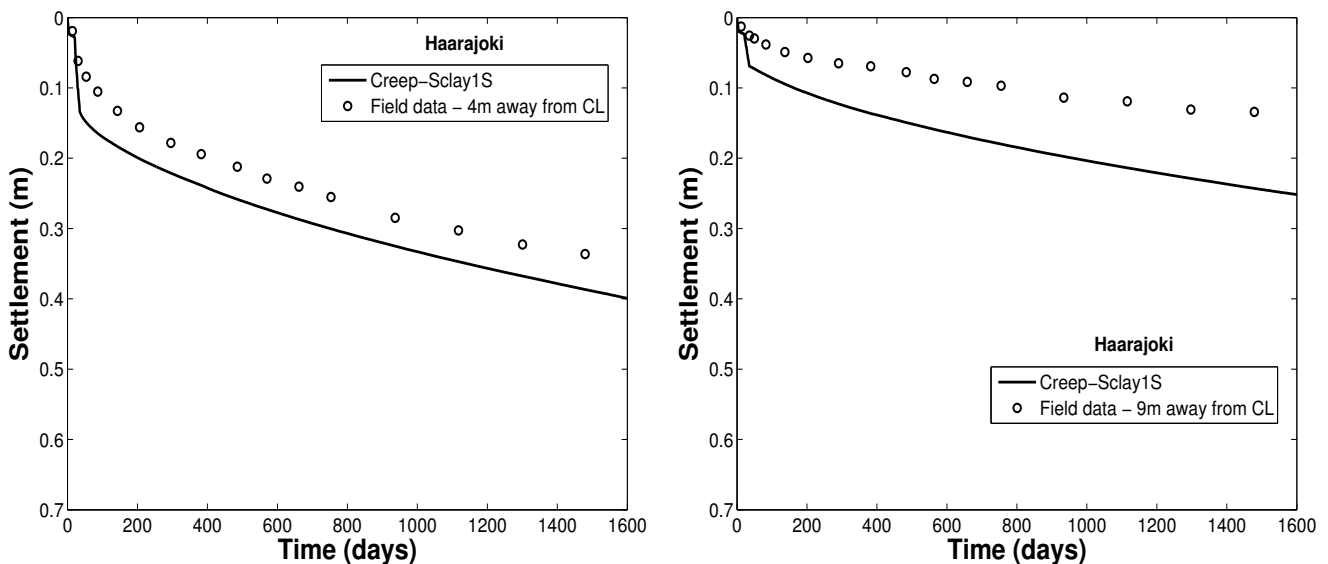


Figure 7.4: (a) Comparison of Creep-Sclay1S simulation with field data for settlement along 4m right of embankment centre line (b) along 9m right of embankment centre line at Haarakjoki

Figure 7.5 shows the comparison of simulation with field data for pore pressure variation with respect to time. The field data shows faster dissipation than simulated values. This can be due to assumption of constant value of low permeability in simulation throughout the consolidation period, whereas in reality, permeability starts from a higher value and decreases correspondingly with consolidation rate. Nevertheless, the result from simulation shows a closer prediction of pore pressure values beyond 7m depth and slightly excess values near surface. As per simulation, after 1500 days, an excess pore pressure of 32 kPa exists around 10–15m.

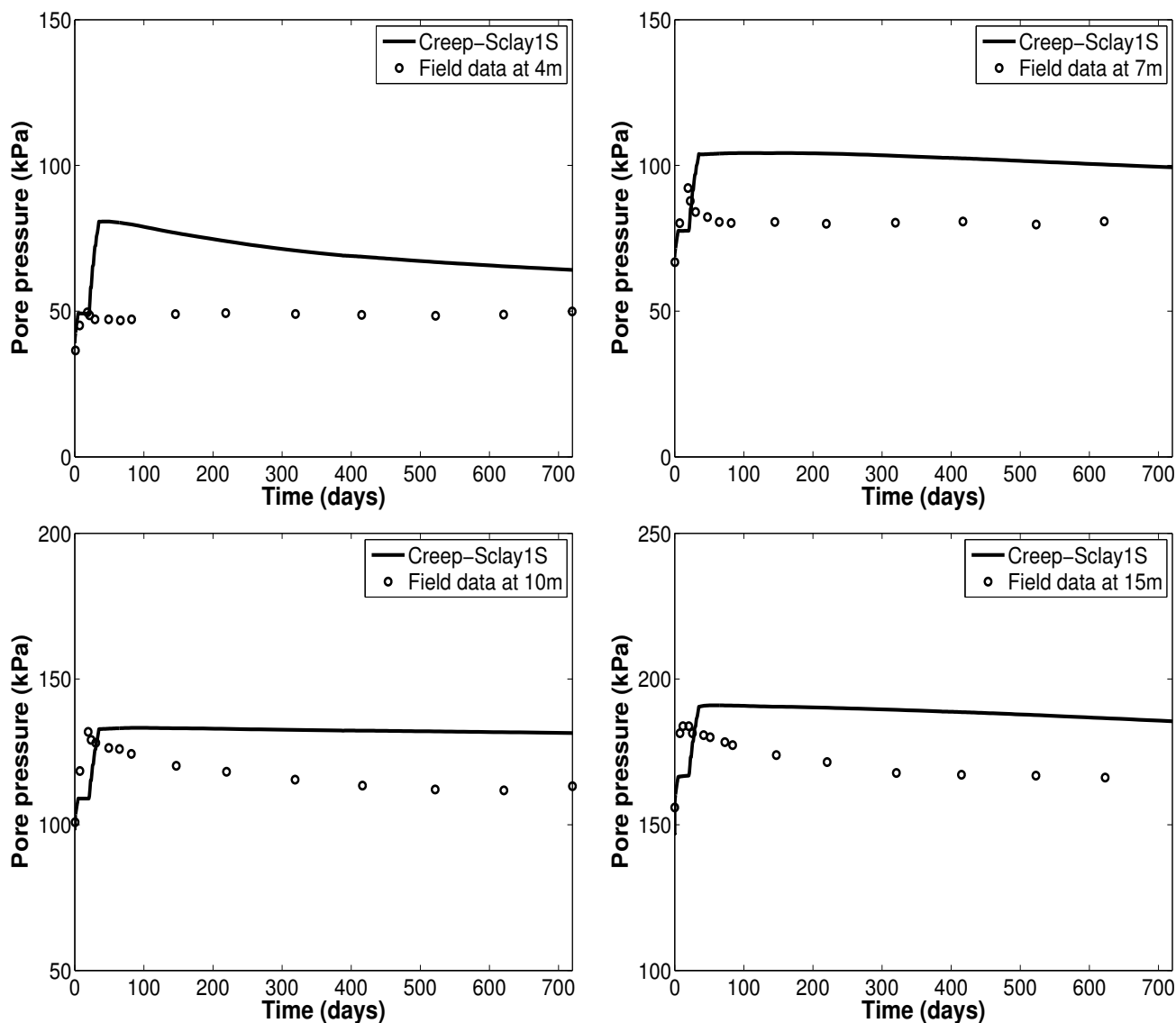


Figure 7.5: Comparison of simulation with field data for pore pressure measurements at different depths in Haarajoki

Figure 7.6 shows the distribution of pore pressures in soil after 1500 days. Maximum pressure is located around 10 - 15m under embankment centre line. This is reasonable since lower permeability values are assigned with increasing depth creating a proportional gradient in dissipation rate.

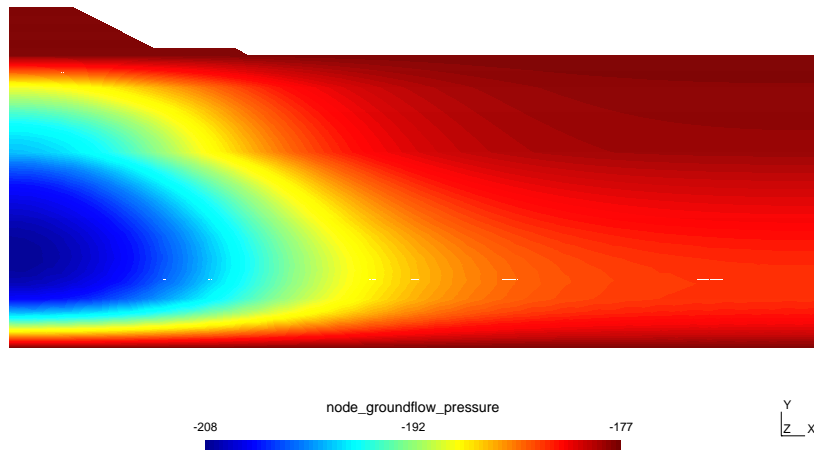


Figure 7.6: Simulation result of groundflow pressure distribution after 1500 days generated in Gmsh for Haarajoki soil

In order to perform an efficient validation for Creep-Sclay1S model, the embankment is simulated for a long period to investigate creep behaviour in soft soil. Figure 7.7 shows the Creep-Sclay1S simulation for settlement along embankment centre line after 1000 years. This simulation is done to investigate the creep rate in different time period to understand the effect of visco-plastic multiplier in Creep-Sclay1S model. From Figure 7.7, a creep rate of 38 mm/year is observed in the initial 14 years after embankment construction which gradually reduces to 1.85 mm/year between 41 and 100 years. Finally, the creep rate reaches to 0.075 mm/year between 100 and 1000 years showing that maximum deformation, of 1m, has reached at 100 years with negligible creep afterwards.

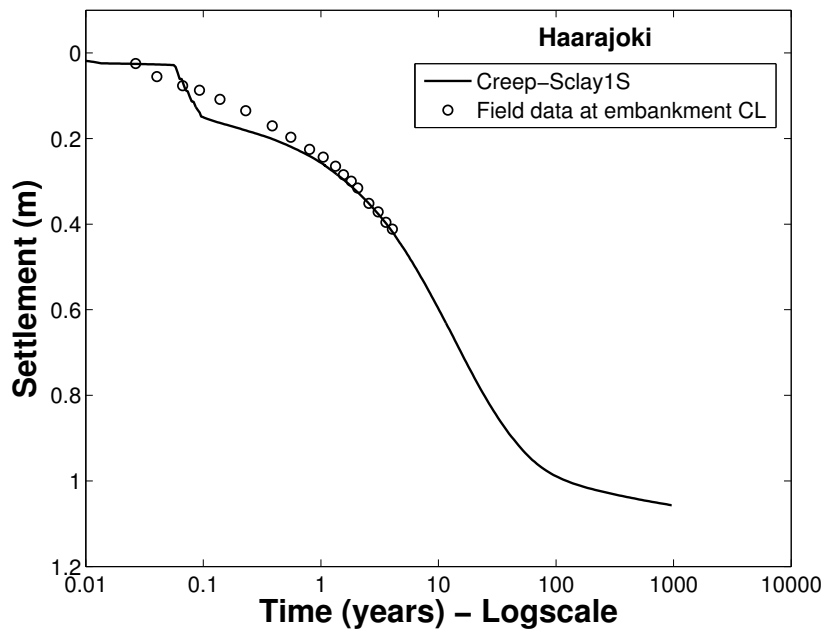


Figure 7.7: Creep-Sclay1S prediction for settlement along embankment centre line at Haarajoki after 1000 years

Figures 7.8 and 7.9 show the lateral deformation predicted from the simulation at 4m and 9m right of embankment CL after 1 and 3 years. Field measurements show less deformation in soft soil layer than simulation. The deformation of dry crust layer at 4m right of embankment CL after 1 and 3 years show good accordance with field values. Predictions are exaggerated at 9m right of embankment CL which is attributed mainly due to stiffness properties of dry crust and soft soil.

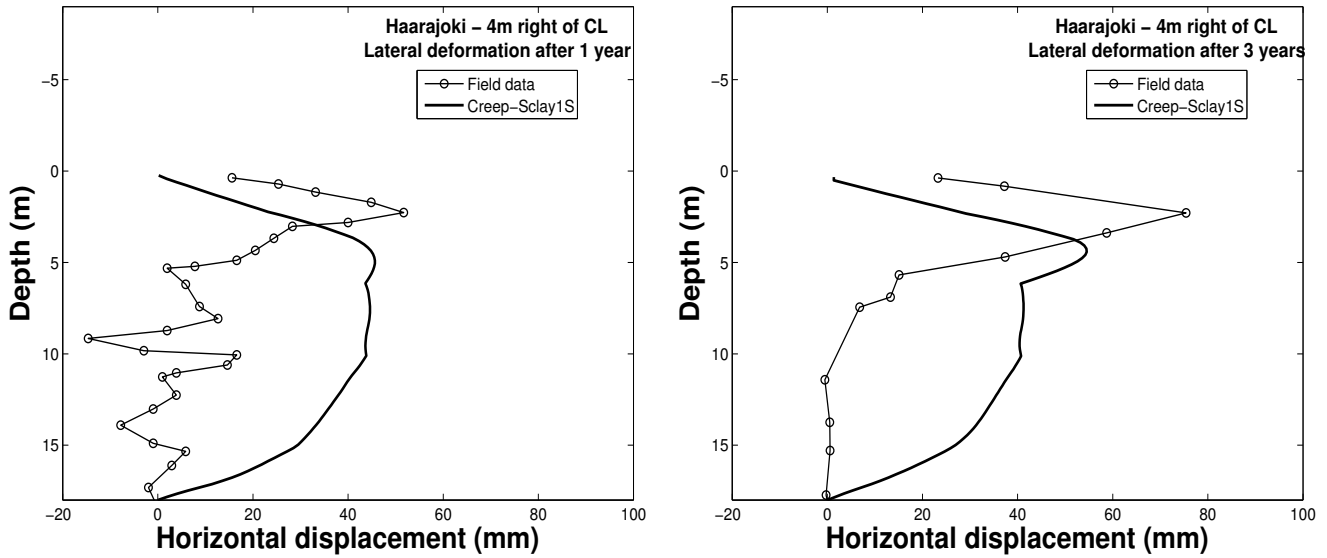


Figure 7.8: (a) Comparison of Creep-Sclay1S simulation with field data for lateral displacement along 4m right of embankment centre line after 1 year (b) after 3 years

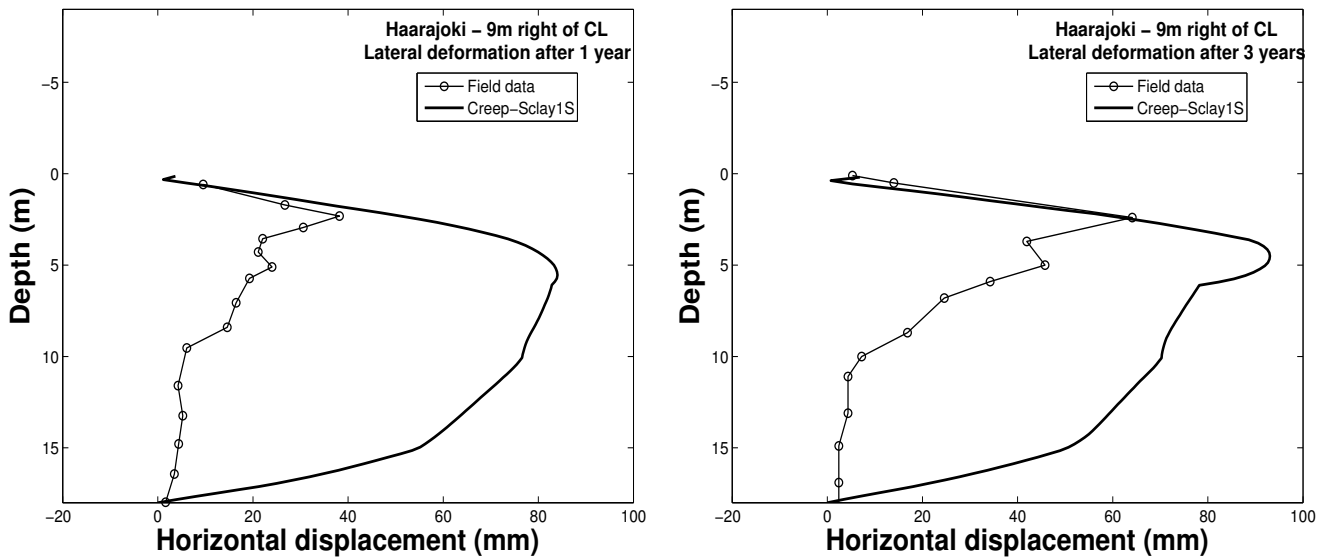


Figure 7.9: (a) Comparison of Creep-Sclay1S simulation with field data for lateral displacement along 9m right of embankment centre line after 1 year (b) after 3 years

In order to find the most critical region, the settlement and pore pressure with time is investigated for all depths. Figure 7.10 (a) shows the settlement along centre line of embankment at different period. It is clearly evident that dry crust layer is the most critical region followed

by initial soft soil layers from 2 - 5m. Figure 7.10 (b) shows the pore pressure variation with time. A peak in pore pressure value is observed after 35 days of embankment construction followed by a slow dissipation rate. Difference can be observed between the new equilibrium state attained after complete dissipation of pore pressures and the equilibrium state before embankment loading. Maximum pore pressures exist around 10 - 15m. Excess pore pressures are completely dissipated after 75 years.

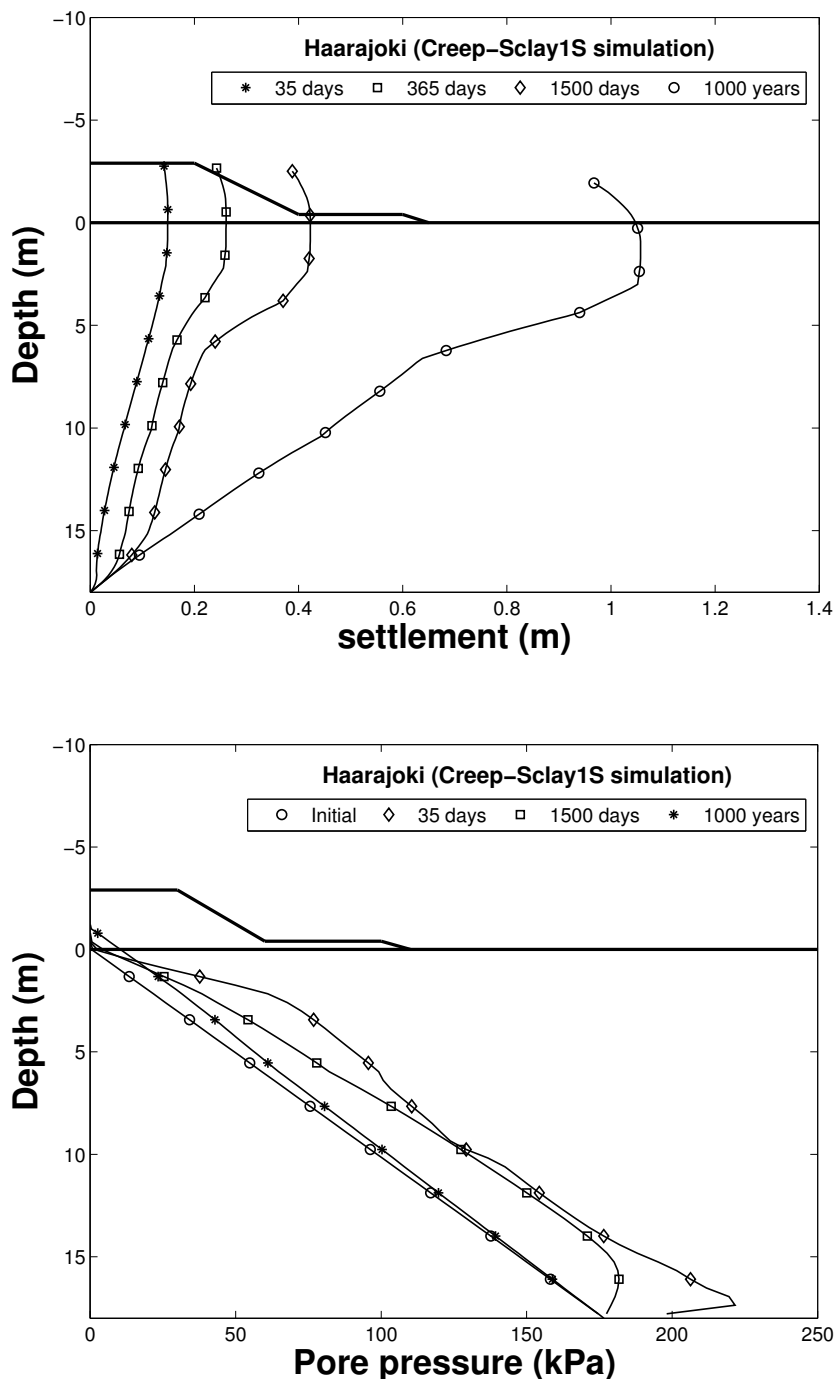


Figure 7.10: (a) Settlements along embankment centre line from simulation for different time period (b) Pore pressure distribution along embankment centre line from simulation for different time period

7.3 Drycrust sensitivity

The sensitivity of dry crust stiffness and its impact on the overall analysis is investigated. The dry crust layer (2m thick) is modelled with an extremely high stiffness and its effect on the analysis is investigated. Due to high stiffness, most of the load from embankment is uniformly distributed onto soft soil. As a consequence, the pore pressures are uniformly dissipated throughout the soil layer leaving excess pressure in the mid region (10 - 15m) as shown in Figure 7.11 (a). Due to this condition, settlement along centre line, 4m and 9m right of embankment exhibit same value as shown in Figure 7.11 (b).

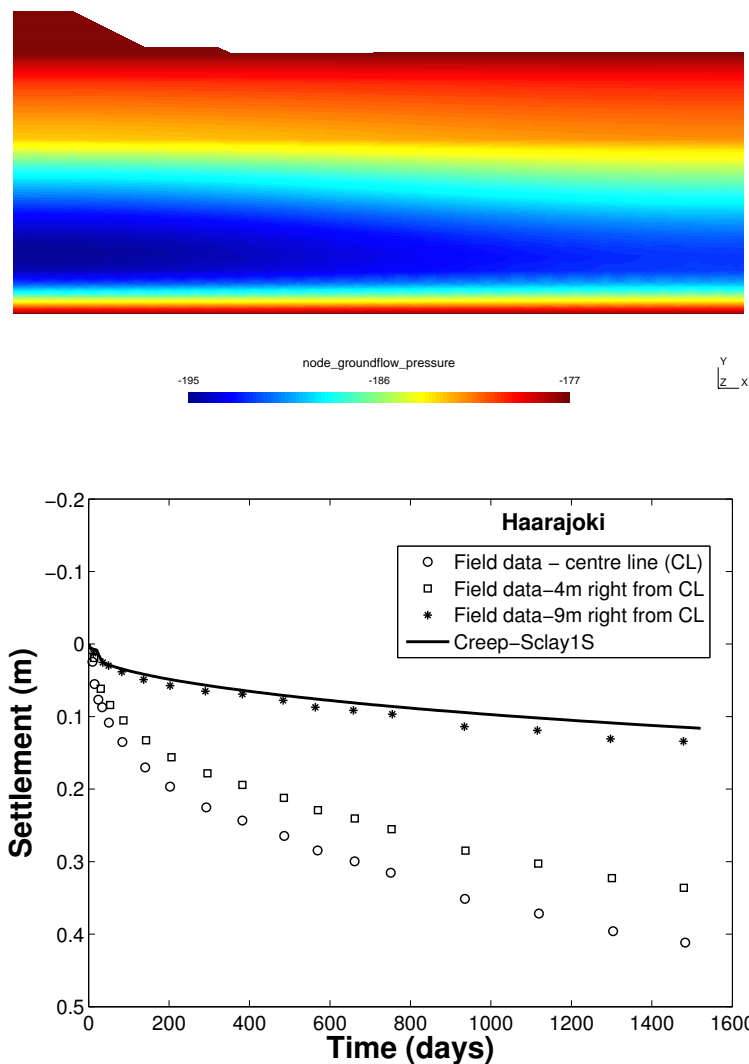


Figure 7.11: (a) Ground flow pressure after 1500 days from simulation with high stiff dry crust layer (b) Comparison of settlement from simulation of high stiff dry crust layer with field data

From Figure 7.12, A large difference in pore pressure development can be observed between analysis done in single dry crust layer with high stiffness and analysis done with three layered dry crust with varying stiffness. The margin of difference is around 50 % and highlights the amount of sensitivity the dry crust exerts on the overall simulation results.

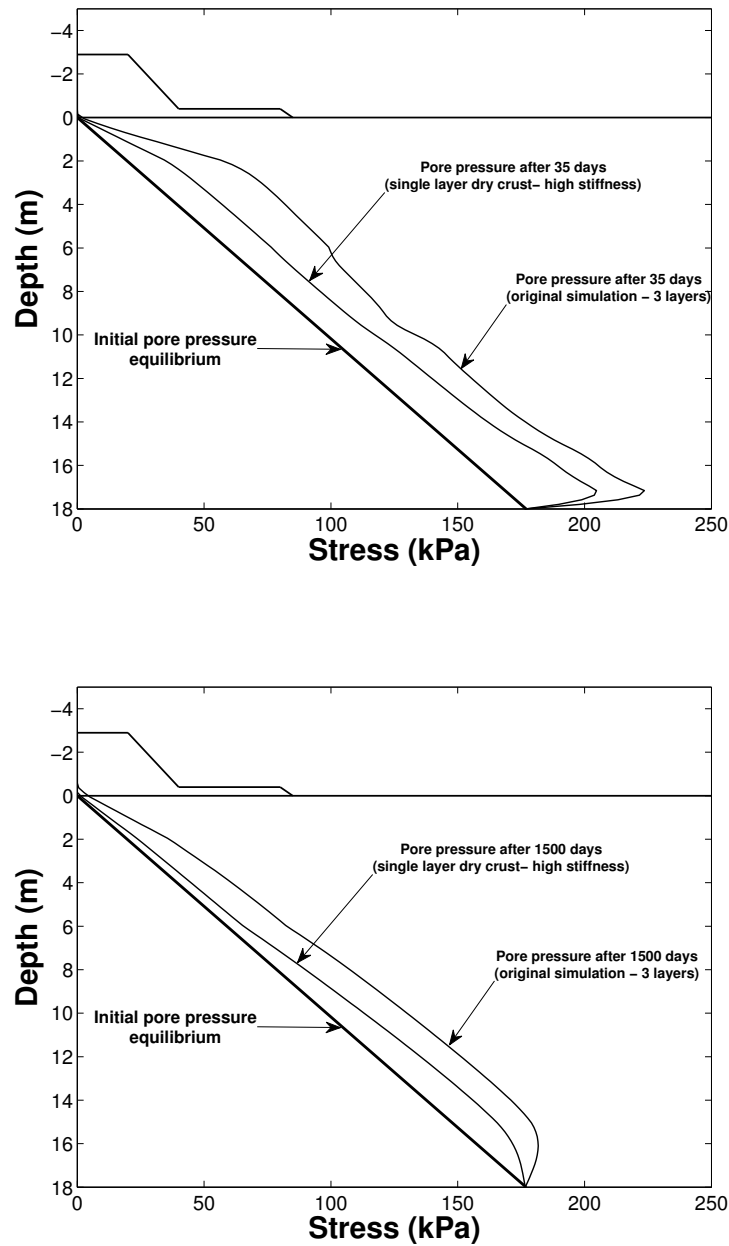


Figure 7.12: (a) Comparison of pore pressure distribution for high stiff dry crust layer analysis with original simulation after 35 days embankment construction (b) after 1500 days

It is evident from above results that the dry crust layer has a significant impact on the overall analysis of embankment loading. Hence, it should be analysed with a spatial differential stiffness model and be able to capture on-site OCR variation.

7.4 Permeability sensitivity

The effect of permeability on the embankment simulation is investigated. Analysis with different permeability values are simulated with the same parameters and boundary conditions as the original simulation. Figure 7.13 show the comparison of analyses between different permeability

values and field data for settlement under embankment centre line. It is evident that the difference is large ranging 28-35 % for the case of 5 times the original permeability value.

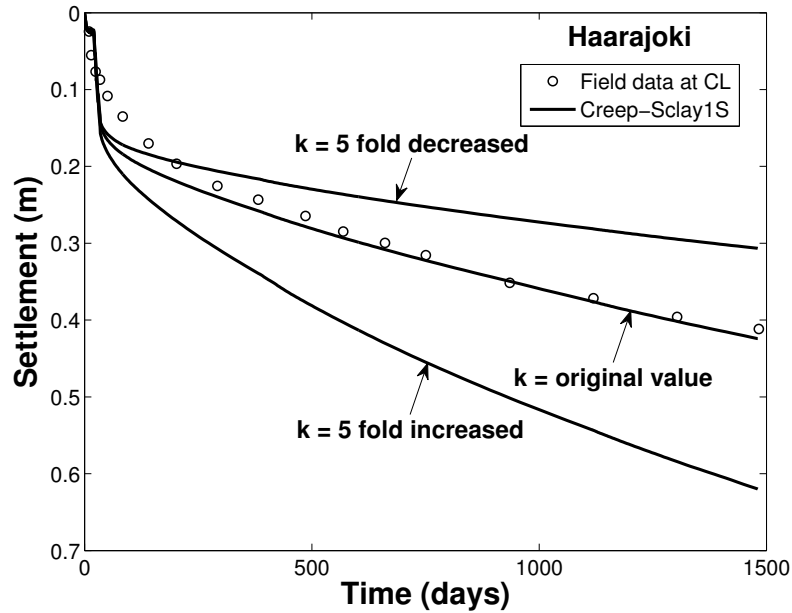


Figure 7.13: Comparison between analyses with different values of permeability with field data for settlement along embankment centre line

Figure 7.14 show the dissipation of pore pressures with time at 4m and 15m respectively. A faster dissipation rate can be observed for increased permeability values, however, the difference is larger at 15m depth due to proximity of drainage boundary compared to a depth of 4m.

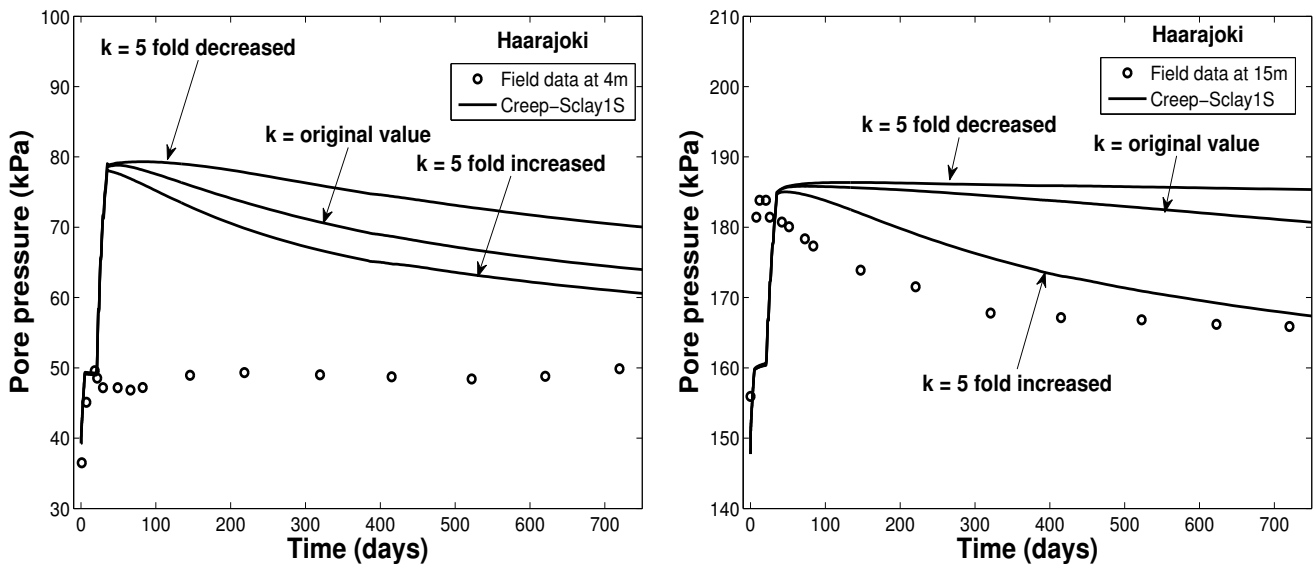


Figure 7.14: (a) Comparison of simulation with field data for pore pressure dissipation at depth of 4m (b) 15m

7.5 Load type sensitivity

An alternative analysis by using a line load instead of an embankment material is investigated using same parameters to analyse difference between a compliant and stiff element on the surface. The magnitude of line load is increased in stages similar to Haarajoki embankment construction. Figure 7.15 shows the comparison of settlement prediction between analysis with line load and embankment material. The settlement predicted is higher with line load analysis along embankment centre line whereas it is contrary at 9m away from centre line. It is evident that load is more concentrated near the centre line when analysed with line load compared to embankment material leading to excess deformation in that area.

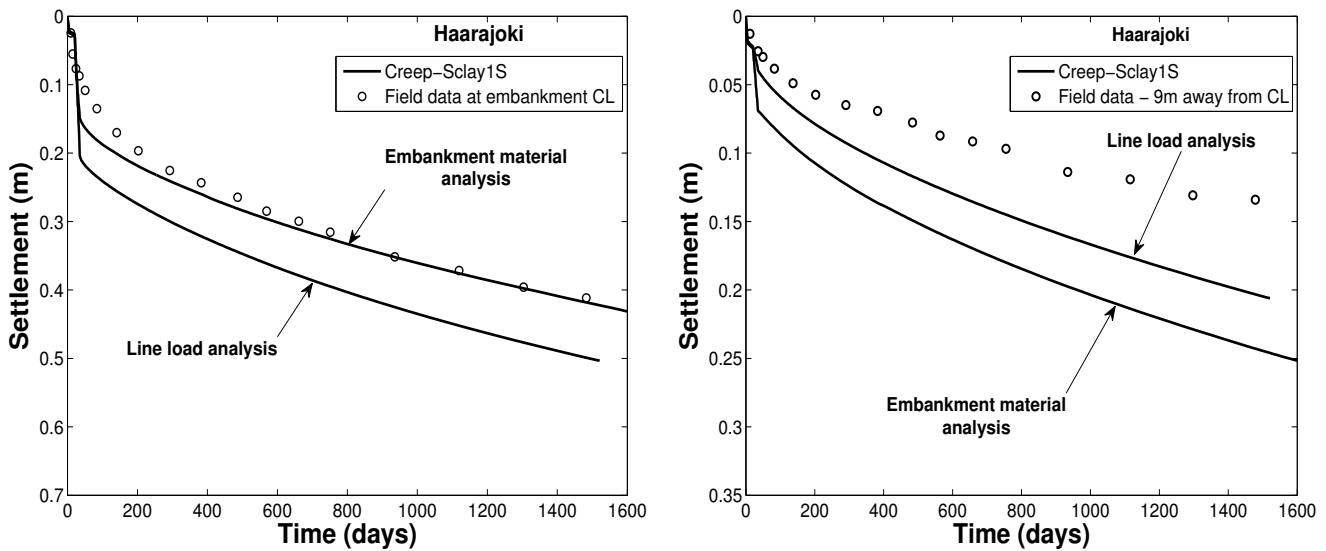


Figure 7.15: (a) Comparison between line load and embankment material analysis with field data for settlement along embankment centre line (b) 9m right of embankment centre line

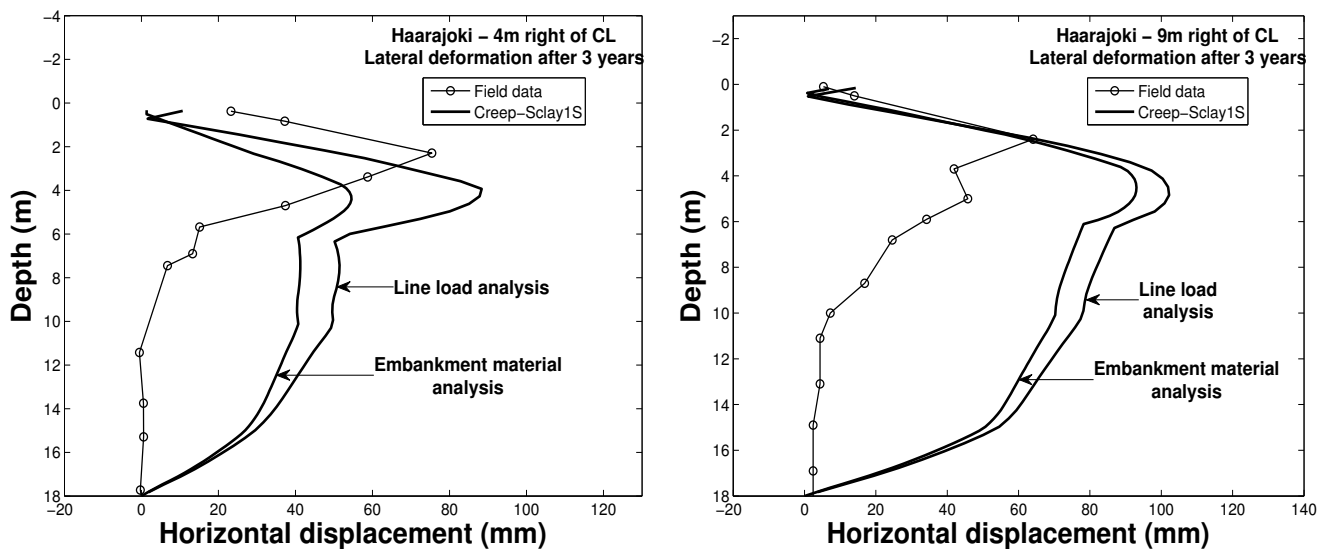


Figure 7.16: (a) Comparison of line load with embankment material analysis for lateral deformations at 4m right of embankment centre line (b) 9m right of embankment centre line

Lateral deformations are exaggerated in line load analysis due to excess deformation along centre line as shown in Figure 7.16. It is clear that using line load as an alternative to embankment material is not advisable.

There are no significant changes in pore pressures between the two analyses with margin of difference ranging between 5 - 9 kPa. The only difference is that pore pressures are higher near the surface from line load analysis due to higher concentration of stress along embankment centre line. The excess pore pressure after 1500 days is similar for both the analysis as shown in Figure 7.18 (b).

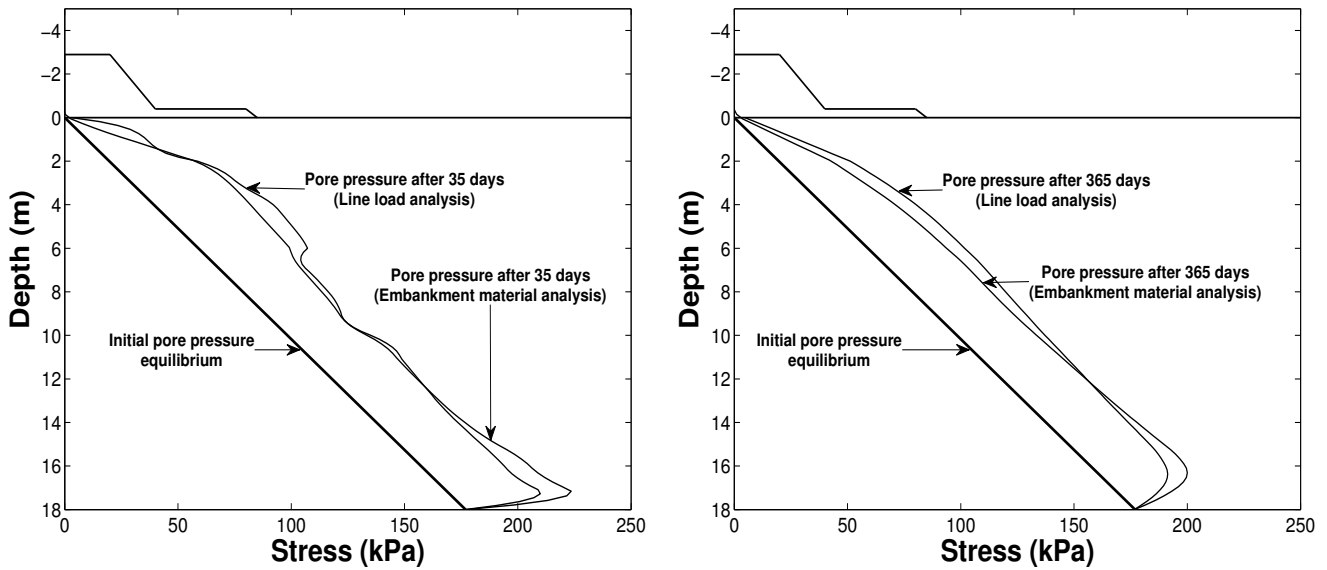


Figure 7.17: (a) Comparison between line load and embankment material analysis for pore pressure distribution after 35 days embankment construction (b) after 365 days

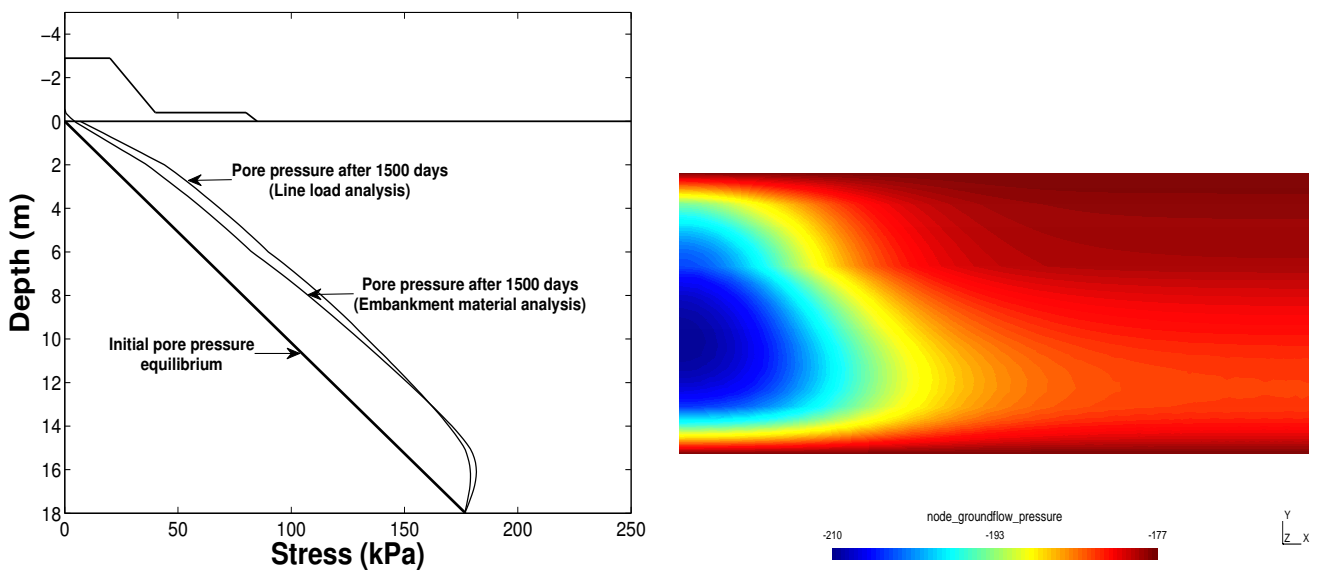


Figure 7.18: (a) Comparison between line load and embankment material analysis for pore pressure distribution after 1500 days (b) Simulation from line load analysis for ground flow pressure after 1500 days in Haarajoki

7.6 Geometry sensitivity

The sensitivity of the geometry on the analysis is investigated. The length of geometry is reduced from 50m to 20m and 15m to check the effect of boundary on result. Figure 7.19 (a), shows the difference in settlement prediction between different geometries simulated with Creep-Sclay1S model. The settlement, after 1500 days along embankment CL, from 20m and 15m geometry is predicted as 0.385m and 0.335m respectively whereas for 50m geometry, the settlement predicted is 0.422m. This difference when scaled in long term analysis such as 10 or 20 years, the accumulation of error can severely distort the prediction. Lateral displacements are affected significantly by the boundary as shown in Figure 7.19.

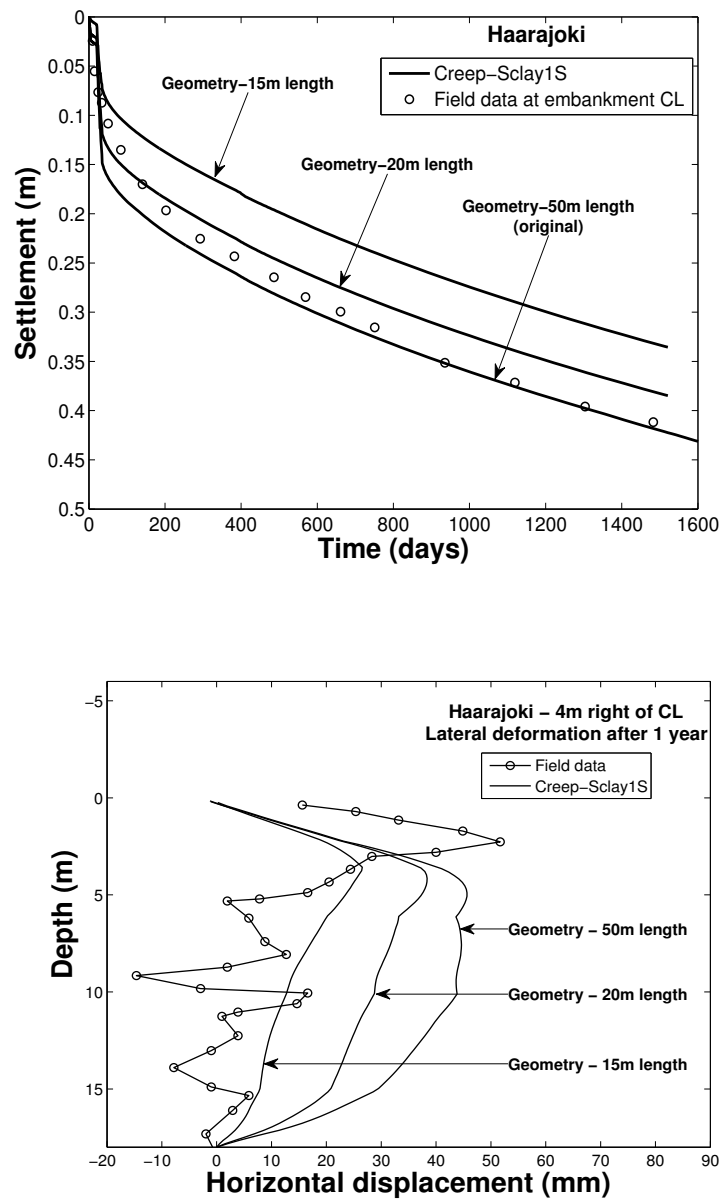


Figure 7.19: (a) Comparison of Creep-Sclay1S simulation of different geometries with field data for settlement along embankment centre line (b) Lateral deformation after 1 year for different geometries at 4m right of embankment centre line

There is no significant difference in pore pressures between different geometries as shown in Figure 7.20. Excess pore pressure of 31 kPa exists after 1500 days around 10-15m.

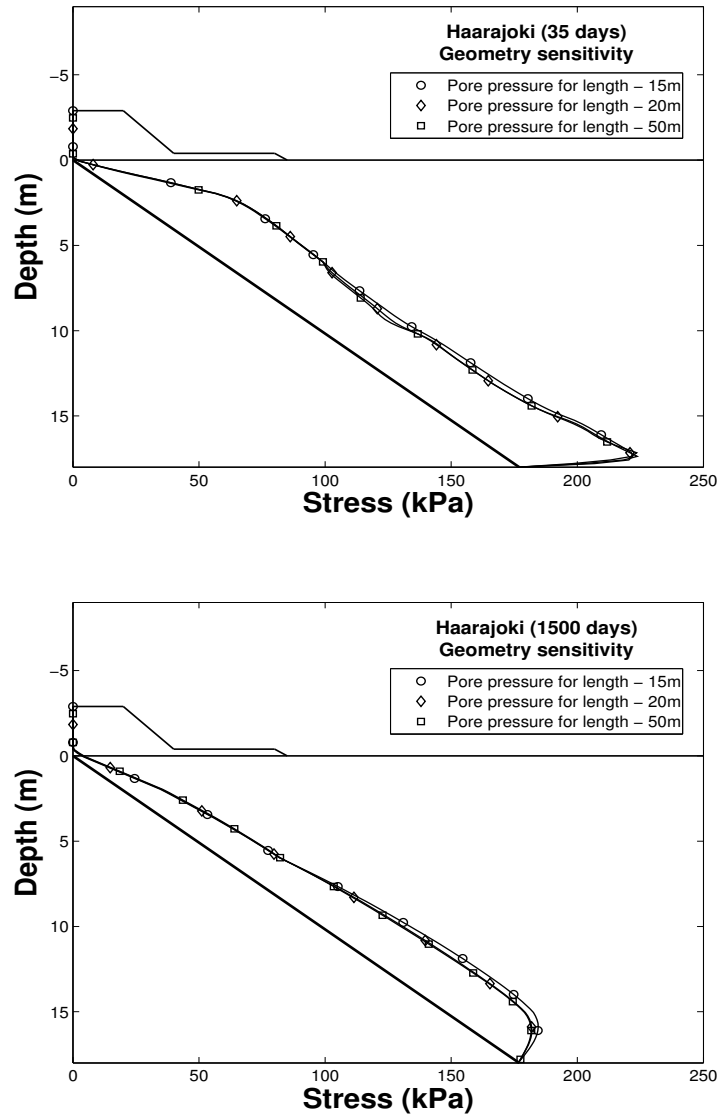


Figure 7.20: (a) Comparison of pore pressure distribution of different geometries after 35 days embankment construction (b) after 1500 days

7.7 Mesh sensitivity

The effect of number of elements on the accuracy of result is investigated. A Geometry with 50m length is chosen for this analysis to avoid boundary effects and meshed in two separate files with 22000 elements and 900 elements for comparison. Figure 7.21 (a) shows the comparison between Creep-Sclay1S simulation with 900 and 22000 elements for settlement along embankment centre line at Haarajoki. The difference between the two analysis is not very large and the margin of error is around 5 %. This can be due to second order elements used in this analysis. In case of first order elements, a large deviation may be expected, however, due to incorporation of flow analysis, first order elements cannot be used.

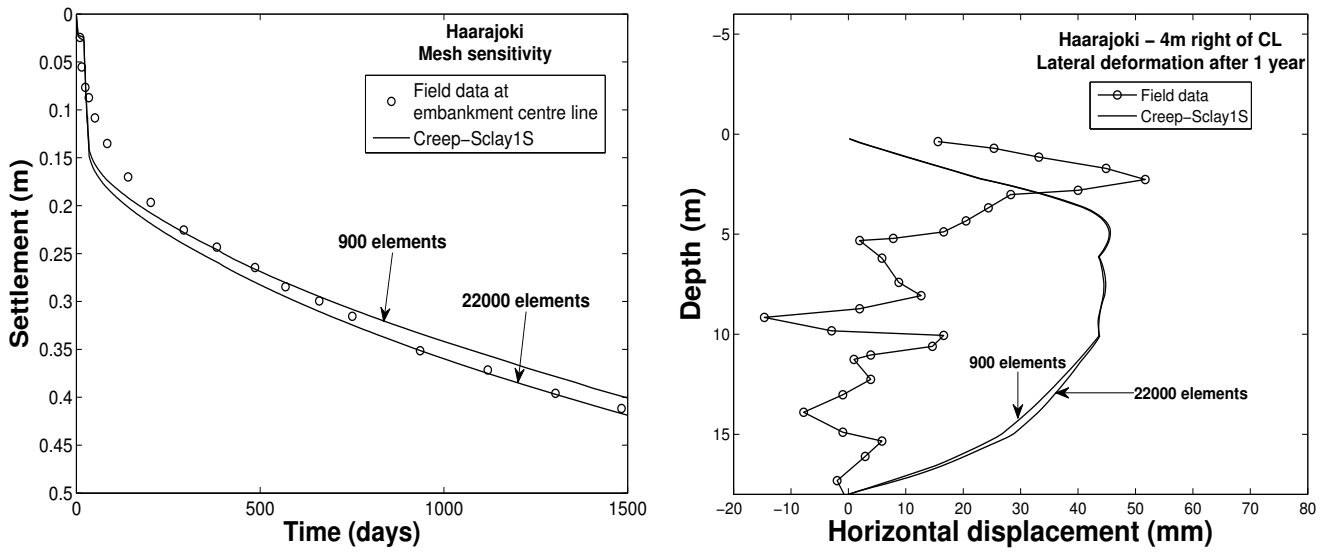


Figure 7.21: (a) Comparison of simulation with 900 and 22000 elements with field data for settlement along embankment CL (b) for lateral displacement at 4m right of embankment CL

Figure 7.22 shows the pore pressure variation with time for simulation with 900 and 22000 elements. After 35 days of embankment construction, the peak pore pressure value for 22000 elements exhibit 25 kPa more at the bottom layer than 900 elements. A difference in pore pressures of 10 kPa at bottom layer can be observed between the two analysis after 1 year.

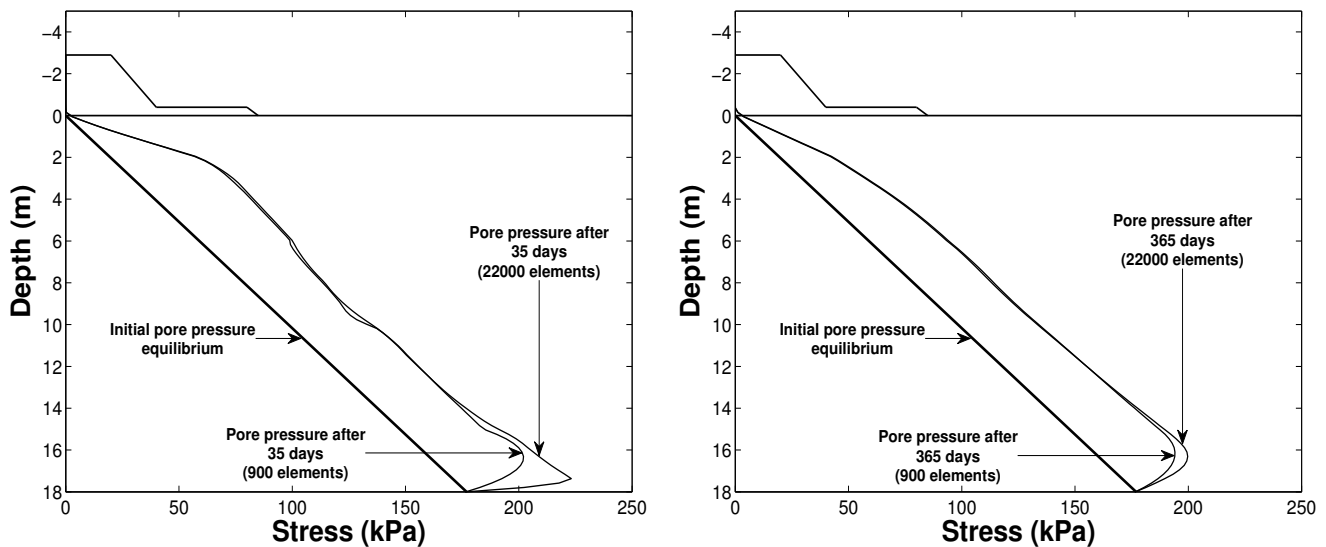


Figure 7.22: (a) Comparison of simulation with 900 and 22000 elements for pore pressure behaviour after 35 days embankment construction (b) after 365 days

From the above results, the number of elements does have a marginal impact on the result. However, the margin of error can vary for different geometry and boundary condition making it a case specific problem. Hence a mesh sensitivity analysis should be investigated to avoid a possible large deviation in any analysis.

8 Conclusions & Recommendations

8.1 Conclusions

The thesis presents novel routines implemented in MATLAB for automated determination of the model parameters of an advanced constitutive model for soft soils. In this case the CREEP-SCLAY1S model is selected as the benchmark case is a test embankment with long-term monitoring (4 years) on soft sensitive clay.

In addition to the strength and stiffness parameters (M , κ , λ_i) also the creep index (μ_i^*) and pre-consolidation pressure are directly evaluated from the laboratory data (1D incremental oedometer test, anisotropically consolidated undrained and drained triaxial tests in compression). The processing showed that with some non-linear interpolation data with a limited number of data points and noise still could be adequately processed. The batch processing required little additional user intervention to complete the task properly. At this stage of the research the additional hardening parameters were set to best practice recommended values as those doesn't seem to affect the results significantly. The initial K_0 distribution is also determined from the well known OCR relations and the strength properties.

The element level simulations with the newly derived model parameters have first been shown to be in close agreement laboratory test data for the 1D incremental pedometer test and the drained triaxial test. On the other hand the CRS compression tests showed larger discrepancies resulting from the complexities of the CRS test that require coupled analysis and rate dependency in the constitutive model as well as high quality samples which were not available.

Furthermore, the new model parameter set is shown to lead to the best predictions of the test embankment so far. The predictions are in good accordance with field measurements for settlement and pore pressure distribution. The most influential parameters for embankment simulation includes the permeability, dry crust stiffness and modified creep index. The settlements are exaggerated when creep index values corresponding to in-situ stress condition are used. This value does not have a significant impact on the element test simulations due to short duration of tests and smaller domain. Dry crust has been found to be the most sensitive layer followed by initial soft soil layer (2-4m depth) which is the same as field observations. It is recommended to use a spatial differential stiffness model for dry crust analysis with proper capturing of OCR variation with strain increment.

It can be concluded that the performance of Creep-Sclay1S model combined with accurate parameter determination is efficient in capturing experimental and field behaviour of soft soil.

8.2 Recommendations

The following recommendations are proposed for further research:

- Automated model parameter derivation should be the de facto approach for numerical modellers to increase the efficiency and reduce the human bias in the model parameter set.
- Improved modelling and characterisation of the in-situ dry crust is paramount for increasing the accuracy of predictions of stability and safety of structures on and/or in soft soils. Given the complexity of the material, at first in-situ plate load tests or strength assessment should be considered before systematically studying the behaviour in the laboratory (if sampling is possible at all).
- In cases where advanced constitutive models require validation against high quality data from advanced physical model tests on natural soils (these include field scale experiments) it is recommend to complement the test instrumentation with site investigation on high quality samples and using non standard stress path testing to capture all intricate features of the constitutive model used.
- Although the current rate dependent models seem to be a genuine improvement upon the previous generations, still additional validation and modification (unloading/reloading) should be carried out.

References

- Berre, T. (2013). Test fill on soft plastic marine clay at Onsøy in Norway. *Canadian Geotechnical Journal* (ahead of print).
- Björk, S. (2008). The late Quaternary development of the Baltic Sea, 398–407.
- Brinkgreve, R. B. J., Broere, W., and Waterman, D. (2008). PLAXIS-2D (Version 9.0).
- Casagrande, A. (1936). The determination of the preconsolidation load and its practical significance. *Proceedings of the 1st International Conference on Soil Mechanics and Foundation Engineering* 1.
- Clayton, L. et al. (1991). Glaciation of Wisconsin.
- Cundy, M. and Neher, H. (2003). Numerical analysis of a test embankment on soft ground using an anisotropic model with destructuration. *Proc., Int. Workshop on Geotechnics of Soft Soils-Theory and Practice, Noordwijkerhout, The Netherlands*, 265–270.
- Darcy, H. (1956). Détermination des lois d'écoulement de l'eau à travers le sable. *Les Fontaines Publiques de la Ville de Dijon*, 590–594.
- Dijkstra, J. and Karstunen, M. (2014). *Survey of benchmark field tests for validation of creep models*. Tech. rep. Chalmers University of Technology.
- Forsström, L. and Eronen, M. (1985). Flandrian and Eemian shore levels in Finland and Adjacent Areas - a Discussion, 135–145.
- Gens, A. (1982). Stress-strain and strength characteristics of a low plasticity clay. PhD thesis. *Gmsh reference manual* (2015). Version 2.9.3. URL: <http://geuz.org/gmsh/doc/texinfo/gmsh.pdf>.
- Grimstad, G. et al. (2010). Modelling creep and rate effects in structured anisotropic soft clays. *Acta Geotechnica*. DOI: 10.1007/s11440-010-0119-y.
- Grimstad, G. and Degago, S. A. (2010). A non-associated creep model for structured anisotropic clay (n-SAC).
- Grimstad, G. et al. (2008). Modelling creep and rate effects using the time resistance concept in a model for anisotropy and destructuration. *Nordic Geotechnical Meeting, Sandefjord, Norway*, 195–202.
- Holtz, R. D. and Kovacs, W. D. (1981). *An Introduction to Geotechnical Engineering*. Prentice Hall. ISBN: 0-13-484394-0.
- Jaky, J. (1948). Pressure in Silos. *International conference on Soil mechanics and Foundation engineering, Rotterdam, The Netherlands*, 103–107.
- Janbu, N. (1969). The resistance concept applied to deformation of soils. *Proceedings of the 7th international conference on soil mechanics and foundation engineering, Mexico city*, 191–196.
- Karstunen, M. et al. (2005). Effect of Anisotropy and Destructuration on the Behaviour of Murro Test Embankment. *International Journal of Geomechanics*, 87–97.
- Karstunen, M. et al. (2013). Modelling rate-dependent behaviour of structured clays. *International Conference on Installation Effects in Geotechnical Engineering*.
- Knappett, J. A. and Craig, R. F. (2014). *Craig's Soil Mechanics*. Spon Press. ISBN: 978-0-415-56126-6.
- Kulhawy, F. H. and Mayne, P. W. (1990). *Manual on estimating soil properties for foundation design*. Electric Power Research Institute Palo Alto, CA.
- Leoni, M. et al. (2008). Anisotropic creep model for soft soils. *Géotechnique*, 215–226. DOI: 10.1680/geot.2008.58.3.215.

- MATLAB manual* (2008). *Ordinary Differential Equations*. Version 7.8. Mathworks. URL: <http://www.mathworks.com/access/helpdesk/help/techdoc/ref/ode45.html>.
- Muir Wood, D. (1991). *Soil behaviour and critical state soil mechanics*. Cambridge University Press. ISBN: 0-521-33782-8.
- Muir Wood, D. (2010). *Soil Mechanics - a one dimensional introduction*. Cambridge University press. ISBN: 978-0-521-18730-5.
- NEEM (2013). Eemian interglacial reconstructed from a Greenland folded ice core. *Nature*, 489–493. DOI: 10.1038/nature11789.
- Nenonen, J. and Portaankorva, A. (2009). The Geology of the Lakeland Finland area.
- Näätänen, A., Vepsäläinen, P., and Lojander, M. (1998). Finite element calculations on Haarajoki test embankment. *Proc., 4th European Conf. on Numerical Methods in Geotechnical Engineering (NUMGE), Udine, Italy*, 151–160.
- Olsson, M. (2010). “Calculating long term settlements in soft clays - with special focus on Gothenburg region”. Licentiate Thesis. Chalmers University of Technology, Sweden.
- Perzyna, P. (1963). Constitutive equations for work hardening and rate sensitive plastic materials. *Proc., Vibration problems*.
- Perzyna, P. (1966). Fundamental problems in viscoplasticity. *Advanced applied mechanics*.
- Rouainia, M. and Muir Wood, D. (2000). A kinematic hardening model for natural clays with loss of structure. *Géotechnique* **50(2)**.
- Schmertmann, J. H. (1953). Estimating the true consolidation behaviour of clay from laboratory test results, 1–26.
- Sivasithamparam, N. (2012). Modelling Creep behaviour of Soft Soils.
- Stapelfeldt, T., Vepsäläinen, P., and Yin, Z.-Y. (2009). Numerical modelling of a Test embankment on soft clay improved with vertical drains.
- Sällfors, G. (1975). Preconsolidation pressure of soft, high plastic clays. PhD Thesis.
- Taylor, D. W. (1948). *Fundamentals of soil mechanics*.
- Tochnog Professional User's manual* (2015). Version 22. FEAT-Finite Element Application Technology. URL: <http://www.feat.nl/manuals/user/user.pdf>.
- Vepsäläinen, P., Lojander, M., and Koskinen, M. (1997). Competition to calculate settlements at Haarajoki test Embankment. Competition programme, Competition materials, FinnRA, Finland.
- Wefer, G. et al. (2002). *Climate Development and History of the North Atlantic Realm*. Springer. ISBN: 978-3540432012.
- Wheeler, S. J. et al. (2003). An anisotropic elastoplastic model for soft clays. *Canadian Geotechnical Journal*, 403–418.
- Yildiz, A., Karstunen, M., and Krenn, H. (2009). Effect of Anisotropy and Destructuration on Behaviour of Haarajoki Test Embankment. *International Journal of Geomechanics*, 153–168. DOI: 10.1061/(ASCE)1532-3641(2009)9:4(153).
- Yin, Z.-Y., and Karstunen, M. (2011). Modelling strain rate dependency of natural soft clays combined with anisotropy and destructuration. *Acta mechanica solida sinica*, 216–230. DOI: 10.1016/S0894-9166(11)60023-2.
- Yin, Z.-Y. et al. (2011). Modelling Time Dependant Behaviour of Soft Sensitive Clay. *Journal of Geotechnical and Geo-Environmental engineering*, 1103–1113. DOI: 10.1061/(ASCE)GT.1943-5606.0000527.

A Instrument installation

A.1 Layout

The embankment layout is divided into station numbers fixed for each location as a reference point which are mentioned in the FinnRA report (Vepsäläinen et al. 1997). Field measurements for area without ground improvement are recorded at station number 35840 as shown in Figure A.1, where horizontal displacement, settlements and pore pressure measurements at different depth are available. Hence cross-section at station number 35840 has been considered for the analysis. Some of the instruments are installed before the construction of the embankment. Piezometers tips, inclinometer pipes, ground screws and extensometers are installed in areas without ground improvement before the construction of the work base. Settlement plates and pressure cells are installed in the same area simultaneously with spreading of the material. In areas with prefabricated vertical drains, all instruments are installed immediately after drain installation.

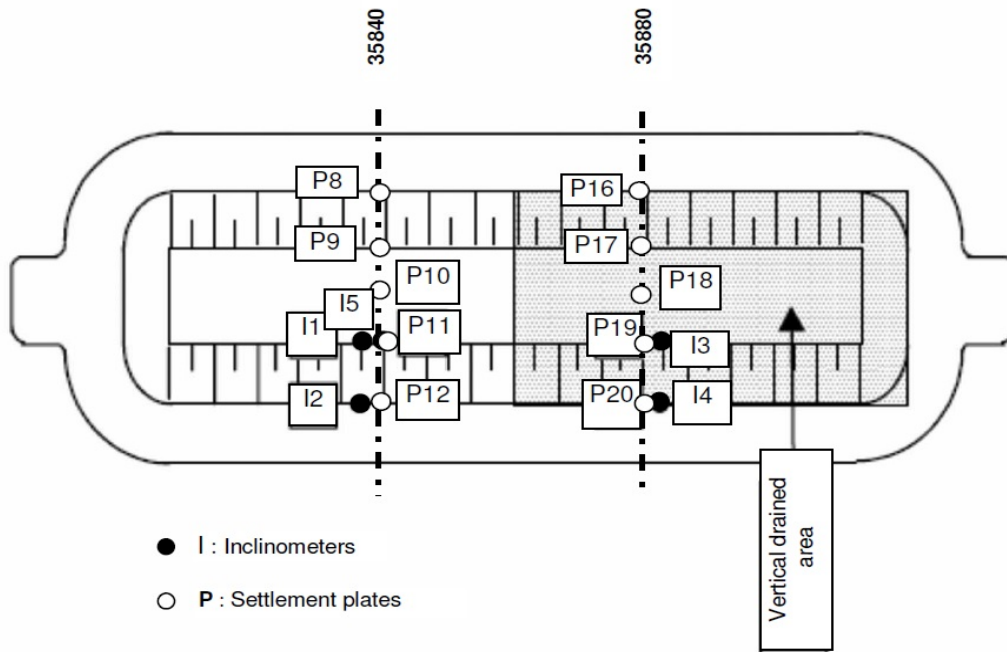


Figure A.1: Layout of Haarajoki test embankment with instrument positions (Yildiz et al. 2009)

A.2 Installation procedure

Piezometer tips are installed two months prior to the construction of the embankment to measure the initial pore water pressure. In ground improved areas, piezometer tips are installed in the centre of the square of vertical drain strips. Inclinometers are also installed two months prior to the embankment construction in unimproved areas and in ground improved areas it is installed immediately after vertical drain installation. The inclinometer pipes are extended as work on the embankment proceeds and installed in such a way that the bottom of the pipe is

anchored in dense moraine. Settlement plates of size 30cm x 30 cm and 1 cm thick are laid under the embankment to measure the overall settlement of the layer. The plates are installed immediately after drain installation in ground improved areas. The plates, connected to a rod, are laid in their assigned position in an excavated area of 0.5m x 0.5m of the work base and compacted as tight as possible. The vertical alignment of the rods are checked regularly during installation. The pressure cells are installed in the same procedure as for settlement plates. During construction of top surface of the embankment, settlement control points are installed by sinking half the length of a concrete pipe, 30 cm diameter, which is then filled with concrete and fastened with bolts on the top surface for determination of coordinates. By levelling the bolts in the control points, it is possible to observe the overall transition of the embankment. The installation schedule and location for all instruments are mentioned in the report provided by FinnRA (Vepsäläinen et al. 1997).

A.3 Instrument position

Table A.1: Location of instruments under Haarajoki embankment for unimproved ground

| Instruments | Reference ID | Station number | Location |
|--------------------|---------------------|-----------------------|-----------------|
| Settlement plates | P8 | 35840 | 9m left |
| | P9 | 35840 | 4m left |
| | P10 | 35840 | Centre line |
| | P11 | 35840 | 4m right |
| | P12 | 35840 | 9m right |
| Piezometer tips | B1 | 35837 | Centre line |
| | B2 | 35837 | Centre line |
| | B3 | 35837 | Centre line |
| | B4 | 35837 | Centre line |
| | B5 | 35837 | Centre line |
| Inclinometers | I1 | 35838 | 4m right |
| | I2 | 35838 | 9m right |
| | I5 | 35838 | 4m right |

B Embankment construction schedule

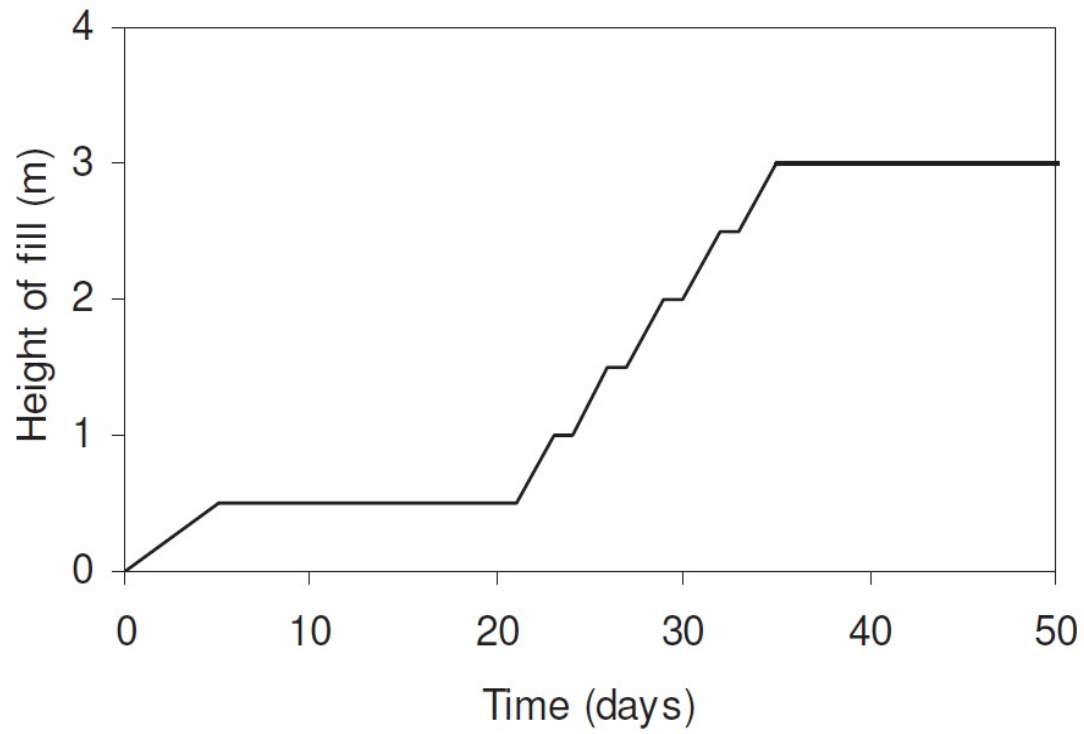
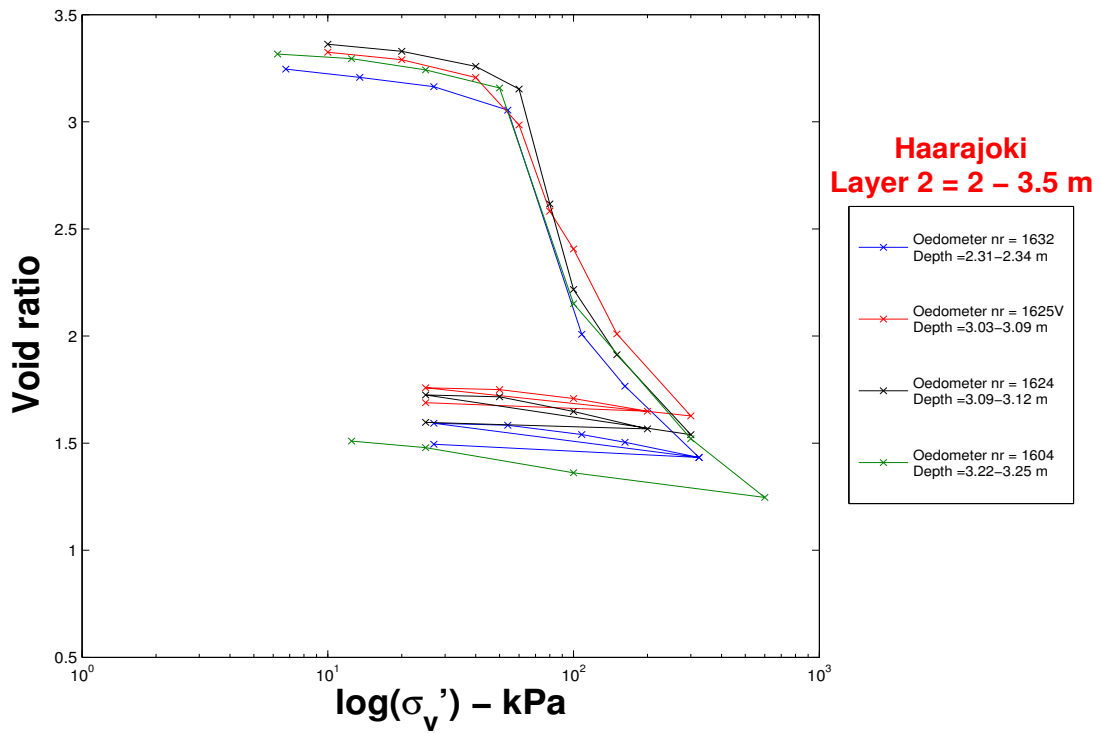
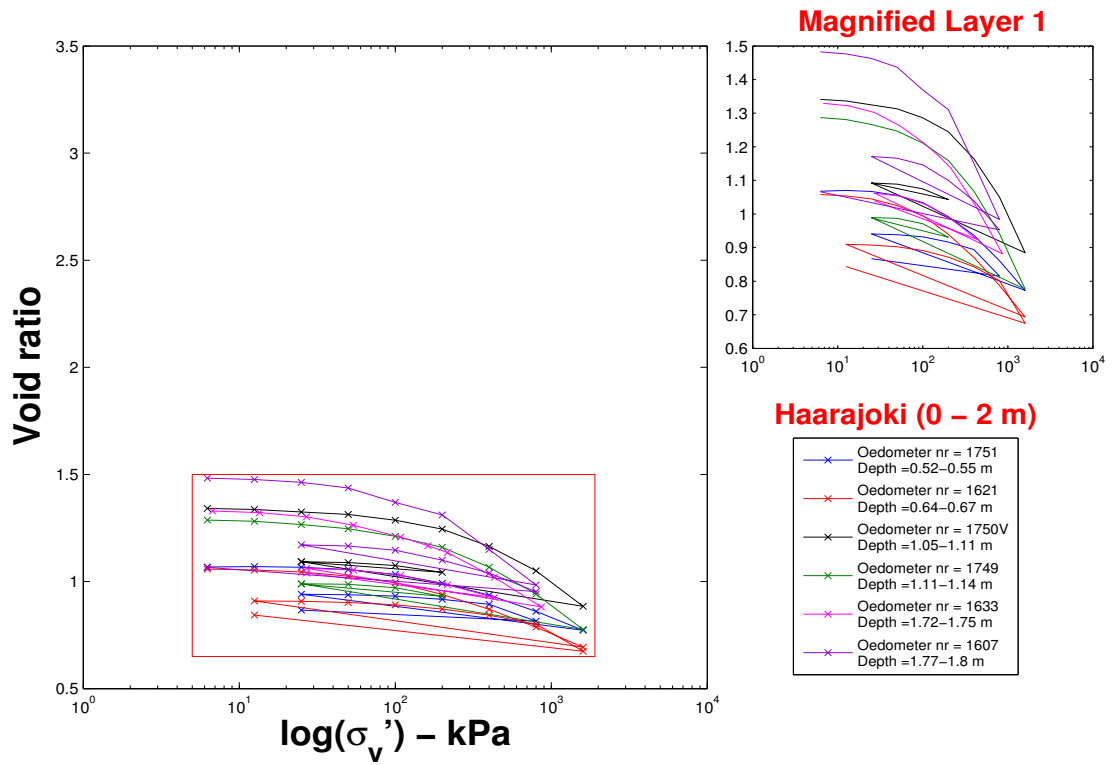
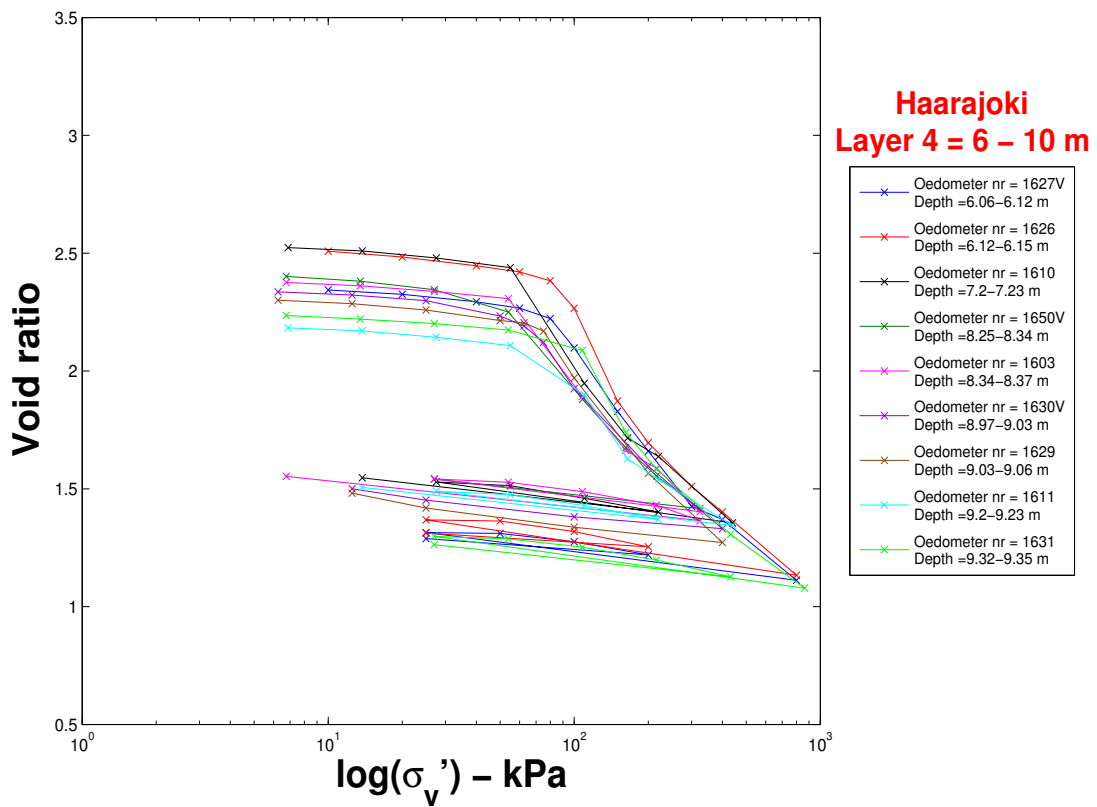
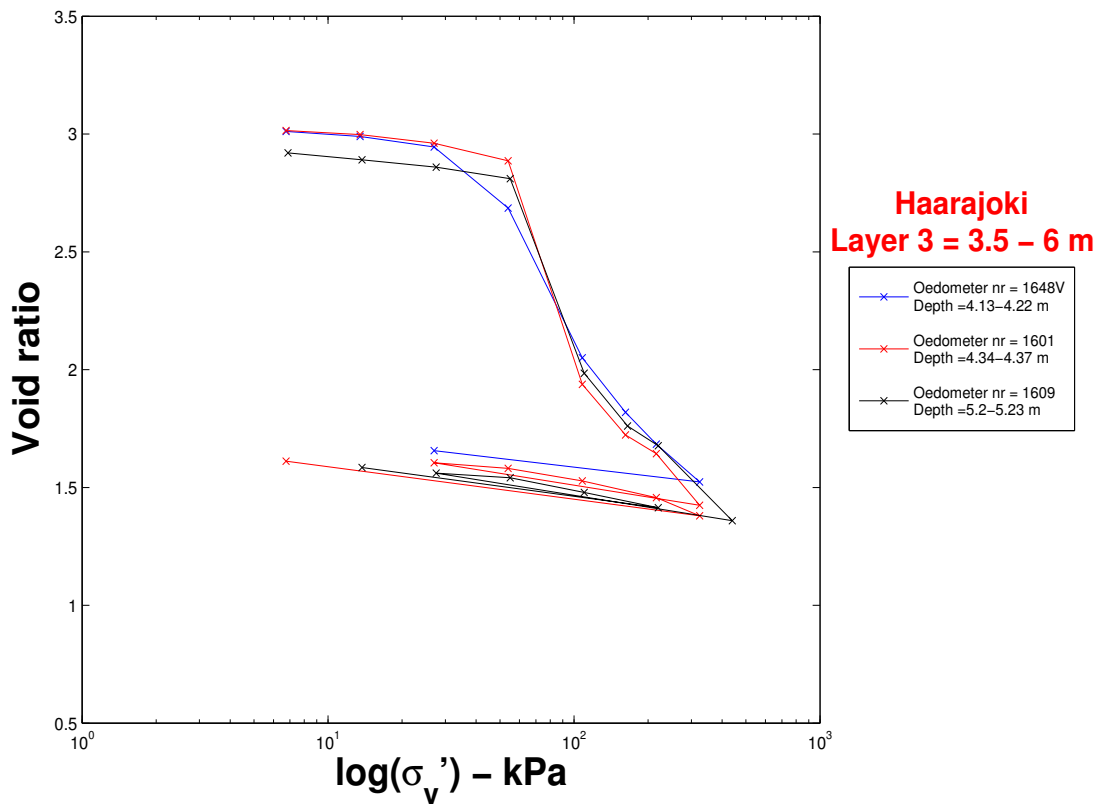
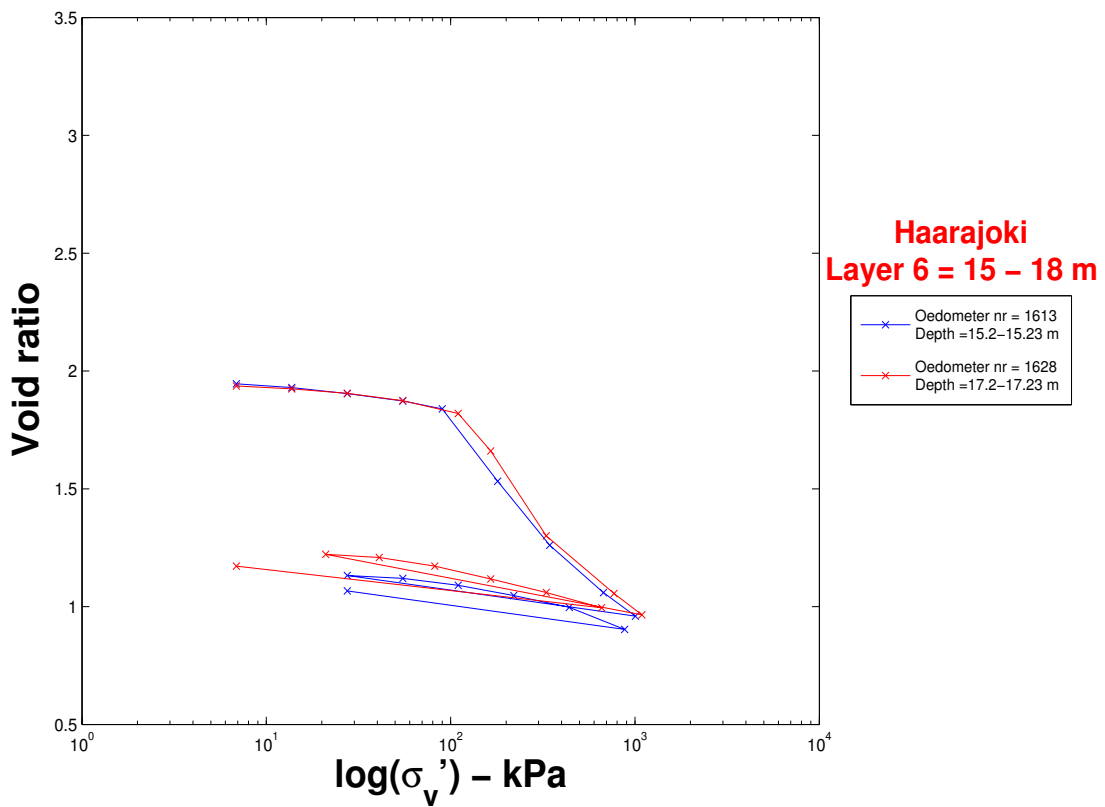
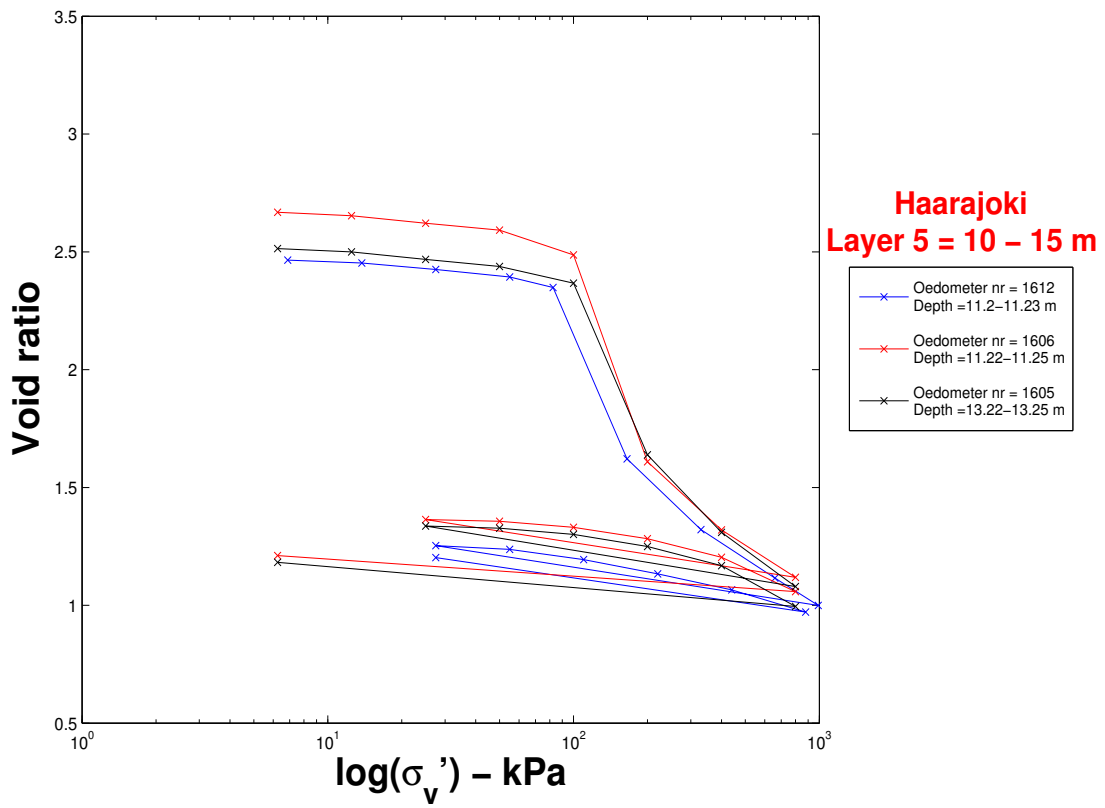


Figure B.1: Illustration of schedule for embankment construction at Haarajoki

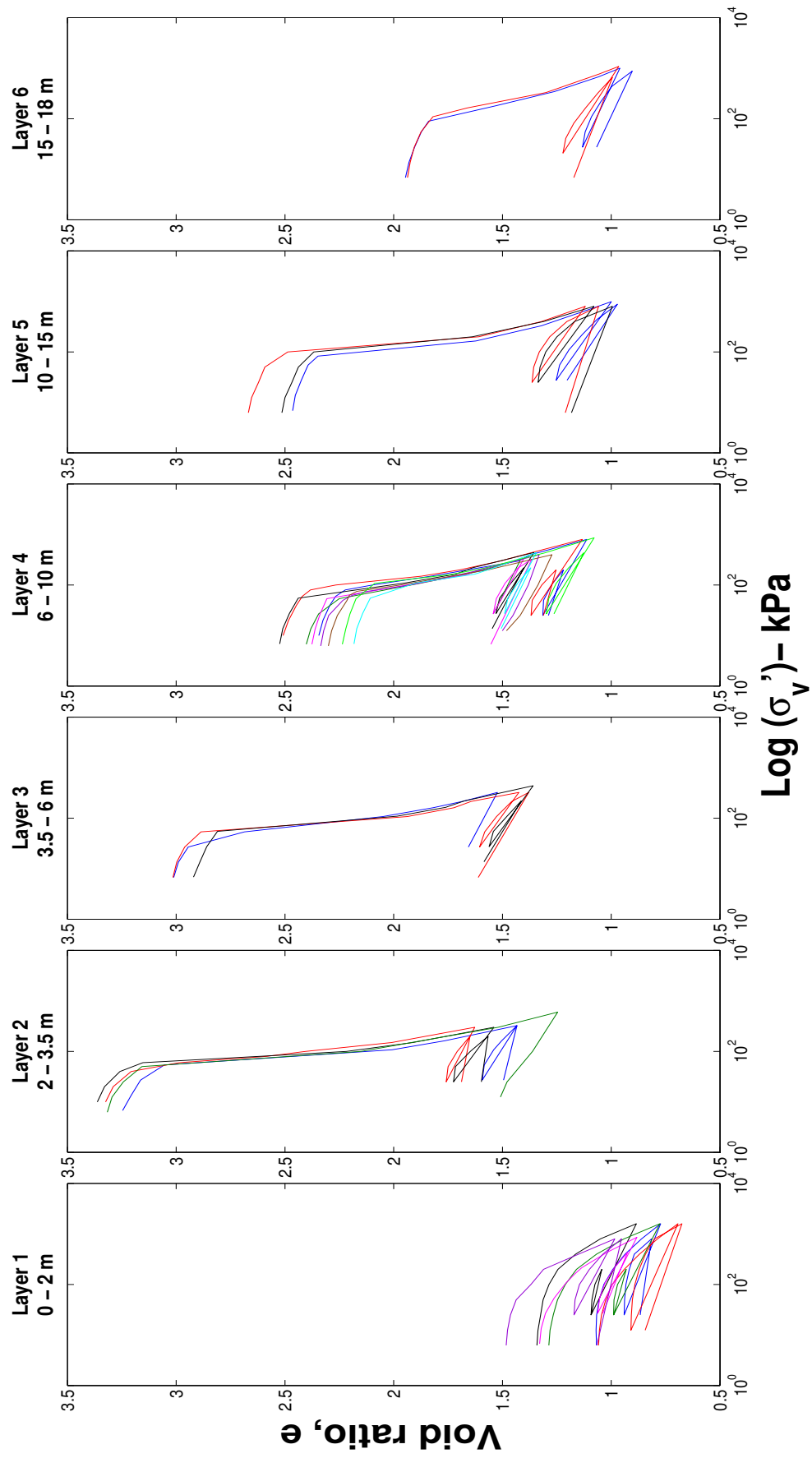
C Layering







SUMMARY



D Summary of parameters

Table D.1: Summary of Creep-Sclay1S parameters derived from laboratory tests for Haarajoki samples

| Type | Parameters | Symbol | Depth of layers (m) | | | | | | | | | |
|---------------------------------|---|---------------|---------------------|---------|---------|---------|---------|---------|-------|--|--|--|
| | | | 0 - 2 | 2 - 3.5 | 3.5 - 6 | 6 - 10 | 10 - 15 | 15 - 18 | | | | |
| Isotropic parameters | Swelling index | κ^* | - | 0.030 | 0.036 | 0.034 | 0.040 | 0.040 | 0.041 | | | |
| | Intrinsic compression index | λ_z^* | - | 0.100 | 0.105 | 0.101 | 0.090 | 0.086 | | | | |
| | Poisson's ratio | ν' | 0.350 | 0.180 | 0.18 | 0.180 | 0.180 | 0.280 | | | | |
| | Critical state in compression | M_c | 1.800 | 1.450 | 0.940 | 1.240 | 1.100 | 1.560 | | | | |
| | Critical state in extension | M_e | 1.130 | 0.977 | 0.720 | 0.877 | 0.805 | 1.030 | | | | |
| Anisotropic parameters | Friction angle | ϕ'_{ev} | 43.814 | 35.726 | 23.976 | 30.919 | 27.697 | 38.248 | | | | |
| | Initial inclination of yield surface | α_0 | 0.76 | 0.56 | 0.37 | 0.47 | 0.42 | 0.61 | | | | |
| | Absolute effectiveness in rotational hardening | ω | - | 23 - 46 | 24 - 48 | 30 - 60 | 35 - 70 | 40 - 80 | | | | |
| | Relative effectiveness in rotational hardening | ω_d | 0.95 | 0.98 | 0.43 | 0.8 | 0.64 | 1.02 | | | | |
| | Initial bonding | χ_0 | 1.76 | 14.58 | 25.14 | 33.98 | 48.46 | 61.0 | | | | |
| | Absolute rate of destructuration | ξ | 9.0 | 9.0 | 9.0 | 9.0 | 9.0 | 9.0 | | | | |
| | Relative rate of destructuration | ξ_d | 0.2 | 0.2 | 0.2 | 0.2 | 0.2 | 0.2 | | | | |
| | Creep coefficient | μ_z^* | 0.0010 | 0.0060 | 0.0065 | 0.0080 | 0.0040 | 0.0050 | | | | |
| | Reference time (days) | τ | 1.0 | 1.0 | 1.0 | 1.0 | 1.0 | 1.0 | | | | |
| | Initial void ratio | e_0 | 1.33 | 3.35 | 3.03 | 2.38 | 2.58 | 1.96 | | | | |
| Initial stress state parameters | Unit weight for each layer (kN/m ³) | γ' | 17.25 | 13.78 | 14.1 | 14.78 | 14.6 | 15.9 | | | | |
| | Preconsolidation pressure (kPa) | σ'_p | - | 49 | 51 | 65 | 87 | 92 | | | | |
| | Lateral earth pressure at rest | K_0^{NC} | 0.308 | 0.416 | 0.594 | 0.486 | 0.535 | 0.381 | | | | |
| | Overconsolidation ratio | OCR | - | 2.524 | 1.889 | 1.358 | 1.310 | 1.070 | | | | |
| | Preoverburden pressure (kPa) | POP | - | 29.29 | 26.00 | 13.50 | 20.78 | 8.87 | | | | |

E Initial in-situ stress condition

Table E.1: Initial in-situ stress condition prior to embankment loading in Haarajoki soil profile

| Layer | Depth (m) | σ_v (kPa) | u (kPa) | σ'_v (kPa) | PCP (kPa) | OCR (-) | POP (kPa) | ϕ'_{cv} | K_0 | σ'_h (kPa) |
|-----------|-----------|------------------|----------------|-------------------|------------------|----------------|------------------|--------------|-------|-------------------|
| 0 - 2m | 0.535 | 9.710 | 5.400 | 4.316 | - | - | - | 0.765 | 0.803 | 3.468 |
| | 0.655 | 11.830 | 6.570 | 5.258 | - | - | - | | 0.803 | 4.224 |
| | 1.08 | 19.600 | 10.890 | 8.711 | - | - | - | | 0.803 | 6.999 |
| | 1.125 | 20.130 | 11.180 | 8.947 | - | - | - | | 0.732 | 6.553 |
| | 1.735 | 30.900 | 17.170 | 13.734 | - | - | - | | 0.308 | 4.226 |
| | 1.785 | 31.780 | 17.660 | 14.126 | - | - | - | | 0.658 | 9.300 |
| 2 - 3.5 m | 2.325 | 40.000 | 22.960 | 17.043 | 50.209 | 2.946 | 33.165 | 0.624 | 0.782 | 13.327 |
| | 3.06 | 50.330 | 30.310 | 20.016 | 48.505 | 2.423 | 28.489 | | 0.698 | 13.965 |
| | 3.105 | 50.740 | 30.610 | 20.135 | 55.633 | 2.763 | 35.499 | | 0.753 | 15.166 |
| | 3.215 | 52.260 | 31.690 | 20.570 | 52.030 | 2.529 | 31.455 | | 0.715 | 14.714 |
| | 3.235 | 52.530 | 31.880 | 20.650 | 43.546 | 2.109 | 22.896 | | 0.643 | 13.284 |
| 3.5 - 6 m | 4.175 | 66.150 | 41.400 | 24.750 | 40.641 | 1.642 | 15.890 | 0.418 | 0.726 | 17.973 |
| | 4.355 | 68.270 | 42.870 | 25.400 | 50.682 | 1.996 | 25.290 | | 0.786 | 19.963 |
| | 5.215 | 80.410 | 51.310 | 29.110 | 53.390 | 1.834 | 24.280 | | 0.760 | 22.110 |
| 6 - 10 m | 6.09 | 93.060 | 60.040 | 33.020 | 70.891 | 2.147 | 37.870 | 0.540 | 0.720 | 23.772 |
| | 6.135 | 93.500 | 60.330 | 33.170 | 83.167 | 2.508 | 50.000 | | 0.780 | 25.861 |
| | 6.175 | 94.530 | 61.020 | 33.510 | 38.319 | 1.144 | 4.810 | | 0.521 | 17.454 |
| | 6.355 | 96.740 | 62.490 | 34.250 | 47.306 | 1.381 | 13.060 | | 0.574 | 19.656 |
| | 7.215 | 109.390 | 70.930 | 38.460 | 51.181 | 1.331 | 12.720 | | 0.563 | 21.657 |
| | 8.295 | 125.720 | 81.820 | 43.910 | 45.189 | 1.029 | 1.280 | | 0.493 | 21.665 |
| | 8.355 | 126.170 | 82.110 | 44.060 | 51.472 | 1.168 | 7.420 | | 0.527 | 23.202 |
| | 9 | 135.880 | 88.580 | 47.290 | 55.052 | 1.164 | 7.760 | | 0.526 | 24.860 |
| | 9.045 | 136.320 | 88.880 | 47.440 | 65.619 | 1.383 | 18.180 | | 0.574 | 27.248 |
| | 9.215 | 138.820 | 90.550 | 48.270 | 74.276 | 1.539 | 26.000 | | 0.607 | 29.286 |
| 9.335 | 140.590 | 91.720 | 48.860 | 95.003 | 1.944 | 46.140 | 0.684 | 33.431 | | |
| 10 - 15 m | 11.215 | 168.100 | 110.170 | 57.940 | 74.391 | 1.284 | 16.450 | 0.483 | 0.601 | 34.830 |
| | 11.235 | 168.400 | 110.360 | 58.030 | 85.998 | 1.482 | 27.960 | | 0.643 | 37.291 |
| | 13.235 | 197.590 | 129.980 | 67.610 | 87.798 | 1.299 | 20.190 | | 0.604 | 40.858 |
| 15 - 18 m | 15.215 | 226.720 | 149.410 | 77.310 | 80.400 | 1.040 | 3.080 | 0.668 | 0.390 | 30.175 |
| | 17.215 | 257.900 | 169.030 | 88.870 | 103.114 | 1.160 | 14.240 | | 0.418 | 37.119 |

F Other methods of determining pre-consolidation pressure

Pre-consolidation pressure (σ'_p) is the maximum overburden pressure sustained by a soil in its history. It is also defined as the yielding point of a soil beyond which a transition is observed from elastic to elasto-plastic behaviour. An accurate determination of σ'_p is necessary due to sensitivity of soft soil behaviour to loading. A number of methods have been proposed by different researchers to estimate an approximate value for pre-consolidation pressure. Casagrande 1936 proposed the most commonly used method of deriving σ'_p from $e - \log(\sigma'_v)$ plot. The steps recommended from this method is mentioned in Holtz and Kovacs 1981 and explained subsequently.

A point of maximum curvature is chosen from observation (Point A from Figure F.1) from $e - \log(\sigma'_v)$ curve. An horizontal line and a tangent is drawn from point A and intersected. The angle formed from this intersection is bisected and a straight line is drawn from the normally consolidated region. The point of intersection between this line and the bisected line (Point B from Figure F.1) is taken as the value of pre-consolidation pressure.

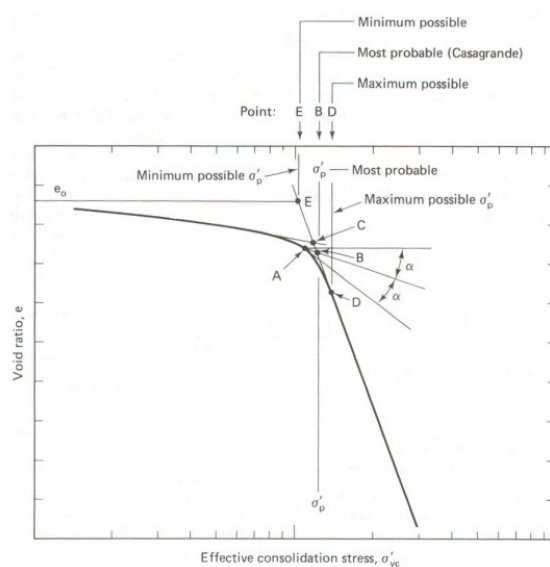


Figure F.1: Illustration of Casagrande's method for determination of pre-consolidation stress (Holtz and Kovacs 1981)

Due to effects of sampling disturbance, there is an expected decrease in the slope of the virgin compression line and the magnitude of error depends on the rate of disturbance of the sample. Hence it can be assumed that the slope of virgin compression line determined in laboratory tests are, in most cases, slightly less than that found in in-situ conditions. This affects the determination of pre-consolidation stress since accurate values are necessary to obtain the transition point of soil behaviour from elastic to elastic-plastic region. Schmertmann 1953 pointed out that the slope of virgin compression line for disturbed samples would intersect its in-situ counterpart at a void ratio around 0.42 times the initial void ratio of the sample.

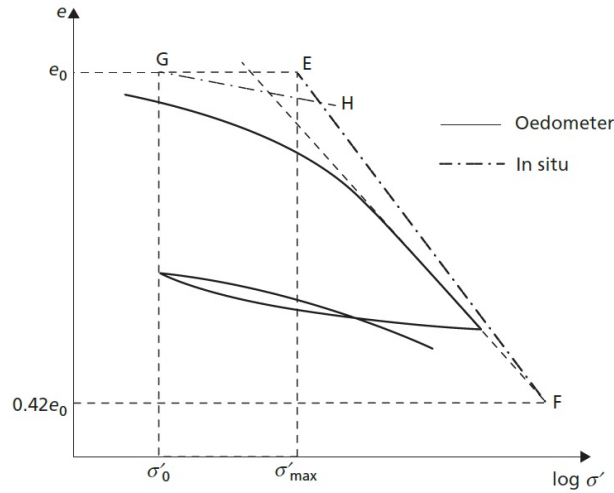


Figure F.2: Illustration of Schmertmann’s proposal of eventual intersection of virgin compression line between laboratory and in-situ samples at $e = 0.42e_0$ (Knappett and Craig 2014)

It is widely known that soft soils are highly strain-rate dependant which implies that the pre-consolidation stress would differ for different strain rates. This shows that the pre-consolidation value is sensitive to rate of loading. Sällfors 1975 proposed a methodology for the evaluation of pre-consolidation pressure from constant strain-rate (CRS) tests. This method is commonly used in Sweden. Soil samples are loaded at a constant strain-rate of $0.7\%/hour$. The results are plotted in an arithmetic scale corresponding to $10 \text{ kPa stress}/1\% \text{ strain ratio}$. The linear part from the elastic and elastic-plastic region is intersected and an isosceles triangle is drawn as shown in Figure F.3. Finally, the point σ'_c is identified as the pre-consolidation pressure for that sample.

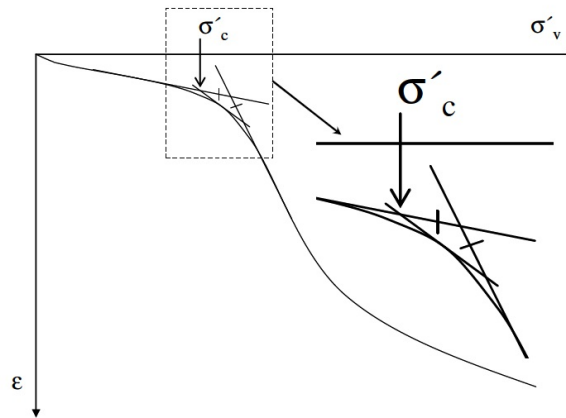


Figure F.3: Principle for evaluation of pre-consolidation stress according to Sällfors (1975)

G Determination of modified intrinsic creep index

Creep effect is recognized as one of the most important aspects of soft soil behavior. Different models have been developed to account for viscous effects. Creep-Sclay1S model, an extension of the S-CLAY1S model, incorporates creep effect. The model makes use of a visco-plastic multiplier Grimstad et al. 2008 which is expressed from equation G.1.

$$\dot{\Lambda} = \frac{\mu_i^*}{\tau} \cdot \left(\frac{p^{eq}}{(1 + \chi) \cdot p'_{mi}} \right)^{\frac{\lambda_i^* - \kappa^*}{\mu_i^*}} \cdot \frac{M_c^2 - \alpha_0^2}{M_c^2 - \eta_0^2} \quad (\text{G.1})$$

where μ_i^* is the intrinsic creep index and its determination is explained by a time resistance concept according to Grimstad et al. 2010. The time resistance concept is first introduced by Janbu 1969. The time resistance, R , is given by the relation in equation G.2. The time resistance number (r_s) is obtained by numerical differentiation from equation G.2.

$$R = \frac{dt}{d\epsilon} \quad (\text{G.2})$$

$$r_s = \frac{d(\partial t / \partial \epsilon_a)}{dt} = \frac{dR}{dt} = \frac{(\partial t / \partial \epsilon_a(t) - R_{ref})}{t - \tau} \quad (\text{G.3})$$

$$\frac{dt}{d\epsilon}(t) = r_s \cdot (t - \tau) + R_{ref} = r_s \cdot t \quad (\text{G.4})$$

$$\frac{d\epsilon_v^{vp}}{dt} = \frac{1}{r_s \cdot t} \Rightarrow \Delta \epsilon_v^{vp} = \frac{1}{r_s} \ln \frac{t}{\tau} \quad (\text{G.5})$$

From equation G.5, the modified creep index (μ^*) parameter used in Creep-Sclay1S model is similar to the time resistance number which is given by the relation $r_s = 1/\mu^*$. Grimstad and Degago 2010 claims that no creep would occur if limit t_{max} or OCR_{max} is reached. Figure G.1 shows the comparison of time resistance number between reconstituted and undisturbed sample. The initial structure is defined according to equation G.6.

$$\chi_0 = \frac{r_{si} - r_{s,min}}{r_{s,min}} \quad (\text{G.6})$$

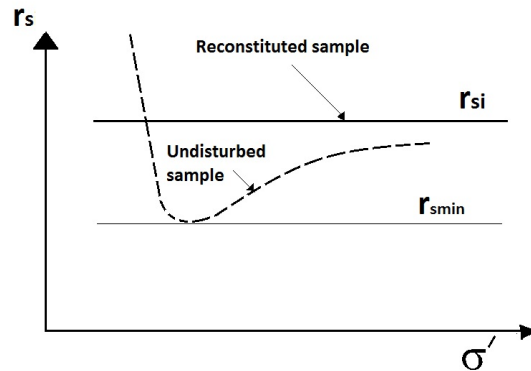


Figure G.1: Determination of intrinsic creep value from Grimstad and Degago 2010

H Experimental procedure

H.1 Oedometer test

Oedometer tests are designed to create a one-dimensional loading condition that represents the field condition for soils. Samples for this test are usually 20 mm thick and 50 mm wide diametrically, however, this standard differs for different region. The soil is placed in a cylindrical confining ring which prevents lateral deformation. In order to reduce friction, silicon paste is applied on the surface of the ring enclosing the sample or rings made of teflon material are also used. However, the type of method used for Haarajoki samples to reduce friction from confining ring is not specified. During the test, the sample is covered in water to make it air tight. Porous stones are placed on the top and bottom of the sample. The difference between the oedometer incremental loading (IL) tests and constant strain-rate is attributed to the loading condition. A standard IL procedure comprises of incremental load steps which is doubled on each step and kept constant for 24 hours. For oedometer CRS tests, the sample is compressed at a constant displacement rate with varying load and the rate differs for different region. In Sweden, a standard deformation rate of 0.0024 mm/min (0.72%/hour) is used. Continuous monitoring is required for CRS tests to maintain a constant rate of displacement. In most cases, CRS tests are preferred over incremental loading as it takes less time and cost.

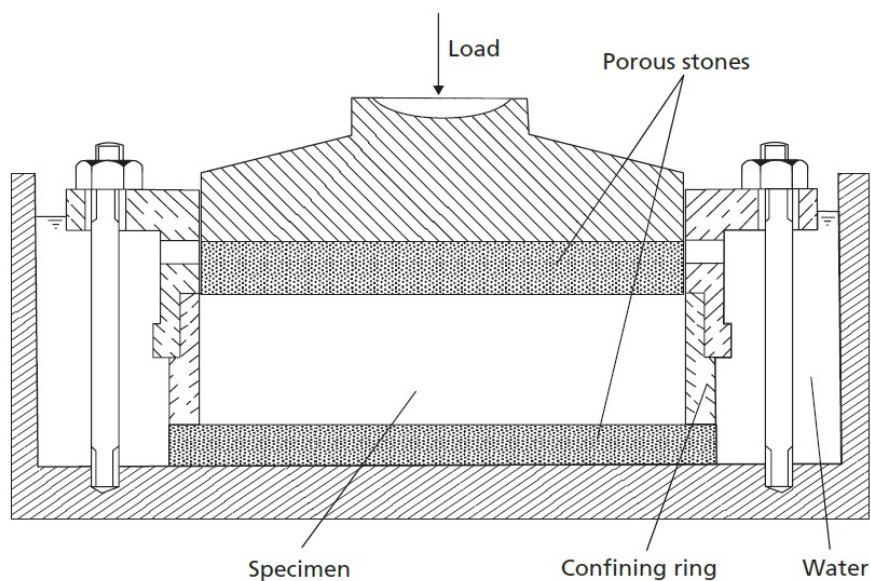


Figure H.1: Schematic diagram of an Oedometer apparatus (Knappett and Craig 2014)

H.2 Triaxial test

Another most commonly used laboratory testing for measuring soil behaviour is the triaxial apparatus which is suitable for all types of soil. The advantage of using this test over oedometer is that drainage can be controlled and pore pressure measurements be obtained. In the load cell, the cylindrical soil sample is covered in a thin rubber membrane. Generally, the height of the sample is taken as twice its diameter. The cell is filled with liquid, mostly water, and pressurized to a constant cell pressure. The sample is then loaded axially with a ram in addition to the cell pressure to initiate deviatoric stress in the sample until failure takes place, usually on a diagonal plane through the sample. The test can be conducted in drained condition and in undrained conditions where excess pore pressures can be measured. For triaxial compression test, the ram is pushed down at a constant rate which acts as the major principal stress with cell pressure acting radially on the sample. For triaxial extension tests, the cell pressure acts as the major principal stress and the soil shears in extension. Triaxial test is useful in deducing friction angle (ϕ'_{cv}), dilatancy angle (ψ'), cohesion (c), slope of critical state (M) and other parameters. The stress path of the sample can be plotted in $p' - q$ plane and corresponding volumetric and deviatoric strains can also be plotted.

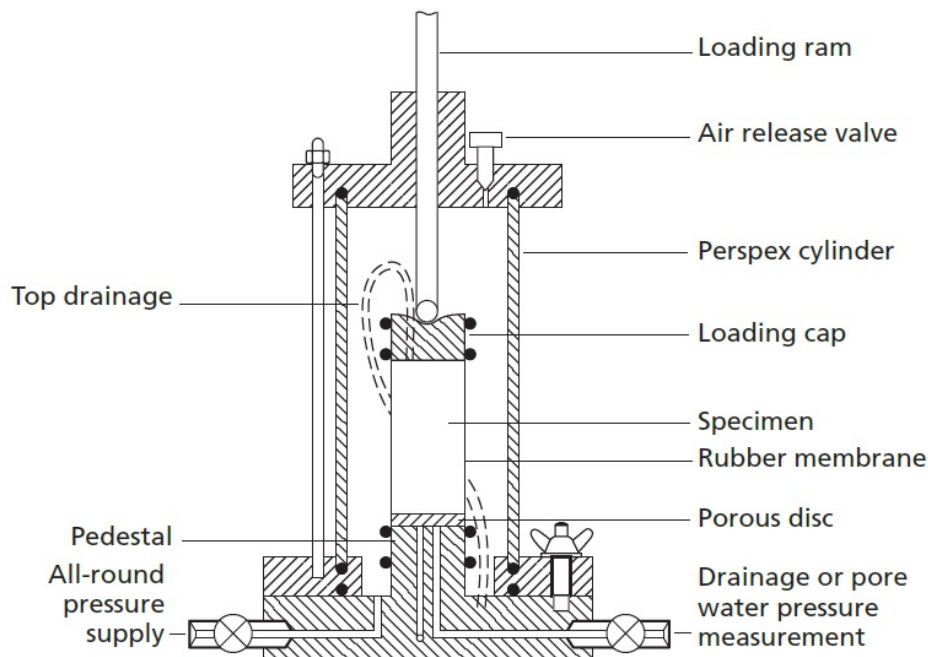


Figure H.2: Schematic diagram of a commonly used triaxial apparatus (Knappett and Craig 2014)

I Parameter sensitivity analysis on CRS simulation

Table I.1: Sensitivity of Creep-Sclay1S model's parameters on oedometer CRS simulation for Haarajoki samples

| Sl.No. | Parameters | Symbol | Original value | Modified value | Percentage of change | Influence on CRS simulation |
|--------|--|---------------|----------------|----------------|----------------------|--|
| 1 | Relative effectiveness of rotational hardening | ω_d | 1.02 | 0.02 | 98.04 | Increase in plastic compression but not significant |
| 2 | Absolute effectiveness of rotational hardening | ω | 60.00 | 2.00 | 96.67 | Almost no change, so negligible |
| 3 | Pre-overburden pressure (kPa) | POP | 87.00 | 67.00 | 22.99 | Significant change at the start of elasto-plastic region |
| 4 | Swelling index | κ^* | 0.041 | 0.030 | 26.83 | Significant change in the elastic region |
| 5 | Intrinsic Compression index | λ_i^* | 0.089 | 0.100 | 12.36 | Significant change in the plastic region |
| 6 | Modified intrinsic creep index | μ_i^* | 0.005 | 0.001 | 80.00 | Marked difference in the plastic stress path |
| 7 | Initial bonding | χ_0 | 67.00 | 47.00 | 29.85 | Quite significant change at the end of plastic compression stress path |
| 8 | Critical state in compression | M_c | 1.56 | 1.00 | 35.90 | Not as significant as the other isotropic parameters but has a reasonable difference |
| 9 | Initial void ratio | e_0 | 1.96 | 3.96 | 102.04 | No change |
| 10 | Unit weight in KN/m ³ | γ | 16.0 | 14.0 | 12.50 | No change |
| 11 | Poisson's ratio | ν' | 0.28 | 0.15 | 46.43 | Slight change in the elastic region but not significant |

J Flow equation

Darcy's law formulated by Henry Darcy (Darcy 1956) governs the flow of water through a porous medium. In Geotechnical engineering, the flow of liquids in soft soil is generally slow. First, it is necessary to understand the Bernoulli's proposal describing the hydrostatic condition in soil which is given in equation J.1.

$$u + \rho_f g z + \frac{1}{2} \rho_f v^2 = \text{constant} \quad (\text{J.1})$$

Where ρ_f is the density of fluid, u is the pore pressure and v is the velocity of fluid in the porous medium. In the absence of frictional loss, the sum of pressure, potential energy and kinetic energy along a flow path is considered a constant. Hence the total head, H , of a hydraulic system can be rewritten from equation J.1 as J.2.

$$H = (u/\rho_f g) + z + h_v = \text{constant} \quad (\text{J.2})$$

where h is the pressure head, z is the elevation head and h_v is the velocity head. For stationary fluid, which is the initial condition prior embankment loading, there is no kinetic energy and the velocity head can be ignored ($h_v = 0$). From Darcy's law, the discharge velocity (q_v) is proportional to conductivity (k) and hydraulic gradient which is given by equation J.3.

$$q_v = \frac{Q}{A} = -k \frac{dH}{dx} \quad (\text{J.3})$$

$$q_v = -k \left[\frac{\partial u}{\partial x} \frac{1}{\rho_f g} + \frac{\partial z}{\partial x} \right] \Rightarrow -\frac{k}{\gamma_f} \left[\frac{\partial u}{\partial x} - \rho_f g \frac{\partial z}{\partial x} \right] \quad (\text{J.4})$$

By considering three dimensional flow, the equation J.4 is modified to J.5

$$q_v = -\frac{k}{\gamma_f} \left[\nabla u - \rho_f g \right] \quad \text{where } \nabla = \frac{\partial}{\partial x} + \frac{\partial}{\partial y} + \frac{\partial}{\partial z} \quad (\text{J.5})$$

Since the z coordinate is considered in the vertical direction, the components of gravity with respect to the three axes is given as, $g_x = 0$, $g_y = 0$ and $g_z = -g$.

$$q_{v_x} = -\frac{k}{\gamma_f} \frac{\partial u}{\partial x} \quad q_{v_y} = -\frac{k}{\gamma_f} \frac{\partial u}{\partial y} \quad q_{v_z} = -\frac{k}{\gamma_f} \left(\frac{\partial u}{\partial z} + \rho_f g \right) \quad (\text{J.6})$$

$$\nabla q_v = \frac{\partial q_{v_x}}{\partial x} + \frac{\partial q_{v_y}}{\partial y} + \frac{\partial q_{v_z}}{\partial z} = -\nabla \cdot \left(\frac{k}{\gamma_f} \nabla u \right) \quad (\text{J.7})$$

Due to assumption of homogeneous material, the hydraulic conductivity (k) and volumetric weight of fluid (γ_f) are considered to be constants. Hence equation J.7 reduces to J.8

$$\nabla q_v = -\frac{k}{\gamma_f} \nabla^2 u \quad \text{where } \nabla^2 = \frac{\partial^2}{\partial x^2} + \frac{\partial^2}{\partial y^2} + \frac{\partial^2}{\partial z^2} \quad (\text{J.8})$$

From equation J.8, the change in flow is quadratically proportional to the change in pore pressure. This is one of the reasons for opting second order elements when flow analysis is incorporated.

K Settlement results from embankment simulation

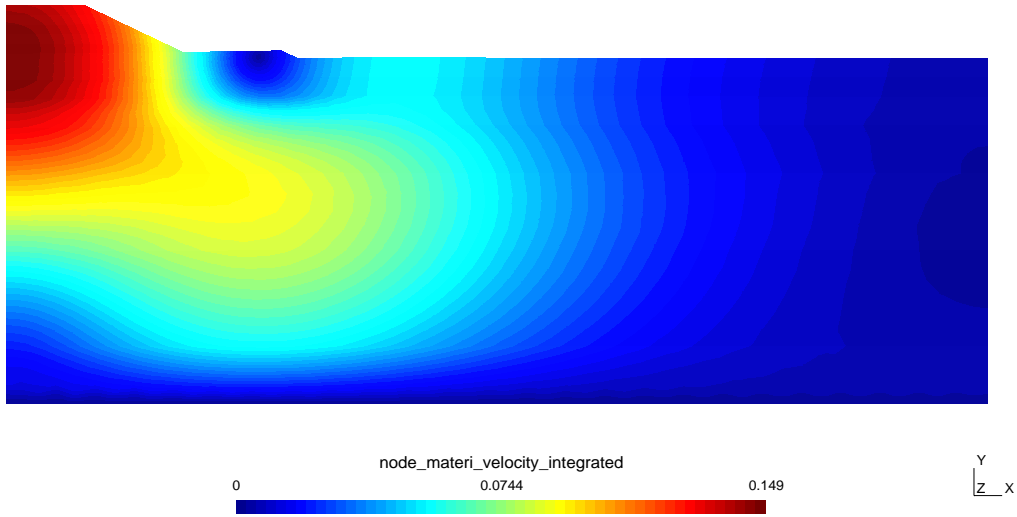


Figure K.1: Settlement with maximum value of 0.149m under embankment centre line after 35 days of embankment construction at Haarajoki

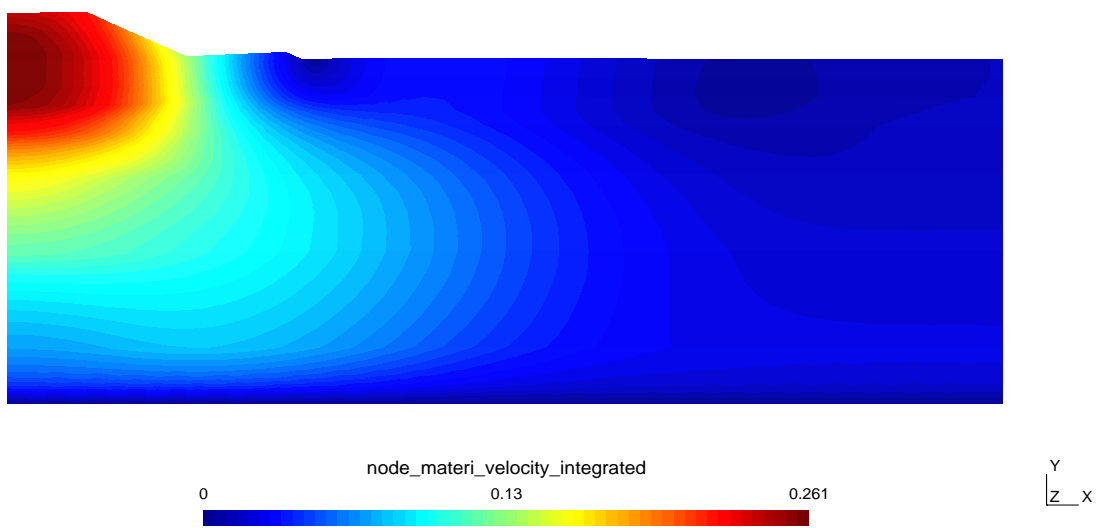


Figure K.2: Settlement with maximum value of 0.261m under embankment centre line after 365 days at Haarajoki

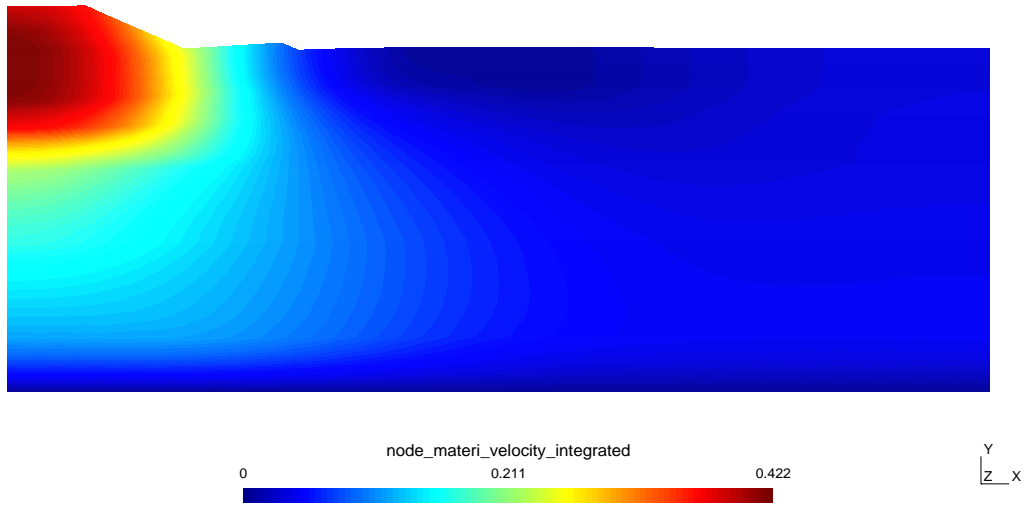


Figure K.3: Settlement with maximum value of 0.422m under embankment centre line after 1500 days at Haarajoki

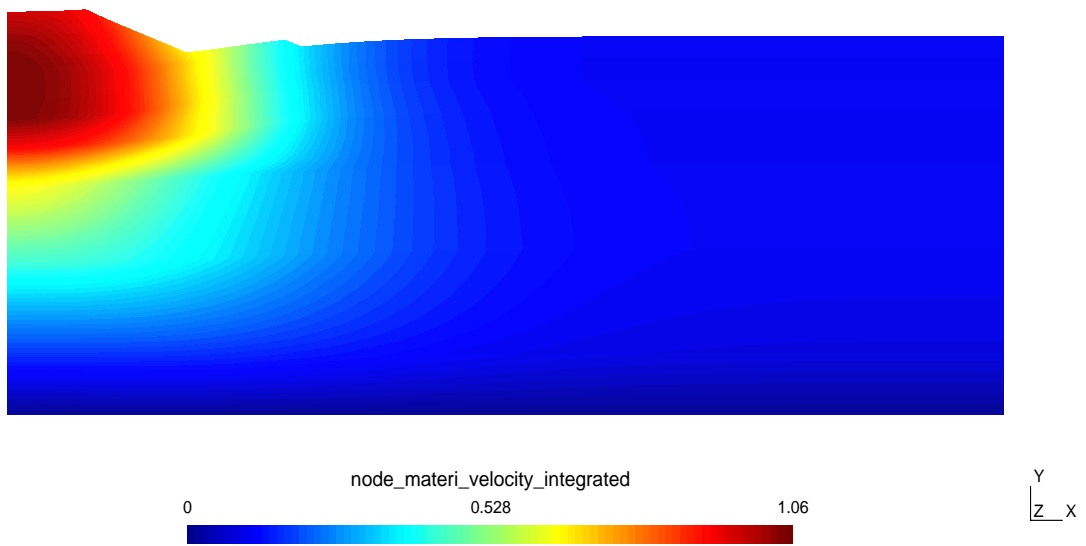


Figure K.4: Settlement with maximum value of 1.060m under embankment centre line after 1000 years at Haarajoki

L Pore pressure results from Embankment simulation

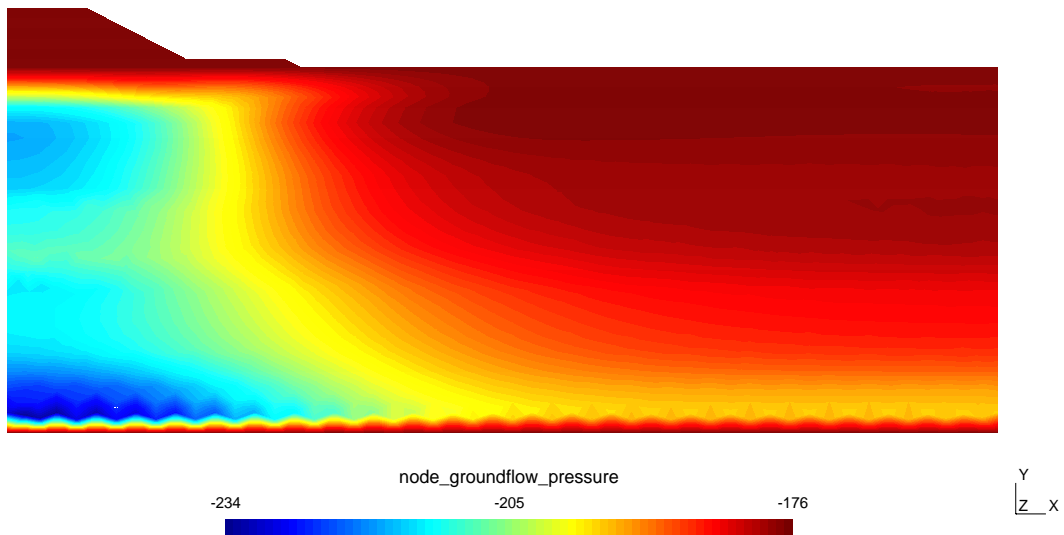


Figure L.1: Groundflow with maximum excess pore pressure upto 58 kPa around 16m depth after 35 days of its construction for Haarajoki soil deposit

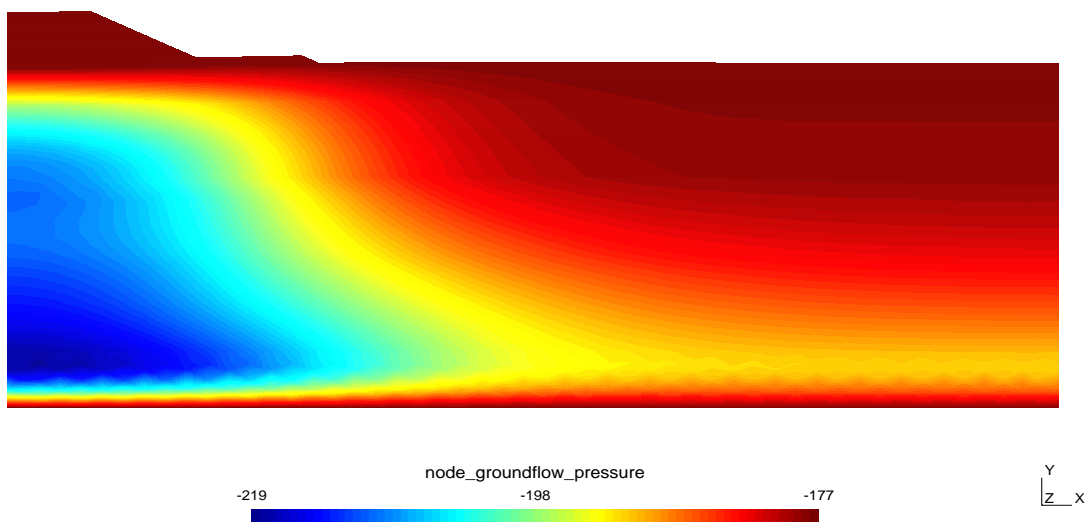


Figure L.2: Groundflow with maximum excess pore pressure upto 42 kPa around 12 - 16m depth after 365 days of embankment loading for Haarajoki soil deposit

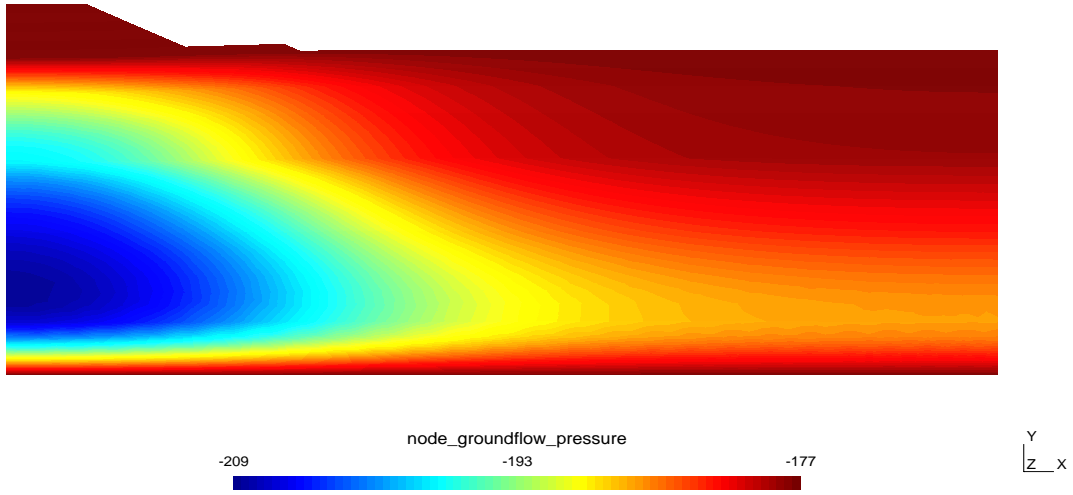


Figure L.3: Groundflow with maximum excess pore pressure upto 32 kPa around 8 - 15m depth after 1500 days of embankment loading for Haarajoki soil deposit

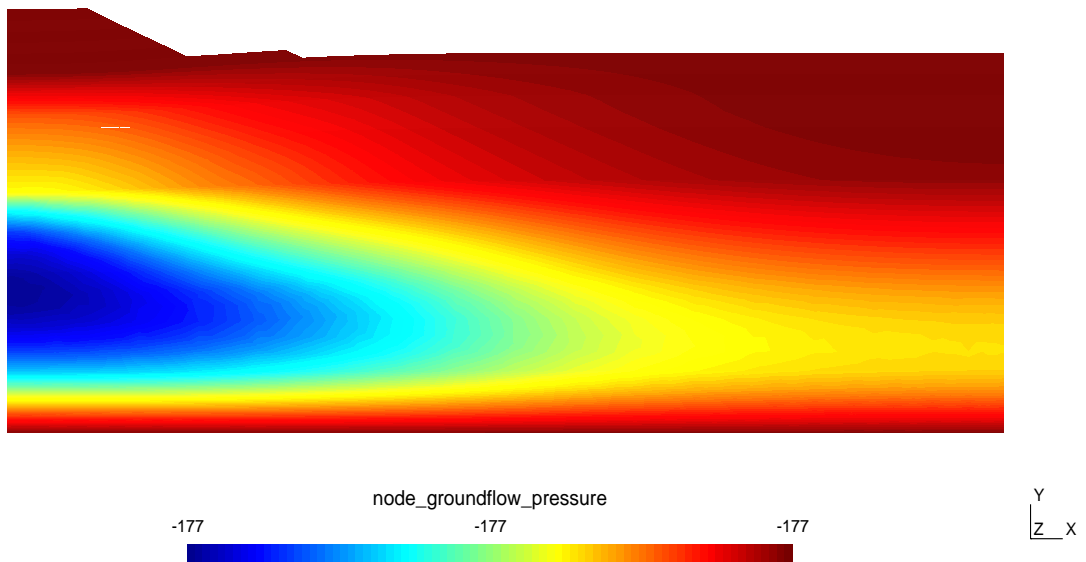


Figure L.4: Groundflow with no excess pore pressures after 1000 years of embankment loading for Haarajoki soil deposit